NAVAL POSTGRADUATE SCHOOL
Monterey, California

THESIS

TROPICAL CYCLONE MOTION DUE TO ENVIRONMENTAL INTERACTIONS REPRESENTED BY EMPIRICAL ORTHOGONAL FUNCTIONS OF THE VORTICITY FIELDS

by
Mark J. Gunzelman

June 1991

Thesis Advisor: Russell L. Elsberry

Approved for public release; distribution unlimited

REPORT DOCUMENTATION PAGE

Form Approved
OMB No 0704 0188

1a REPORT SECURITY CLASSIFICATION Unclassified	1b RESTRICTIVE MARKINGS
2a SECURITY CLASSIFICATION AUTHORITY	3 DISTRIBUTION / AVAILABILITY OF REPORT Approved for public release; distribution is unlimited.
2b DECLASSIFICATION / DOWNGRADING SCHEDULE	
4 PERFORMING ORGANIZATION REPORT NUMBER(S)	5 MONITORING ORGANIZATION REPORT NUMBER(S)
6a NAME OF PERFORMING ORGANIZATION Naval Postgraduate School 6b OFFICE SYMBOL (If applicable) 35	7a NAME OF MONITORING ORGANIZATION Naval Postgraduate School
6c ADDRESS (City, State, and ZIP Code) Monterey, CA 93943-5000	7b ADDRESS (City, State, and ZIP Code) Monterey, CA 93943-5000
8a NAME OF FUNDING / SPONSORING ORGANIZATION 8b OFFICE SYMBOL (If applicable)	9 PROCUREMENT INSTRUMENT IDENTIFICATION NUMBER
8c ADDRESS (City, State, and ZIP Code)	10 SOURCE OF FUNDING NUMBERS PROGRAM ELEMENT NO / PROJECT NO / TASK NO / WORK UNIT ACCESSION NO

11 TITLE (Include Security Classification)
TROPICAL CYCLONE MOTION DUE TO ENVIRONMENTAL INTERACTIONS REPRESENTED BY EMPIRICAL ORTHOGONAL FUNCTIONS OF THE VORTICITY FIELDS

12 PERSONAL AUTHOR(S)
Mark J. Gunzelman

13a TYPE OF REPORT	13b TIME COVERED	14 DATE OF REPORT (Year, Month, Day)	15 PAGE COUNT
Master's Thesis	FROM _____ TO _____	June 1991	115

16 SUPPLEMENTARY NOTATION
The views expressed in this thesis are those of the author and do not reflect the official policy or position of the Department of Defense or the U.S. Government.

17 COSATI CODES			18 SUBJECT TERMS (Continue on reverse if necessary and identify by block number)
FIELD	GROUP	SUB-GROUP	Tropical Cyclone Interactions, EOF, Representation, Vorticity

19 ABSTRACT (Continue on reverse if necessary and identify by block number)

Tropical cyclone motion influenced by adjacent synoptic features is examined with relative vorticity fields at 700, 400 and 250 mb computed from operationally-analyzed wind fields. When a empirical orthogonal function (EOF) method is used to map the vorticity onto the spatial grids, a smoother but more dependable depiction of the vorticity dynamics is provided than by the original fields. The effect of five processes that contribute to motion relative to the steering flow during periods of interaction with adjacent circulations are evaluated for their contributions to binary rotation and to changing the separation distance between the interacting circulations. This vorticity dynamics approach indicates tropical cyclones interact with various features at different levels. The Fujiwhara effect is most evident with stronger interaction events. Only the convergence effect of one tropical cyclone circulation on another tropical cyclone can explain the cases with decreasing separations. By

20 DISTRIBUTION / AVAILABILITY OF ABSTRACT	21 ABSTRACT SECURITY CLASSIFICATION
☒ UNCLASSIFIED/UNLIMITED ☐ SAME AS RPT ☐ DTIC USERS	Unclassified
22a NAME OF RESPONSIBLE INDIVIDUAL Russell L. Elsberry	22b TELEPHONE (Include Area Code) (408) 646-2373 22c OFFICE SYMBOL MR/Es

19. ABSTRACT (continued)

contrast, the advection by the tropical cyclone circulation of the vorticity gradient of the other cyclone could not explain the decreasing separations. The Beta effect depends on the orientation of two interacting systems of different sizes, but the environmental vorticity gradient is not just due to earth vorticity in these interacting cases. The effects of environmental shear strongly depend on the orientation of the ITCZ and the geographical orientation of the two cyclones.

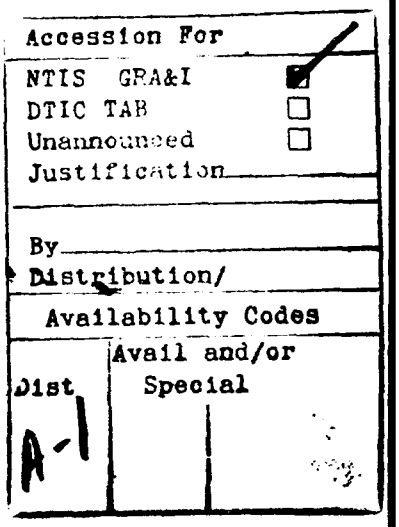

Approved for public release; distribution is unlimited.

Tropical Cyclone Motion Due to
Environmental Interactions
Represented by Empirical Orthogonal
Functions of the Vorticity Fields

by

Mark J. Gunzelman
Lieutenant, United States Navy
B.S., Florida State University, 1979

Submitted in partial fulfillment of the
requirements for the degree of

MASTER OF SCIENCE IN METEOROLOGY AND OCEANOGRAPHY

from the

NAVAL POSTGRADUATE SCHOOL
June 1991

Author: _____
Mark J. Gunzelman

Approved by: _____
Russell L. Elsberry, Thesis Advisor

_____
George M. Dunnavan, Second Reader

_____
for Robert L. Haney, Chairman
Department of Meteorology

_____
Gordon E. Schacher,
Dean of Faculty and Graduate Studies

ABSTRACT

Tropical cyclone motion influenced by adjacent synoptic features is examined with relative vorticity fields at 700, 400 and 250 mb computed from operationally-analyzed wind fields. When an empirical orthogonal function (EOF) method is used to map the vorticity onto spatial grids, a smoother but more dependable depiction of the vorticity dynamics is provided than by the original fields. The effect of five processes that contribute to motion relative to the steering flow during periods of interaction with adjacent circulations are evaluated for their contribution to binary rotation and to changing the separation distance between interacting circulations. This vorticity dynamics approach indicates tropical cyclones interact with various features at different levels. The Fujiwhara effect is most evident with stronger interaction events. Only the convergence effect of one tropical cyclone circulation on another tropical cyclone can explain the cases with decreasing separations. By contrast, the advection by the tropical cyclone circulation of the vorticity gradient of the other cyclone could not explain the decreasing separations. The Beta effect depends on the orientation of two interacting systems of different sizes, but the environmental vorticity gradient is not just due to earth vorticity in these interacting cases. The effects of environmental shear strongly depend on the orientation of the ITCZ and geographical orientation of the two cyclones.

TABLE OF CONTENTS

I.	INTRODUCTION		1
	A.	BACKGROUND AND MOTIVATION	1
	B.	OBJECTIVES	3
II.	LITERATURE REVIEW		5
	1.	The Beta Effect	5
	2.	The Fujiwhara Effect	8
	3.	The Convergent Flow Effect	9
	4.	The Vorticity Advection Effect	10
	5.	The Environmental Shear Effect	11
III.	DATA BASE DEVELOPMENT		13
	A.	FIELD DEFINITION	13
	B.	DATA RETRIEVAL	14
	C.	RELATIVE VORTICITY FIELDS	15
IV.	EMPIRICAL ORTHOGONAL FUNCTIONS		17
	A.	BACKGROUND	17
	B.	THE EOF METHOD	17
V.	RESULTS		33
	A.	COMPARISON OF THE EOF FILTERED AND RAW VORTICITY FIELDS	33
	B.	SELECTION OF CASE STUDIES	34
	C.	CASE 1 - SYPERTYPHOON ABBY (STAGE 1)	36
		1. Synoptic Discussion	36
		2. Analysis Procedures and Vortex Parameters	41
		3. Evaluation of Secondary Effects in Stage 1	43
	D.	CASE 1 - SUPERTYPHOON ABBY (STAGE 2)	48
		1. Synoptic Discussion	48
		2. Vortex Parameters	51
		3. Evaluation of Secondary Mechanisms in Stage 2	53
		4. Summary of Mechanisms in Case 1	57

E. CASE 2 - MULTIPLE STORM INTERACTION 59
1. Synoptic Discussion 59
2. Limitations Due to Grid Resolution 61
3. Interaction of Pat and Odessa 66
4. Evaluation of the Secondary Mechanisms 66
F. CASE 3 - INTERACTON OF TY DINAH AND TY ED 70
1. Synoptic Discussion 70
2. TY Dinah's Interaction with an Anticyclone (AC) 73
3. Evaluation of Secondary Effects between TY Dinah and an Anticyclone 77
G. CASE 4 - INTERACTION OF TY MAC AND TS NANCY 84
1. Synoptic Discussion 84
2. Evaluation of Secondary Effects on the Interaction of Weak Cyclones 87

VI. CONCLUSIONS AND RECOMMENDATIONS 92

LIST OF REFERENCES 97

INITIAL DISTRIBUTION LIST 99

LIST OF TABLES

Table 1.	MEAN EIGENVALUES AT 95 PERCENT CONFIDENCE LEVEL	32
Table 2.	PERCENTAGE OF EXPLAINED VARIANCE WITH 45 MODES	32
Table 3.	RATIO OF THE RELATIVE VORTICITY AMPLITUDE OF TROPICAL STORM (TS) BEN COMPARED TO TYPHOON (TY) ABBY DURING STAGE ONE	42
Table 4.	RELATIVE MOTION AND ROTATION OF THE TRACKS OF TY ABBY AND TS BEN DURING STAGE ONE	47
Table 5.	RATIO OF RELATIVE VORTICITY AMPLITUDE OF THE EXTRATROPICAL (ET) CYCLONE COMPARED TO TY ABBY DURING STAGE TWO	53
Table 6.	RELATIVE MOTION AND ROTATION OF THE TRACKS OF TY ABBY AND THE ET CYCLONE DURING STAGE TWO	57
Table 7.	RATIO OF THE RELATIVE VORTICITY AMPLITUDE OF THE HYBRID CENTER (HC) COMPARED TO TY PAT	66
Table 8.	RELATIVE MOTION AND ROTATION OF THE TRACKS OF TY PAT AND THE HYBRID CENTER	69
Table 9.	RATIO OF THE RELATIVE VORTICITY AMPLITUDE OF THE ANTICYCLONE (AC) COMPARED TO TY DINAH	77
Table 10.	RELATIVE MOTION AND ROTATION OF THE TRACKS OF TY DINAH AND THE ANTICYCLONE	84
Table 11.	RATIO OF THE RELATIVE VORTICITY AMPLITUDE OF TS NANCY COMPARED TO TY MAC	87

Table 12. RELATIVE MOTION AND ROTATION OF THE TRACKS OF TS NANCY AND TY MAC 91

LIST OF FIGURES

Figure 1.	The western North Pacific region	1
Figure 2.	Linear Beta effect	7
Figure 3.	Nonlinear vorticity advection effect	7
Figure 4.	Resultant displacement due to Beta effect	8
Figure 5.	The Fujiwhara effect	9
Figure 6.	Convergent flow effect of Chang (1983)	10
Figure 7.	The vorticity advection effect of DeMaria and Chan (1984)	11
Figure 8.	The environmental shear effect of Dong and Neumann (1983)	12
Figure 9.	Relocatable 527-point grid	14
Figure 10.	Relative vorticity at 700 mb for 00 UTC 14 August 1983	16
Figure 11.	Average vorticity at 700 mb for all 682 cases	19
Figure 12.	Standard deviation of vorticity at 700 mb for all 682 cases	19
Figure 13.	Average vorticity at 400 mb as in Fig. 11	20
Figure 14.	Standard deviation of vorticity at 400 mb as in Fig. 12	20
Figure 15.	Average vorticity at 250 mb as in Fig. 11	21
Figure 16.	Standard deviation of vorticity at 250 mb as in Fig. 12	21
Figure 17.	Mode 1 eignevector at 400 mb	23
Figure 18.	Mode 2 eigenvector at 400 mb	24
Figure 19.	Mode 3 eigenvector at 400 mb	25
Figure 20.	Mode 4 eigenvector at 400 mb	26
Figure 21.	Mode 5 eigenvector at 400 mb	26
Figure 22.	Mode 6 eigenvector at 400 mb	27
Figure 23.	Reconstructed 400 mb vorticity field	29
Figure 24.	Example of mode selection for eigenvalues	30
Figure 25.	Reconstructed vorticity fields at 400 mb with 45 modes	31

Figure 26.	Original vorticity field at 700 mb	33
Figure 27.	Filtered EOF vorticity field at 700 mb	34
Figure 28.	Binary interaction of Pat and Odessa about a singular point	35
Figure 29.	Best track of Supertyphoon (STY) Abby during August 1983	37
Figure 30.	Tracks of Abby, TS Ben and an extratropical cyclone	38
Figure 31.	Vorticity and winds (kt) for 00 UTC 12 August 1983 at 700 mb	39
Figure 32.	Vorticity and wind field for 00 UTC 13 August 1983 at 700 mb	39
Figure 33.	Vorticity and wind field for 00 UTC 14 August 1983 at 700 mb	40
Figure 34.	Vorticity and wind field for 00 UTC 15 August 1983 at 700 mb	40
Figure 35.	Vorticity along line connecting STY Abby and TS Ben	42
Figure 36.	Beta effect in Abby-Ben case (stage 1)	45
Figure 37.	Fujiwhara effect applied to the Abby-Ben case (stage 1).	45
Figure 38.	Convergent circuation effect of Chang (1983) for Abby-Ben case	46
Figure 39.	Vorticity advection effect of DeMaria and Chan (1984)	46
Figure 40.	Environmental shear of Dong and Neumann (1986) for Abby-Ben case (stage 1).	47
Figure 41.	Relative vorticity and wind fields for 400 mb at 00 UTC 12 August	49
Figure 42.	Relative vorticity and wind fields for 400 mb at 00 UTC 13 August similar to Fig. 41.	49
Figure 43.	Relative vorticity and wind fields for 400 mb at 00 UTC 14 August similar to Fig. 41.	50
Figure 44.	Relative vorticity and wind fields for 400 mb at 00 UTC 15 August similar to Fig. 41.	50
Figure 45.	Relative vorticity and wind fields for 400 mb at 00 UTC 16 August similar to Fig. 41.	51
Figure 46.	Vorticity of Abby and a midlatitude cyclone	52

Figure 47.	Beta effect during stage 2	52
Figure 48.	Fujiwhara effect during stage 2	55
Figure 49.	Convergent flow effect during stage 2	55
Figure 50.	Vorticity advection effect during stage 2	56
Figure 51.	Environmental shear effect during stage 2	56
Figure 52.	Separation distances (n mi) between TY Odessa and TS Ruby	60
Figure 53.	Relative vorticity at 700 mb for 00 UTC 27 August 1985	61
Figure 54.	Relative vorticity at 700 mb for 12 UTC 27 August 1985	63
Figure 55.	Schematic of the vorticity fields at 700 mb for 12 UTC 27 August 1985	64
Figure 56.	Binary motion of the hybrid vorticity center (HC)	65
Figure 57.	Positions (cross symbols) of TY Pat, Odessa and TS Ruby	65
Figure 58.	Vorticity along line connecting Pat and hybrid vorticity center	67
Figure 59.	Tracks of TY Dinah and TY Ed	71
Figure 60.	Vorticity at 700 mb along the axis connecting Dinah and Ed	72
Figure 61.	Vorticity at 700 mb of TY Dinah compared to TY Ed	73
Figure 62.	Vorticity at 400 mb along the axis connecting Dinah and the AC.	75
Figure 63.	Relative vorticity and wind fields for 400 mb at 00 UTC 29 August.	76
Figure 64.	Relative vorticity and wind fields for 400 mb at 00 UTC 30 August similar to Fig. 63	76
Figure 65.	Relative vorticity and wind fields for 400 mb at 00 UTC 31 August similar to Fig. 63	78
Figure 66.	Beta effect for Dinah and the anticyclone (AC)	79
Figure 67.	Separation distances and relative positions of Dinah and the AC at 400 mb.	80
Figure 68.	Fujiwhara effect between Dinah and the AC at 400 mb	80

Figure 69. Convergent flow effect between Dinah and the AC at 400 mb 81

Figure 70. Vorticity advection effect between Dinah and the AC at 400 mb. 82

Figure 71. Environmental shear effect for Dinah and the AC at 400 mb 83

Figure 72. Tracks of a weakened TY Mac and TS Nancy 85

Figure 73. Vorticity field at 700 mb for TY Mac 86

Figure 74. Vorticity along the axis connecting Mac and Nancy at 700 mb 88

Figure 75. Beta effect between TY Mac and TS Nancy at 700 mb 89

Acknowledgements

The completion of this study involved the dedicated assistance of many individuals. In particular, I want to express a special thanks to Dr. Russ Elsberry who directed this research and taught me many valuable ideas. His acute teaching ability, genuine interest and thorough dedication opened up avenues I never thought I could understand. He taught me how to approach and solve a complex problem one step at a time, helping to keep the big picture in focus. I greatly appreciated his patience and understanding during those weeks when roadblocks brought no results to show.

I am truly grateful to Paul Dobos for his countless dedicated hours of assistance on a wide range of problems. From scratch, Paul patiently taught me certain areas of computer programing previously unfamiliar to me. His continuous guidance and trouble-shooting eroded numerous frustrating roadblocks in piecemeal fashion.

Additionally, the staff of the W. R. Church computer center patiently provided specialized guidance in trouble-shooting many programs and aid in using the mainframe computer. In particular, I wish to thank Dennis Mar for his unwavering patience during his busy schedule, to help me find a "needle in a haystack" type programming glitches; Linda Mauck's tremendous help in protecting and making old feisty "direct access" data files available for proper use; Richard Donat for providing much needed extra computer storage space that saved me lots of time, and finally Larry Frazier for his ingenious magic in reformatting "Gthesis" to certain specifications.

I greatly appreciated the Macintosh graphics insight and help received from 1st Lieutenant Randy Lefevere preparing for my thesis presentation, some of which are included in the thesis.

Finally, I reserve my sincerest thanks of appreciation to last. I would like to dedicate all the long hours, frustrations and accomplishments to my wife, Venida and my two beautiful daughters, Ashley and Megan. Venida and the children's support were my encouragement and light at the end of the tunnel over the past 2 1/2 years. It is not easy raising two lovely children without a husband's normal assistance because my thoughts and effects were often directed towards my graduate studies. The result of those too numerous efforts lies in this completed thesis. My deepest and dearest thanks for making a dream come true.

I. INTRODUCTION

A. BACKGROUND AND MOTIVATION

Tropical cyclone motion is influenced by environmental interactions. The forecasting of such interactions is one of the most difficult problems in tropical meteorology. Reliable forecasts require a certain degree of understanding of the complex interaction of cyclones and their surrounding environment. Sandgathe (1987) explains that current numerical and statistical forecast aids provide reasonable guidance in textbook situations. However, the presence of an adjacent tropical cyclone often leads to large forecast errors. The forecaster in the western North Pacific faces this situation an average of three times per season (Sandgathe 1987).

The western North Pacific region (Figure 1) includes the western North Pacific Ocean, the Philippine Sea, South China Sea, East China Sea, Yellow Sea and the Sea of Japan. An average of 31 tropical cyclones occur each year in this area (Annual Tropical Cyclone Report 1985).

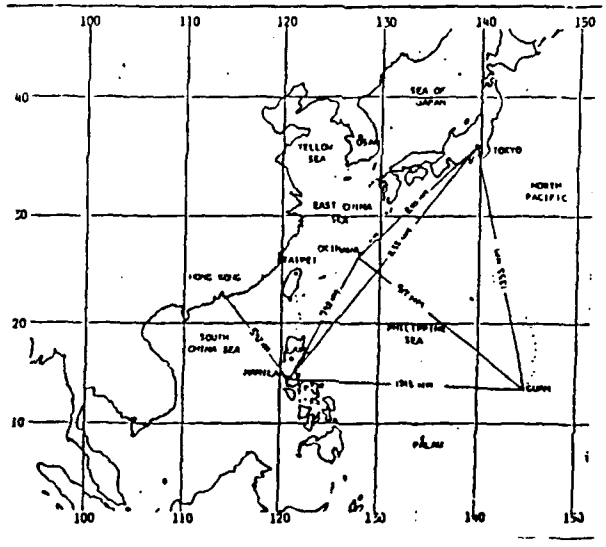

Figure 1. The western North Pacific region is shown with distances between key locations (Sandgathe, 1987).

These cyclones have a major impact on the logistics and operations of both military and civilian populations. The loss of three naval ships, 790 men and 200 planes from a tropical cyclone in December 1944 led to the establishment by May 1945 of weather reconnaissance squadrons to track the movement of tropical cyclones (Halsey and Bryan 1947). New operating orders were written for ships to take correct evasive action. Nevertheless, serious losses of life and property continue to occur. It is imperative to improve the ability to forecast tropical cyclone movement, since storm damage can only be minimized or avoided with early and accurate warnings to ship and shore facilities. Improved warnings can provide a greater lead-time for evasive action to be carried out. To minimize storm damage, the Commander U.S. Seventh Fleet has set the maximum forecast error requirements for tropical cyclones at 50, 100 and 150 n mi for the 24-h, 48-h and 72-h forecast, respectively. This will require a reduction of more than 50 percent in the average annual forecast errors of 116, 232 and 360 n mi at 24, 48 and 72 h, respectively (ATCR 1986).

Sandgathe (1987) ranks seven track forecasting problems in the western North Pacific related to storm-synoptic interaction. His ranking is in terms of the least understood scenarios that need improved forecaster understanding:

(i) Multiple cyclone interaction--the outer wind circulation of one cyclone influences the track of the second.

(ii) Cyclone and midlatitude trough interaction--this type of interaction may cause several types of cyclone movement. The trough influences the cyclone to track more northward, at least temporarily. If the trough is strong enough, the cyclone will continue moving northward and then recurve. However, if the trough influence is overcome by a strengthening subtropical ridge, the cyclone movement will again be towards the west, which results in a stair-step type track. Looping is another track possibility from this interaction.

(iii) Cyclone and subtropical ridge interaction--the cyclone track is determined by the shape and extent of the ridge. The cyclone will either move west under the ridge or gradually recurve around the western end of the ridge. The step and looping type tracks also are possible with this kind of interaction.

(iv) Extratropical transition--the warm core (single air mass) cyclone is transformed into a cold-core or hybrid (two air mass) system.

(v) Terrain interaction--significant orographic features have an effect on the cyclone's steering or storm circulation. This interaction occurs when the cyclone moves over or close to various large island and coastal areas in the western North Pacific basin.

(vi) Monsoon surge interactions--the tropical cyclone track is altered by either the Southwest Monsoon or the Northeast Monsoon. Diurnal fluctuations in the Southwest monsoon flow may vary the cyclone speed, and sometimes cause the storms to become quasi-stationary in the Philippine and South China Sea regions. Late season tropical cyclones are significantly influenced by the Northeast Monsoon, which can result in erratic movements and large forecast errors.

(vii) Cyclone and upper-level low interaction--tropical cyclone motion is influenced by a Tropical Upper Tropospheric Trough (TUTT). In the western North Pacific, these TUTT's may form from the base of a eastward-moving midlatitude trough.

Four storm interaction cases are selected for evaluation. Each case involves more than one interaction category listed by Sandgathe. The numerals in parentheses following the storm name indicate the year and the Roman numerals correspond to the interactions in the list above:

- Supertyphoon (STY) Abby and Tropical Storm (T.S.) Ben; (1983), (i, ii)
- Typhoon (TY) Odessa, Pat and T.S. Ruby; (1985), (i, iii, iv)
- TY Dinah and Ed; (1984) (i, ii, iii, iv, vii)
- TY Mac and TS Nancy; (1979) (i, v, vi)

B. OBJECTIVES

The primary objective of this study is to investigate relative vorticity derived from operationally-analyzed wind fields as a predictor of tropical cyclone motion due to environmental effects. Relative vorticity fields have not been available at the Joint Typhoon Warning Center (JTWC) for use as a predictor of such interactive cyclone motion. The goals are to use vorticity and vorticity advection as predictors that will hopefully give dynamic guidance to the forecaster via:

(i) demonstrating an Empirical Orthogonal Function (EOF) representation of the relative vorticity gives a better depiction of the fields than the raw vorticity fields (Sherman 1988); and

(ii) evaluating individually how five secondary mecahnisms that affect tropical cyclone motion support or do not support the observed results of binary rotation and attraction/repulsion relative to/from the other cyclone.

The primary influence on cyclone motion is the environmental steering flow. Superposed on this effect are five processes that may operate during periods of interaction with adjacent circulations:

(i) Beta effect--combines the linear beta and nonlinear vorticity advection effects;

(ii) Fujiwhara effect--explains the counterclockwise rotation of two vortices;

(iii) Convergent and divergent flow effects--uses the outer circulation flow profile of each storm to explain mutual attraction or repulsion;

(iv) Vorticity advection effect--describes mutual attraction or repulsion through vorticity gradients within each of the interacting circulations; and

(v) Environmental shear effects--evaluates mutual attraction or repulsion due to the environment vorticity gradient outside the interacting circulations.

These mechanisms, which will be described more fully in the next section, are listed in order of increasing dynamic complexity. One goal of this study is to isolate the influences of these five processes in four case studies.

II. LITERATURE REVIEW

This section briefly reviews five studies that evaluated the effect of a particular secondary mechanism in tropical cyclone motion. These physical processes are thought to be applicable during cyclone interaction periods.

1. The Beta Effect

The Beta effect is the simplest secondary factor influencing storm motion. In the Northern Hemisphere, each cyclone will have a tendency for the northwest displacement relative to the steering current.

Elsberry et al. (1987) describes tropical cyclone motion due to the Beta effect with the vorticity equation

$$\frac{\partial \zeta}{\partial t} = - \vec{V} \cdot \nabla \zeta - \beta v - (f + \zeta) \nabla \cdot \vec{V} \qquad (1)$$

where ζ is the vertical component of the relative vorticity, $\vec{V}$ is the horizontal wind vector , β is the meridional gradient of earth vorticity, v is the meridional component and f is the Coriolis parameter. Notice that the twisting term and friction are neglected here. Chan and Williams (1987) consider a symmetric vortex on a Beta plane with no mean flow in a barotropic and non-divergent model. With the assumption of non-divergence, the last term of (1) is zero. With the above assumptions, the streamfunctions and vorticity fields are initially concentric.

In the earlier model by Holland (1983), the effect of β was expressed as an asymmetric vorticity tendency field as in Fig. 2. These asymmetries are the result of the southward (northward) flow to the west (east) of the vortex center advecting higher (lower) earth vorticity values into the region. The cyclone will tend to propagate westward toward the positive tendencies if only this linear Beta effect is considered. However, Chan and Williams (1987) demonstrate that the cyclone center is displaced only a short distance by this linear effect. In Holland's theory, the vorticity tendencies create secondary cyclonic (anticyclonic) gyres to the west

(east) of the center in the Northern Hemisphere. This secondary flow through the center associated with these gyres would advect the cyclone toward the north (Fig. 2). Chan and Williams (1987) demonstrate that the linear beta effect distorts the vorticity pattern and creates a vorticity tendency by the crossing of the streamfunction and vorticity contours (Fig. 3).

The nonlinear vorticity advection effect, which will tend to make the streamlines and the vorticity contours concentric again, will lead to positive (negative) tendencies to the north (south) of the center. Therefore, the consequences of adding only this nonlinear vorticity advection effect is initially a poleward displacement. Chan and Williams show that the inclusion of the nonlinear term soon leads to a northwestward displacement (Fig. 4). Fiorino and Elsberry (1989) demonstrate that it is the outer wind strength of the cyclone that dominates the βv term in (1). If the magnitude of the outer winds in the cyclone are increased, the Beta effect becomes more westward vice northwestward. For the cyclone interaction problem, this more westward displacement of the larger cyclone could lead to an increasing separation from a smaller cyclone to the east.

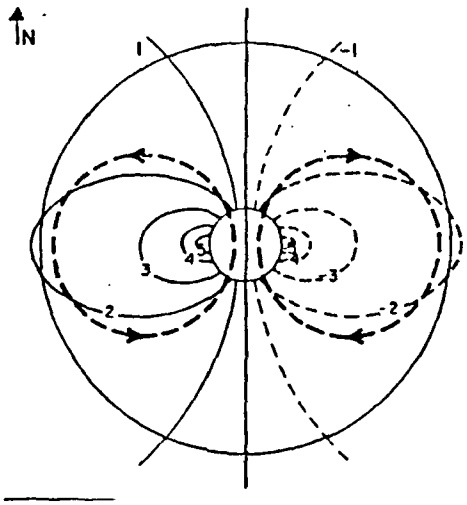

Figure 2. Linear Beta effect expressed as a field $\frac{\partial \zeta}{\partial t}$, in arbitrary units, centered on a symmetric, nondivergent cyclone on a Beta plane with no basic flow (Holland 1983). Heavy dashed lines show the induced secondary circulation resulting from the vorticity tendencies that would advect the cyclone center northward.

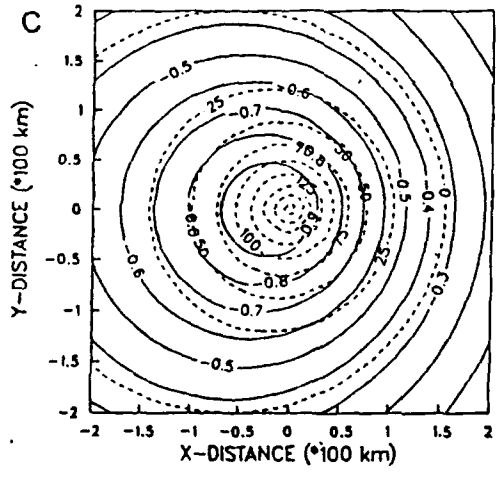

Figure 3. Nonlinear vorticity advection effect illustrated by vorticity (dashed, contour interval = 25 x 10^{-5} s^{-1}) and streamlines (solid, contour interval = 0.1 x 10^{6} $m^2 s^{-1}$) near the center for the linear model after 36 h (Chan and Williams 1987).

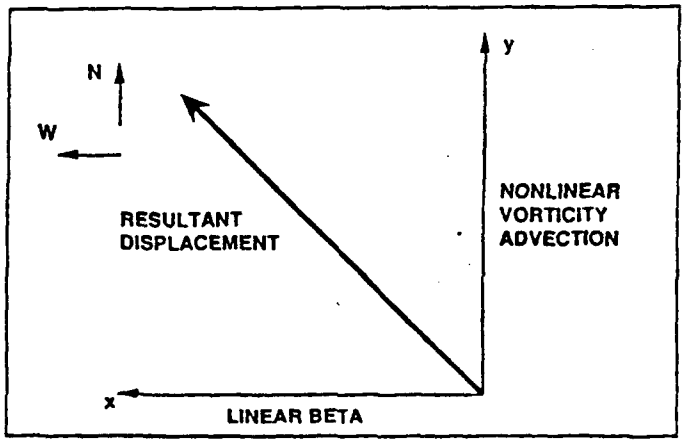

Figure 4. Resultant displacement due to Beta effect if both the linear and nonlinear effects have equal magnitudes.

2. The Fujiwhara Effect

Of the many types of cyclone-cyclone interactions that may occur, the best known is the "Fujiwhara" effect. Fujiwhara (1923, 1931) considered two symmetric, equal magnitude cyclones whose interacting circulations caused a binary rotation (counterclockwise in the Northern Hemisphere). The Annual Tropical Cyclone Report (1985 NAVOCEANCOMCEN/JTWC) describes the Fujiwhara effect as an interaction in which tropical cyclones within about 700 n mi (1296 km) begin to rotate about one another. In Fig. 5, the effect of cyclone A's outer circulation on cyclone B results in storm B moving in the direction of storm A's outer circulation and vice versa. When intense cyclones are within about 400 n mi (741 km), they may begin to move closer to each other. These interaction distances between cyclone centers are somewhat arbitrary and may depend on the size of the

systems. When two tropical cyclone centers come close enough to interact, the wind profile of one cyclone will become the "environment" of the other cyclone.

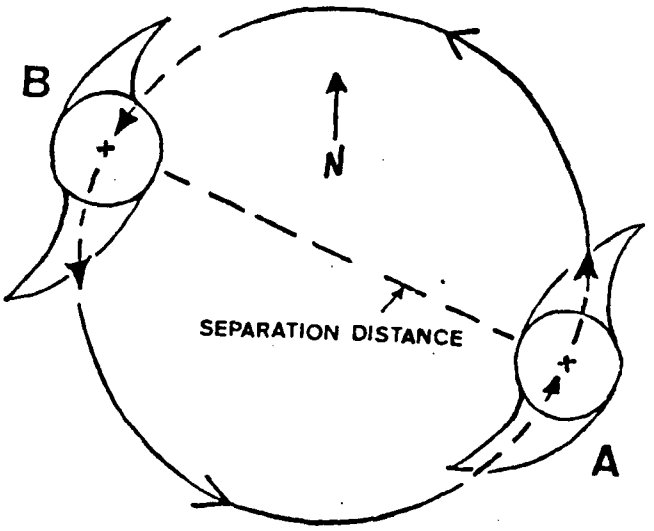

Figure 5. The Fujiwhara effect is the effect of the outer circulation of cyclone A on the movement of cyclone B and vice versa.

3. The Convergent Flow Effect

Chang (1983) used two types of numerical simulations to analyze the effects of convergent flow on the interacting circulations. For symmetric vortices of equal magnitude (Fig. 6), the convergence in the outer region of cyclone A would advect cyclone B towards cyclone A. Similarly, cyclone B's effect on cyclone A would result in a mutual attraction. Conversely, the divergent flows of two interacting anticyclones would lead to mutual repulsion.

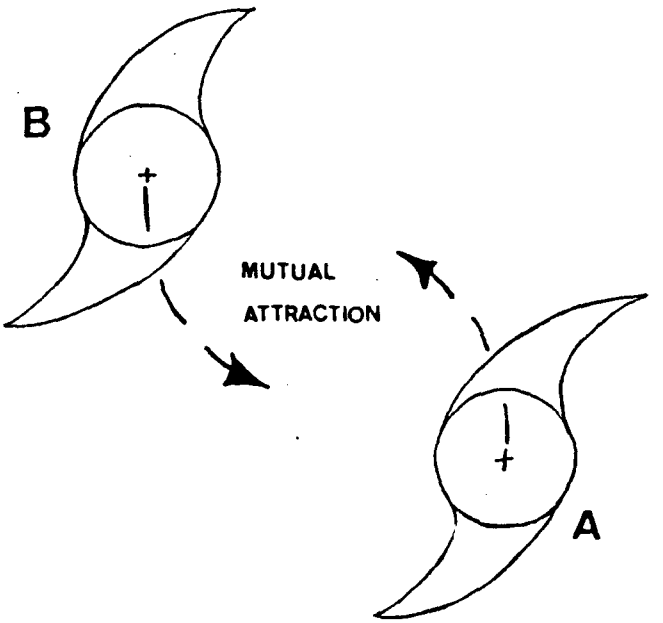

Figure 6. Convergent flow effect of Chang (1983) with the convergent circulation advecting the other cyclone toward the center and resulting in mutual attraction.

4. The Vorticity Advection Effect

DeMaria and Chan (1984) suggested that nondivergent cyclones also could attract or repel depending on the sign of the vorticity gradient between them. That is, the vorticity gradient associated with the other vortex is advected by the vortex circulation similarly to the advection of earth vorticity in the Beta effect. As in Fig. 2, a secondary circulation is induced by the gyres that will tend to move the center of the vortex either away to toward the other vortex. In Fig. 7, the outer wind profile of cyclone A is acting on the vorticity gradient of cyclone B. The outer circulation of cyclone A causes a pair of tyres associated with the positive (negative) vorticity tendencies on either side of storm B. With the vorticity gradients shown, vortices A and B will move outwards due to these secondary circulations. Thus, the

respective positive vorticity tendency areas result in repelling as well as the counterclockwise rotation that was also associated with the Fujiwhara effect.

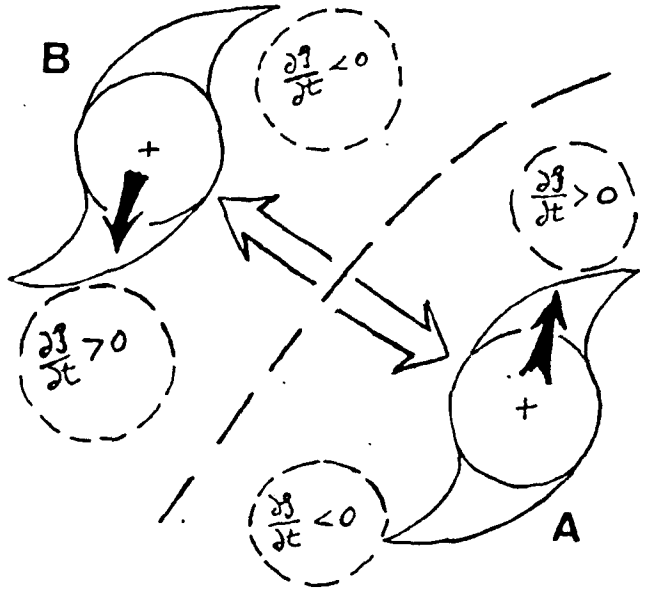

Figure 7. The vorticity advection effect of DeMaria and Chan (1984) created by the outer circulation of one cyclone acting on the vorticity gradient of the other cyclone. Secondary flows associated with the vorticity gyre tendencies develop and cause rotation plus mutual repulsion (solid arrows) for the vorticity gradients shown by the open arrows.

5. Environmental Shear Effect

Dong and Neumann (1983) added the vorticity gradient outside the interacting circulations due to the environmental shear. The environmental vorticity gradient between the larger-scale synoptic flow patterns has an effect similar to the Beta effect. In Fig. 8, the equatorial monsoonal westerlies and the tradewind easterlies would advect the two storms in the direction of the flow (indicated by the arrows), which may contribute to an apparent attraction (decreasing separation) or repulsion. The relative orientation of the two storms is very important. In Fig. 8, the tropical cyclones would separate with time or repel because cyclone A would

move eastward under the influence of the monsoonal westerly flow. Likewise, cyclone B is advected westward by the easterly trade winds. If the storm orientation is northeast-to-southwest vice northwest-to-southeast, this environmental shear would result in attraction. When the storms are oriented east-west within a nearly zonal ITCZ, the environmental shear effect will be small.

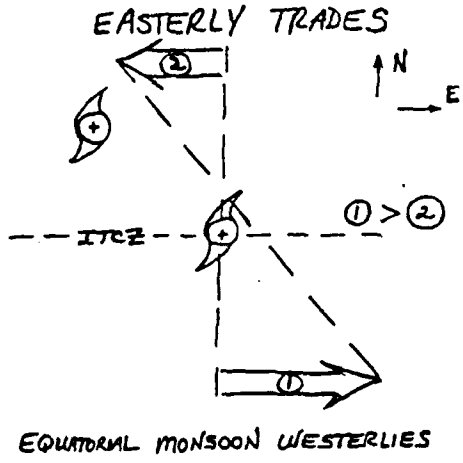

Figure 8. The environmental shear effect of Dong and Neumann (1983) that develop from the larger-scale flows (shown by the arrows) causing a separation (apparent repelling) of cyclones A and B.

III. DATA BASE DEVELOPMENT

A. FIELD DEFINITION

The Global Band Analysis (GBA) are operationally generated by the United States Navy Fleet Numerical Oceanography Center (FNOC). These GBA fields are produced on a Mercator grid from 40.956°S to 59.754°N. The longitudinal coverage is completely around the globe. The 49 x 144 Mercator grid is true along 22.5°N or S latitudes, and the gridpoint spacing is 2.5 degree latitude along this latitude. However, the longitudinal distances between the grid points decrease towards the northern boundary of the GBA grid due to the meridians converging in the higher latitudes. The U. S. Naval Weather Service (1975) provides a detailed description of the GBA.

The geographically oriented grid (Fig. 9) with 17 gridpoints north-to-south and 31 west-to-east that is employed here is the same as in Wilson (1984). The zonal and meridional separation is 255.8 km (150 n mi). The relocatable grid is always storm-centered with the cyclone located at gridpoint (16,7). This point is displaced a little south of the center gird to ensure the data available to the north of the cyclone has sufficient latitudinal extent to describe the future storm track. Only storms with positions south of 34.6°N can be selected if GBA data are to be available for the entire grid in Fig. 9.

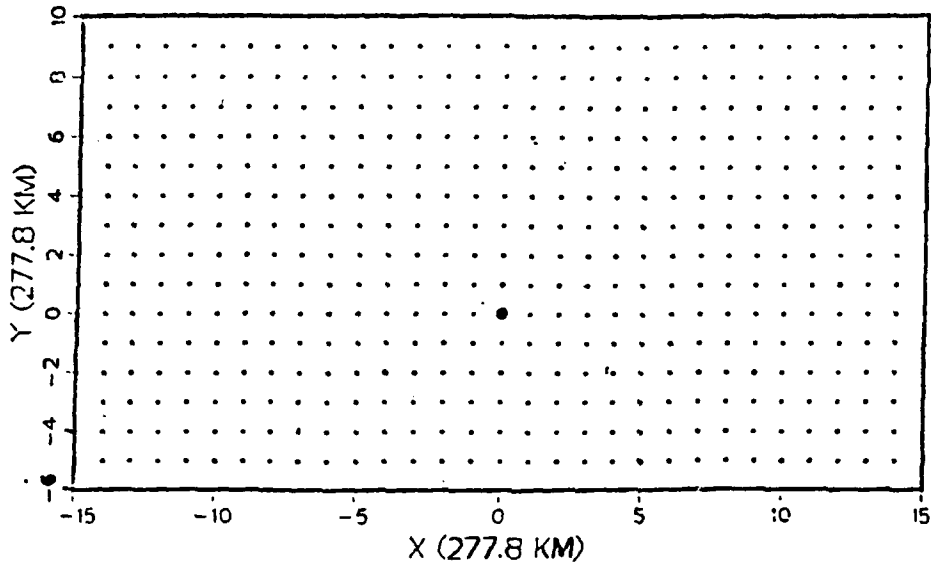

Figure 9. Relocatable 527-point grid with a constant zonal and meridional separation of 277.8 km. The vortex center is located at gridpoint (16,7) from the lower left corner, and is indicated by the large dot (Wilson, 1984).

B. DATA RETRIEVAL

The GBA wind fields at 00 and 12 UTC are composed of meridional (v) and zonal (u) wind components at the 700, 400 and 250 mb levels. The first set of wind fields is that generated by Wilson (1984). This data set comprised 682 cases in a dependent set and 675 in an independent set during 1979-1983. The 682 cases are used to compute the Empirical Orthogonal Function (EOF) coefficients, as described below. A second independent data set included 242 cases during 1984-1985 (216 cases in 1984 and 26 cases in 1985). The wind fields for the 1984-1985 storm cases were generated by Peak (1985) using similar procedures to Wilson (1984). All of these cases meet the following conditions:

(i) a tropical cyclone attaining at least tropical storm strength (maximum sustained winds of 18 m/sec (35 kts) or greater) west of the dateline and east of 100°E;

(ii) a best track position less than 34.6°N (discussed in the previous section); and

(iii) the meridional and zonal wind components of the GBA were available at 700, 400 and 250 mb.

The accuracy of these GBA fields depends on the amount of available data, primarily from rawinsondes and pilot reports. In the tropical western North Pacific region where land masses are scarce, few rawinsondes are available except across the Philippines, and pilot reports are most prevalent at the 250 mb level vice 700 or 400 mb. Therefore, paucity of data is a common problem.

C. RELATIVE VORTICITY FIELDS

The Wilson (1984) program extracts the zonal (u) and meridional (v) winds necessary to compute relative vorticity

$$\frac{\partial v}{\partial x} - \frac{\partial u}{\partial y} \qquad (1)$$

The vorticity at the interior gridpoints in the domain is calculated using centered finite differencing. One-sided differences involving the boundary point and the adjacent interior point are used to estimate the gradients in the four corners and normal to the boundaries of the domain, so that vorticity values are calculated at all 527 gridpoints. A typical relative vorticity pattern with superposed winds from Wilson (1984) is shown in Fig. 10. The primary vorticity centers are associated with Supertyphoon Abby, Tropical Storm Ben (northeast of Abby along 145° E), a subtropical ridge just east of Japan along 40° N and a midlatitude trough east of the Kamchatka Peninsula. The vorticity contours clearly show the amplitude of Abby. The circulation of Abby, which is at least 10° lat. in diameter, is embedded in the monsoon trough that extends southwestward through the Luzon Strait. Ben's circulation is less well-defined and is located at the eastern end of the monsoon trough. The subtropical ridge extends westward into the Sea of Japan.

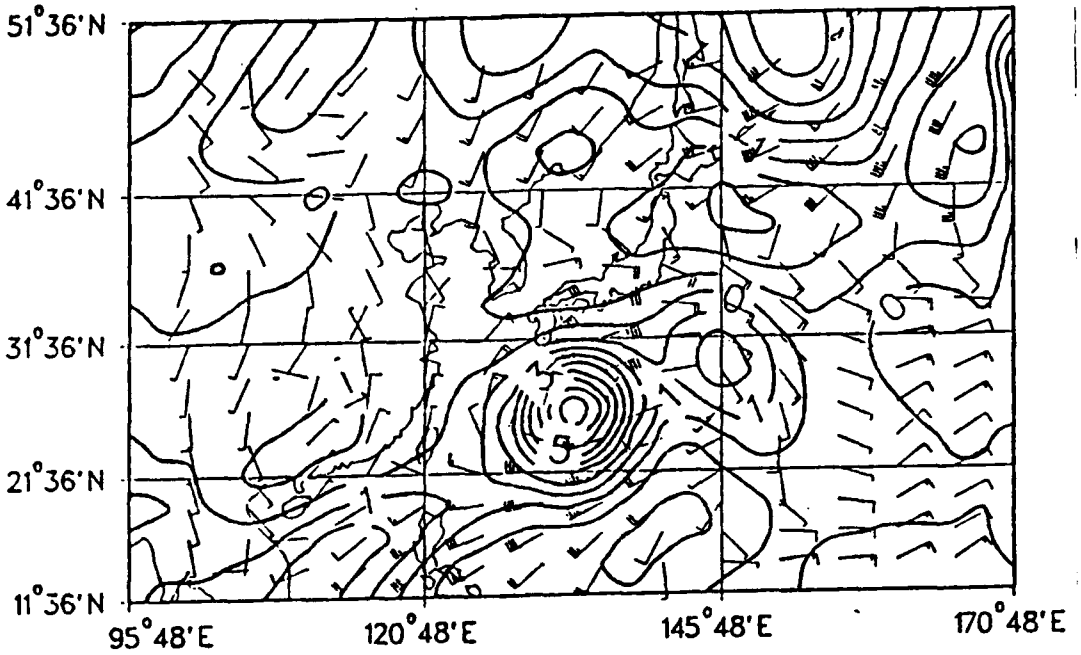

Figure 10. Relative vorticity at 700 mb for 00 UTC 14 August 1983 with superposed wind field.

IV. EMPIRICAL ORTHOGONAL FUNCTIONS

A. BACKGROUND

In Empirical Orthogonal Function (EOF) analysis, mathematical functions are globally adjusted to fit the observed fields on a regular grid such as Fig. 9. These functions are orthogonal, just as in the spectral analysis that uses orthogonal sines and cosines. In EOF analysis, the structure of the geophysical data determines the spatial dependence of the functions. Consequently, the functions are "empirical" because they depend on the particular set of geophysical data used for their derivation.

Lorenz (1956) was the first to apply the EOF method to atmospheric sciences. The eigenvectors derived in the EOF analysis describe the horizontal structure of the atmospheric fields. For example, these EOF's are summed in a similar manner to trigonometric functions in a Fourier series

$$\sum_{i=1}^{527} A_i \zeta_i = A_1\zeta_1 + A_2\zeta_2 + \ldots + A_{45}\zeta_{45} + [A_{46}\zeta_{46} + \ldots + A_{527}\zeta_{527}] \qquad (3)$$

where ζ is the associated eigenfunction or eigenvector (spatial function) and A is the eigenvalue or coefficient (amplitude of the eigenfunction). In this manner, the orthonormal functions can be represented through orthonormal expansion.

B. THE EOF METHOD

The EOF method applied in this study parallels the procedures outline by Wilson (1984), Schott (1985) and Meanor (1987), except that it is applied to relative vorticity rather than the wind components or the vertical wind shear. This EOF method is an expansion of the method used by Kutzbach (1967) and Shaffer (1982). The EOF analysis is on the 527 gridpoint domain in Fig. 9 and is based on 682 cases during 1979-1983.

This method starts with a matrix A of m x n vorticity values, where m is the gridpoint number (1 to 527) and n is the storm case number (1 to 682). Matrices are created for the vorticity field at three pressure levels (700, 400 and 250 mb). Because variability of vortices is generally much larger in the midlatitudes than in the tropics, normalization is necessary to give equal weight to the tropical vortices in the EOF analysis. Matrix A is normalized by subtracting the mean vorticity of the 682 cases at each gridpoint and dividing by the standard deviation at that gridpoint. Figs. 11-16 illustrate the means and standard deviations for all 682 cases at 700, 400 and 250 mb. The mean vorticity fields are nearly vertically stacked near the tropical cyclone (black dot), with large positive vorticity values around the cyclone at 700 mb (Fig. 11) that decrease with height (Fig. 13 and Fig. 15). However, the negative vorticity associated with the subtropical ridge increases with height. The 700 mb vorticity field has the largest difference between the maximum vorticity value and the minimum, and the gradient gradually decreases with height. On the other hand, the standard deviations displayed in Figs. 12, 14 and 16 increase with height and exhibit maxima along the northern boundary, which is due to the greater variability in the midlatitude circulations.

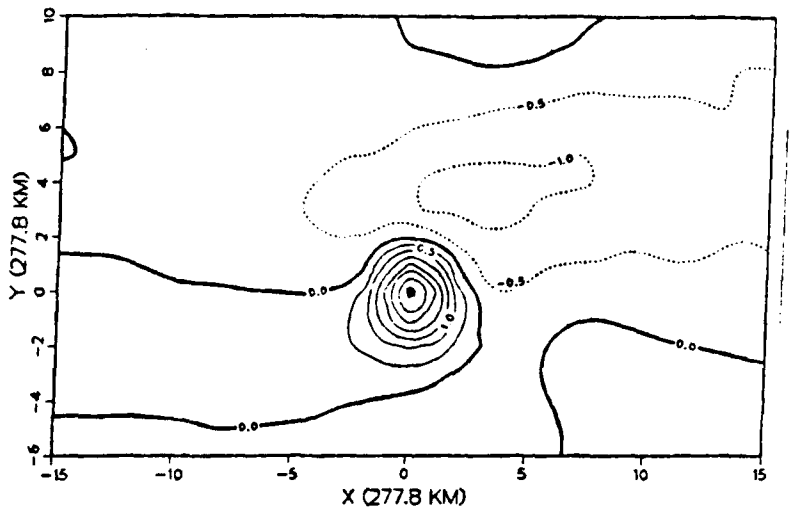

Figure 11. Average vorticity at 700 mb for all 682 cases. The contour inverval is 0.5 x 10^{-5} s^{-1}. Positive (negative) values are solid (dashed). The black dot indicates the storm center position.

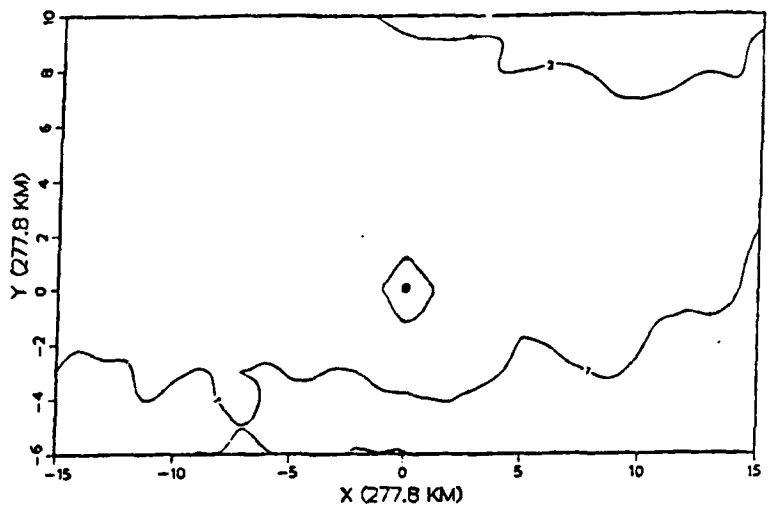

Figure 12. Standard deviation of vorticity at 700 mb for all 682 cases. The contour interval of vorticity is 10^{-5} s^{-1}. The black dot at (0,0) indicates the storm center position.

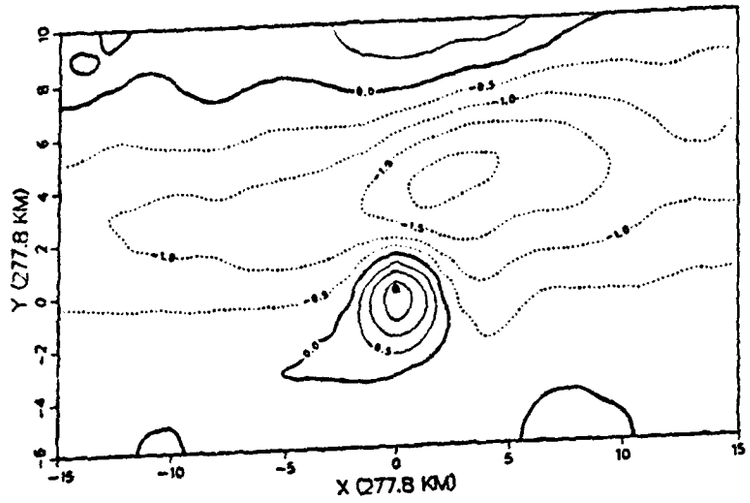

Figure 13. Average vorticity at 400 mb as in Fig. 11.

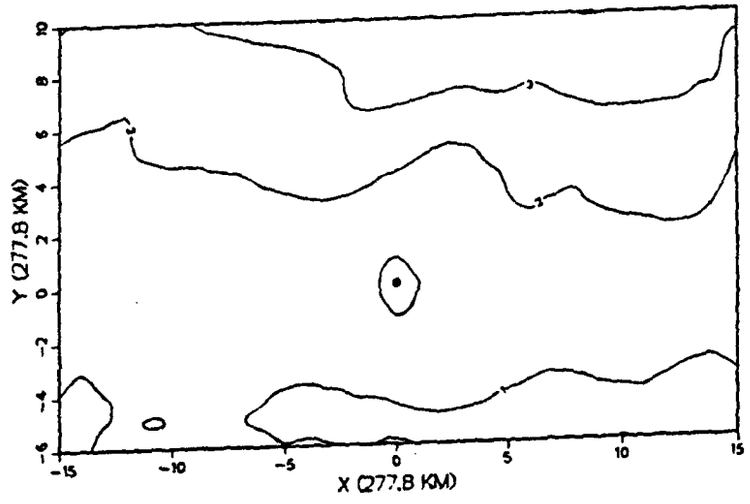

Figure 14. Standard deviation of vorticity at 400 mb as in Fig. 12

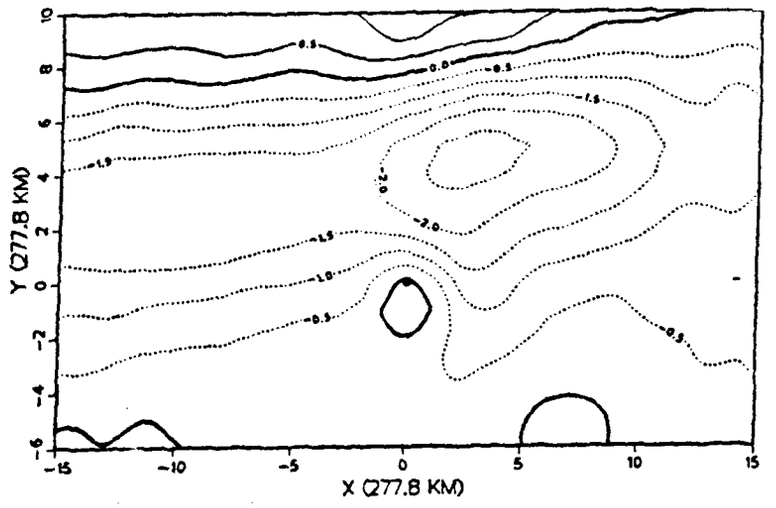

Figure 15. Average vorticity at 250 mb as in Fig. 11.

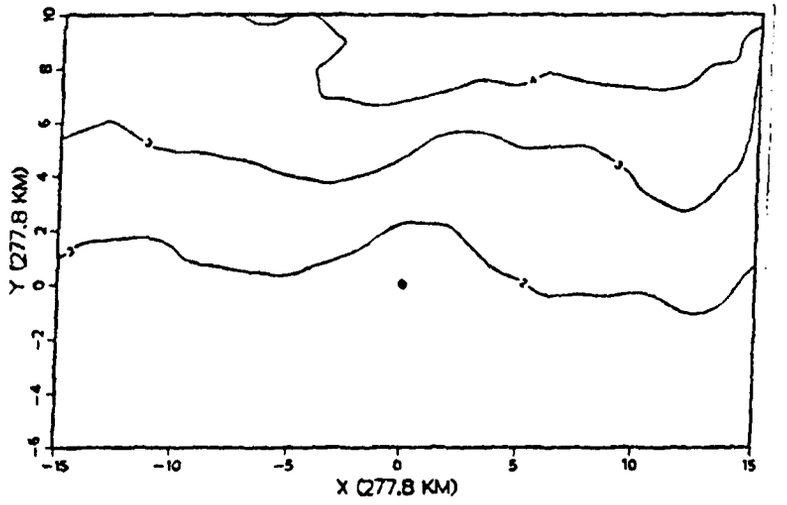

Figure 16. Standard deviation of vorticity at 250 mb as in Fig. 12. Black dot at (0,0) indicates the storm center position.

The elements of the normalized matrix (Z) are defined as

$$z\,(i,j) = \frac{[a(i,j) - b(i)]}{s(i)}\,, \qquad (4)$$

where $z(i,j)$ and $a(i,j)$ are the corresponding elements of matrix Z and A respectively, and $b(i)$ and $s(i)$ are the mean and standard deviation of the vorticity component for all the cases at a particular gridpoint in row "i" elements of matrix A. The Z matrix elements are dimensionless variates with zero mean and a standard deviation of one. A disadvantage to normalizing a matrix is that some slight smoothing occurs in the eigenvector representation (Kutzbach 1967).

Correlation matrix R is

$$R = \frac{ZZ'}{n} \quad , \tag{5}$$

where Z' is the transpose matrix of the normalized matrix and n is the number of cases (682). A maximum constraint method is used to determine a vector **e** in m (527) dimensions that best represents the n (682) observation vectors, and thus describes the most basic geophysical features that are common in the cases. After normalizing vector **e** to unit length 1, where

$$\mathbf{e'e} = 1 \ , \tag{6}$$

the correlation between this vector **e** and the matrix R is defined by

$$k = \mathbf{e'}R\mathbf{e} \ , \tag{7}$$

where k is a scalar correlation between the normalized matrix Z and the vector **e**. Morrison (1967) demonstrated the scalar quantity k can be rewritten in matrix form as

$$EK = ER \ , \tag{8}$$

where the elements of K are the coefficients (eigenvalues) and E is a 527 x 527 eigenvector (EOF) matrix. These EOF's represent components of the field in function space rather than in gridpoint space. Each column of matrix E is an

eigenvector **e** of m dimensions that is associated with one coefficient k_i. These coefficients are derived from the correlation matrix R by

$$| R - KI | = 0 , \qquad (9)$$

where I is the identity matrix and 0 is the null vector. Each of the k_i account for a specific amount of the total field variance.

The eigenvectors are ranked in decreasing order of percentage of explained variance. For example, the first eigenvector ς_1 in (3), which describes 10% of the variance in the field (Fig. 17), depicts only the most broad-scale features of all the cases. These features include a tropical cyclone (black dot) embedded in the equatorial monsoon trough (represented by the positive values) and the subtropical ridge to the north (negative values).

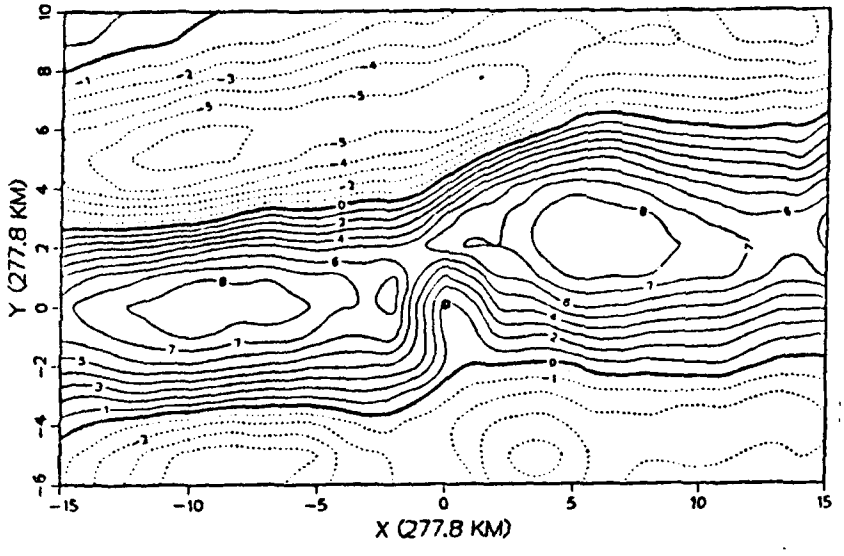

Figure 17. Mode 1 eigenvector at 400 mb explains 10% of the variance. The large black dot represents the cyclone as in Fig. 9, and the eigenvector elements are scaled by multiplying by 10^2. Positive (negative) values are for cyclonic (anticyclonic) vorticity.

The second eigenvector ς_2 (Fig. 18), which explains the next largest amount of variance (8%), is orthogonal to mode 1. That is, each mode evaluates the geophysical field from an orientation that is 90 degrees to the other modes. Notice that the zero contour in mode 1 runs through the maximum positive values of mode 2.

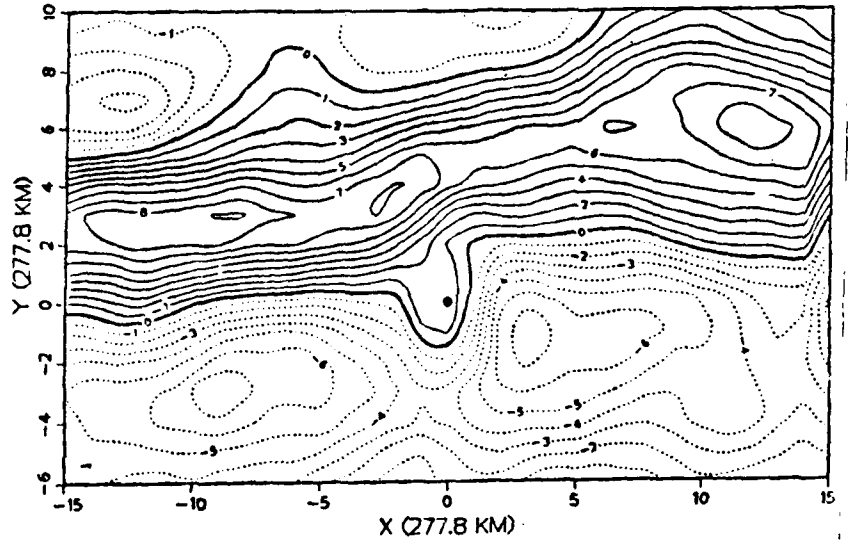

Figure 18. Mode 2 eigenvector at 400 mb explains 8% of the variance.

This methodology continues for all 527 modes so that these fields are 100% explained from 527 different orientations. Eigenvector patterns 3 through 6 are shown in Figs. 19-22. Each of these eigenvectors represents the pattern of positive/ negative vortices as shown or have the opposite sense if the sign of the eigenvector is negative. These figures show changing spatial patterns that become more complex with increasing mode number. There tends to be more contoured centers as the mode number increases. In eigenvector 3 (Fig. 19), the features are tilted rather than being primarily zonal as in the first two modes. Eigenvector 4 (Fig. 20)

may be associated with a pattern of strong cyclonic (positive) vorticity around the tropical cyclone, cyclonic vorticity in the monsoon trough westward from the tropical cyclone and a strong ridge to the north. With such a geophysical interpretation of this eigenvector, the tropical cyclone would be expected to translate westward.

Eigenvectors were also derived for the 700 mb and 250 mb levels. These eigenvectors (not shown) are similar except the gradients increase with height, so that 250 mb has the largest gradients in the eigenvectors.

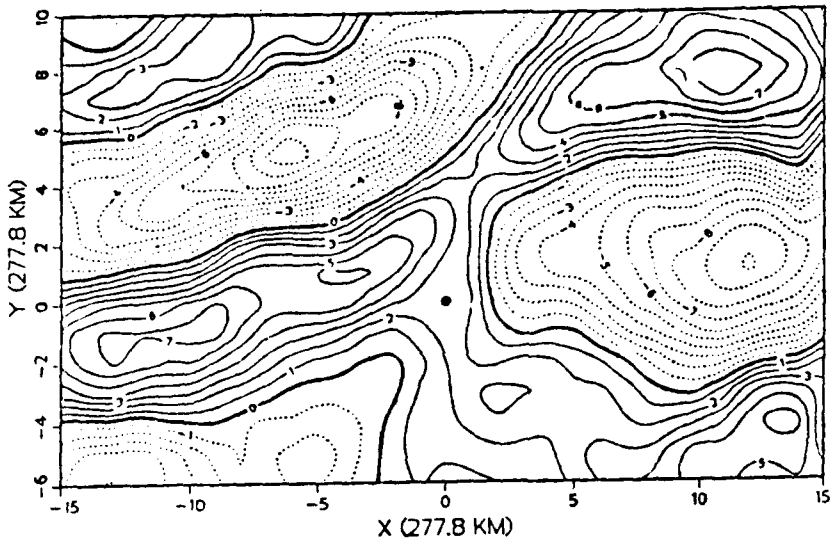

Figure 19. Mode 3 eigenvector at 400 mb explains 4% of the variance.

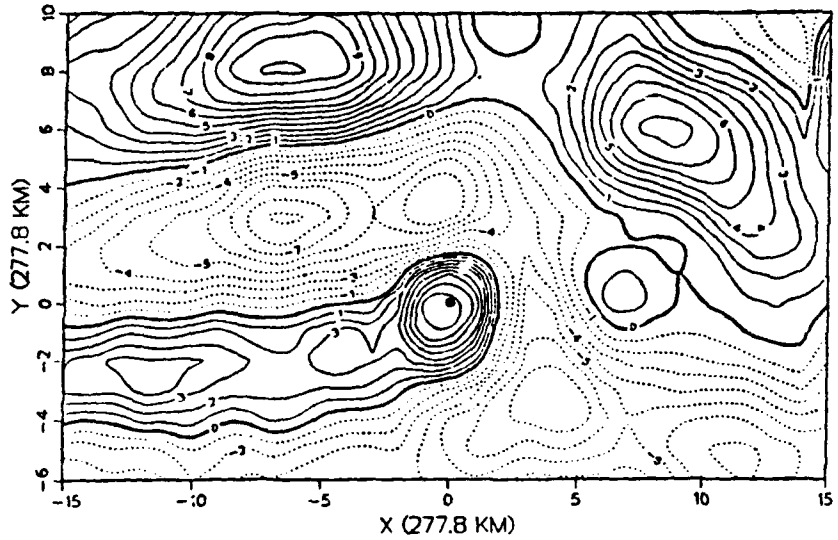

Figure 20. Mode 4 eigenvector at 400 mb explains 3.5% of the variance.

Eigenvector 5 (Fig. 21) is an example of a pattern that is likely to appear with a negative eigenvalue when the tropical cyclone is well developed so that positive vorticity occurs at the (0,0) coordinate. With a negative eigenvalue, the positive values to the northeast of the tropical cyclone would represent a strong subtropical ridge. Eigenvector 6 (Fig. 22) is another example of non-zonal orientation.

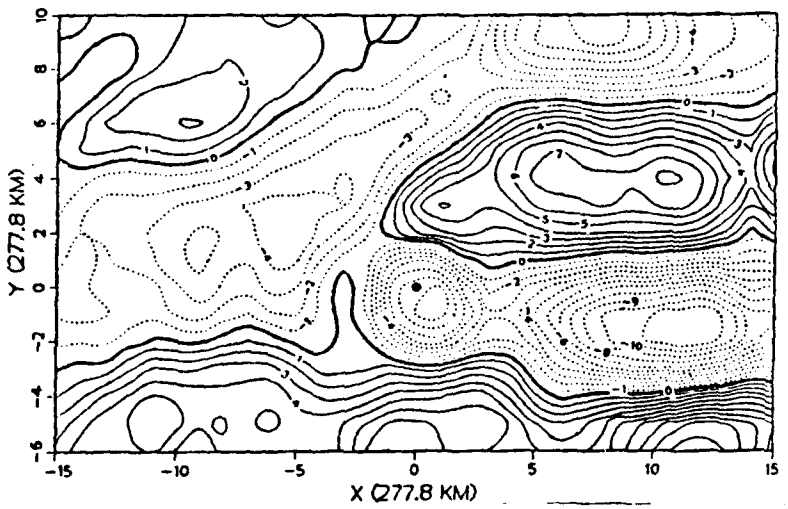

Figure 21. Mode 5 eigenvector at 400 mb explains 3.2% of the variance.

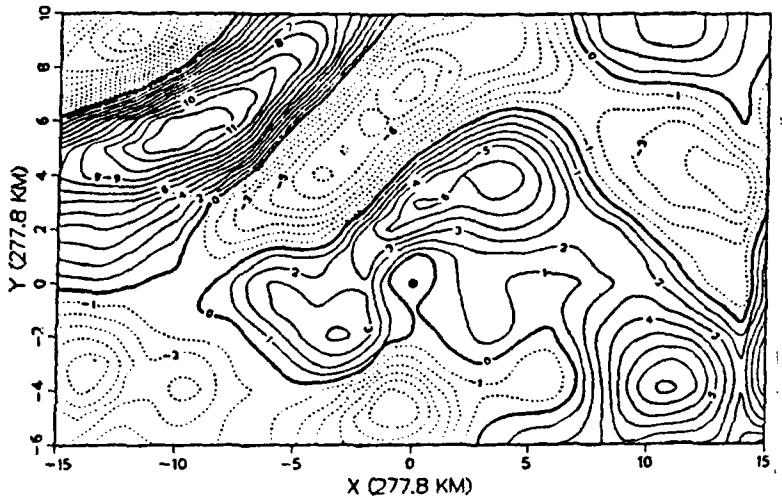

Figure 22. Mode 6 eigenvector at 400 mb explains 2.8% of the variance.

The normalized data matrix Z represents vorticity fields in this study, which may be reconstructed for any case by solving for the EOF coefficients

$$C = E'Z \tag{10}$$

where C is the m(row) by n(column) coefficient matrix (527 x 682) for the dependent sample used in this study and E' is the transpose of the E matrix. From this dependent data set, any other case can be reconstructed by

$$Z = CE \quad . \tag{11}$$

For a particular case (607) in matrix Z, the spatial decomposition of the data is represented by matrix E and the temporal variation by the C matrix. For example, the case (Fig. 23) stored in the 607th (j^{th}) column of the normalized vorticity matrix (Z) can be described in a linear combination of orthogonal coefficients and eigenvectors

$$Z(i,j) = \sum_{i=1}^{m} c(i,j) \times e(i) \qquad \text{for } j = 1, \ldots, n. \tag{12}$$

where $Z(j)$ represents the 607th column vector (j) of matrix Z, and m is the number of eigenvectors $e(i)$ or modes retained. If all 527 modes are retained, 100% of the variance in the original field will be included. However, an unknown amount of noise is included due to the irregular observation grid or computational effects that may distort the vorticity or introduce small-scale features. The pattern in Fig. 23 is much more complex than those represented in modes 1 or 2. Positive relative vorticity values surround Supertyphoon Abby (black dot) with negative values depicting a weak subtropical ridge to the north of Abby. A strong midlatitude trough (large positive values) is evident well to the northeast of Abby.

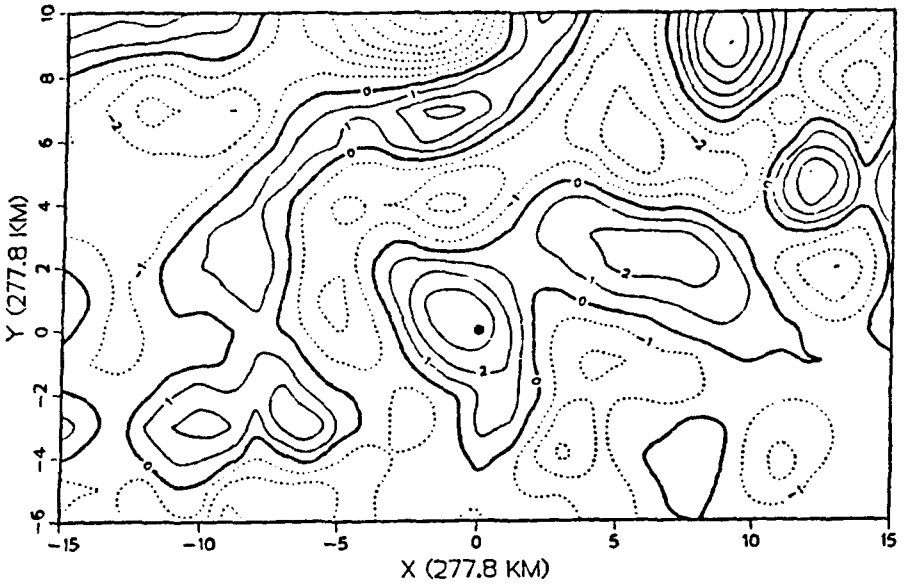

Figure 23. Reconstructed 400 mb vorticity field (10^{-5} s^{-1}) in Supertyphoon Abby on 00 UTC 11 Aug 1983 in which all 527 modes are retained. The typhoon is at the large black dot, and negative (positive) vorticities are dashed (solid).

The key advantage of the EOF approach is the capability to retain only the eigenvectors (a minimum number) that are needed to represent the signal in the field and eliminate unnecessary noise by eliminating higher order modes. Wilson (1984) and Shaffer (1982) used a Monte Carlo technique of Preisendorfer and Barnett (1977) to distinguish between vectors with signal vice those with noise. This technique is better suited for geophysical studies where the sample sizes are not generally large enough to support the approach of Morrison (1967), which requires a large sample of normal data. In the Preisendorfer and Barnett technique, 100 normalized matrices Z are generated from a random number generator. Monte Carlo eigenvalues are calculated for each matrix Z (527 x 682). Mean and standard deviations computed for these random Monte Carlo eigenvalues are represented in Fig. 24 (Wilson's Fig. 7) and compared to the physical data. Table 1 (Wilson's Table 5) shows the results of these comparisons of the mean eigenvalues having 95% confidence level. These mean eigenvalues represent the physical eigenvalues that deviated by more than two standard deviations from the randomly generated

eigenvalues for a particular mode. Because this physical eigenvalue deviates significantly from a random field, it provides reasonable assurance that the associated eigenvector is describing signal rather than noise. In this study, the first 45 modes are used to reconstruct the relative vorticity fields. Retaining 45 modes explained between 59.8 and 76.9 percent of the vorticities at the three pressure levels (Table 3). Wilson (1984) retained only 35 modes to explain 81.7 and 93.2 percent of the u and v fields at the three levels (his Table 7). Because vorticity is the derivative of the wind, the vorticity field inherently contains more noise. Therefore, it is not surprising that more modes would be needed to explain the same variance as in the u and v fields.

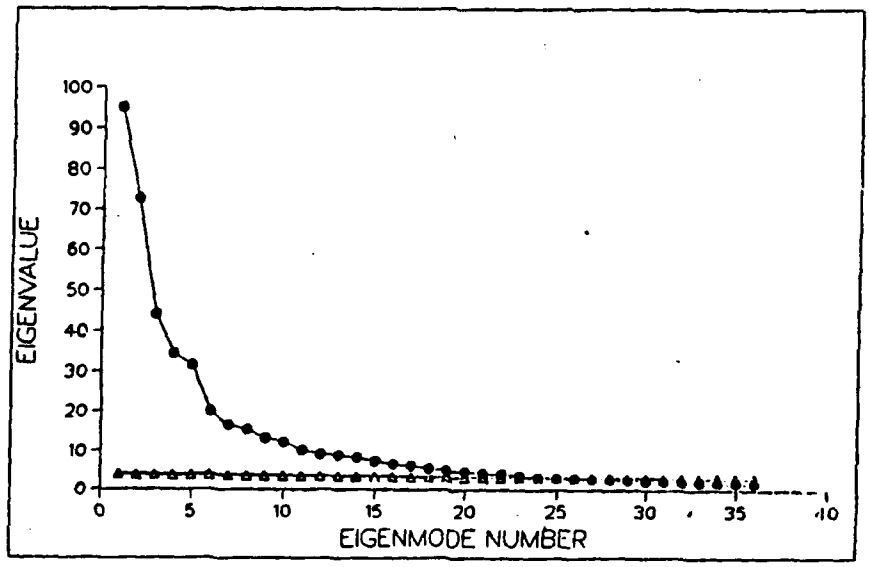

Figure 24. Example of mode selection for eigenvalues of 700 mb zonal modes (circles) and Monte Carlo mean eigenvalues plus two standard deviations (triangles) from Wilson (1984).

The reconstructed vorticity field for Supertyphoon Abby from only 45 modes is shown in Fig. 25 for comparison with the field with 527 modes in Fig. 23. This number of modes represents 75% of the variance with 95% confidence. The basic orientations and relative magnitudes of the main features are retained in the 45-mode representation. the small vorticity centers (especially south and east of Abby) in Fig. 23 that probably are noise-related are not retained in Fig. 25. Any number of orthonormal functions can be chosen to reconstruct the amount of desired variance of the actual field. In (3), only the 45 eigenfunctions (eigenmodes) were used vice the 527 modes to represent the desired amount of the field features. This is what makes the EOF representation an efficient method because the computer running-time and storage capability required to reproduce the fields are greatly reduced.

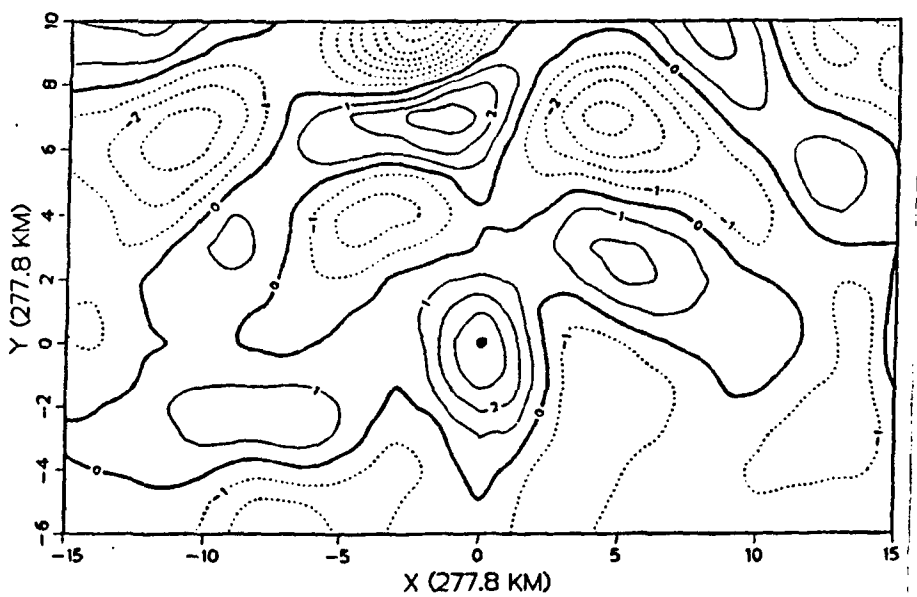

Figure 25. Reconstructed vorticity fields at 400 mb with 45 modes for Supertyphoon Abby (represented by the large black dot) on 00 UTC 11 August 1983. Negative (positive) vorticity contours are dashed (solid).

Table 1. MEAN EIGENVALUES AT 95 PERCENT CONFIDENCE LEVEL computed by the Monte Carlo Technique

MODE	MEAN EIGENVALUE	MEAN EIGENVALUE + 2 σ
1	3.428	8.116
2	3.318	3.989
3	3.299	3.966
4	3.261	3.919
5	3.228	3.880
6	3.211	3.859
7	3.192	3.837
8	3.134	3.773
9	3.110	3.738
10	3.101	3.728
11	3.086	3.710
12	3.048	3.664
13	3.031	3.643
14	2.986	3.589
15	2.970	3.570
16	2.963	3.561
17	2.930	3.522
18	2.917	3.507
19	2.900	3.486
20	2.872	3.452
21	2.850	3.425
22	2.816	3.385
23	2.808	3.375
24	2.797	3.362
25	2.774	3.334
26	2.766	3.325
27	2.743	3.297
28	2.723	3.273
29	2.697	3.242
30	2.681	3.222
31	2.663	3.200
32	2.643	3.177
33	2.636	3.168
34	2.627	3.158
35	2.619	3.149
36	2.591	3.114
•		
100	1.817	2.184
•		
300	0.569	0.684
•		
400	0.238	0.286
•		
527	0.016	0.019

Table 2. PERCENTAGE OF EXPLAINED VARIANCE WITH 45 MODES retained for the relative vortiticy fields.

Level (mb)	Variance
700	72.8
400	76.9
250	59.8

V. RESULTS

A. COMPARISON OF EOF FILTERED AND RAW VORTICITY FIELDS

One of the goals of this study is to use the EOF vorticity fields for cases of tropical cyclone interactions. Sherman (1988) proposed using relative vorticity features as in Fig. 26 to anticipate the future track changes. The corresponding EOF representation for this date is shown in Fig. 27. Notice the EOF field has filtered out much of the noise in the original field, which provides a smoother depiction, and results in a better definition of the field. Certain characteristic features in Fig. 26 (ridge pinch and closed centers) are still well depicted in Fig. 27. Some of the suspicious noise-related features in Fig. 26 (primary and secondary nodes) are smoothed, which provides a more reasonable vorticity representation of the weakness in the subtropical ridge between the positive vorticity contours of the tropical cyclone and the midlatitude trough located east of Japan.

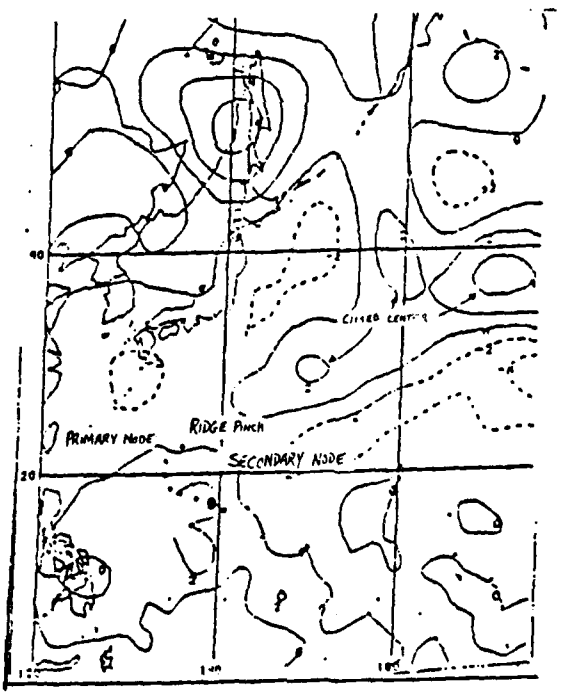

Figure 26. Original vorticity field at 700 mb (10^{-5} s^{-1}) of 00 UTC 03 November 1983 from Sherman (1988).

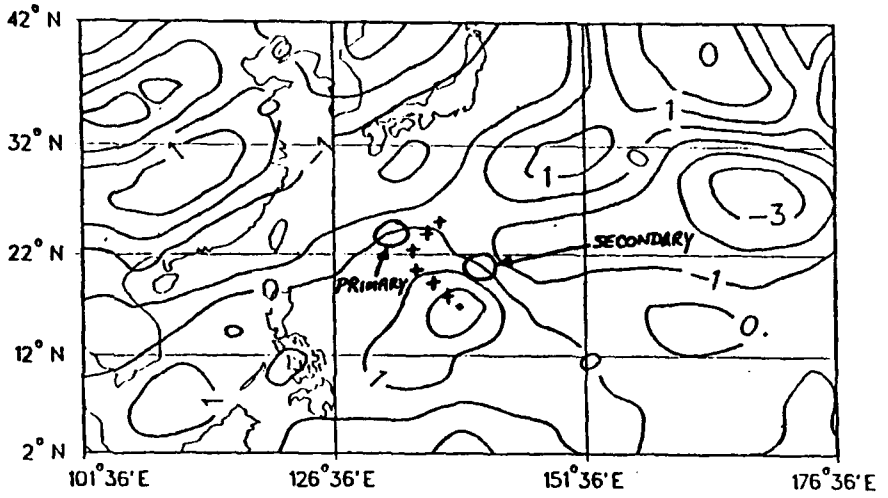

Figure 27. Filtered EOF vorticity field at 700 mb (10^{-5} s^{-1}) for 00 UTC 03 November 1983 reconstructed from 45 EOF modes.

B. SELECTION OF CASE STUDIES

The Annual Tropical Cyclone reports (ATCR) published by the Joint Typhoon Warning Center (JTWC) from 1979-1985 were used to select four case studies:

(1) Supertyphoon (STY) Abby and Tropical Storm (TS) Ben;

(2) Typhoon (TY) Pat and Odessa and TS Ruby;

(3) TY Dinah and TY Ed; and

(4) TY Mac and TS Nancy

These cases were chosen to address tropical cyclone-cyclone interactions, which is the scenario that Sandgathe (1987) listed as least understood by forecasters. However, the analysis of such studies revealed other types of tropical cyclone interactions occurred at different levels. In this research, an interaction is defined as the mutual adjustment of one wind field circulation (tropical cyclone or otherwise) with another circulation feature that can cause a reciprocal action in the tracks. The wind and vorticity analyses represent slices (along a pressure surface)

through the vertical column of the atmosphere where these interactions can take place at one or all three of the analyzed levels. The stronger the circulation, the deeper will be the vertical structure over which the influence will be extended. For example, the more intense a cold-core, upper-level low, the greater the vertical extension downward (towards the surface). The reverse is true for a tropical cyclone.

In Case 1, STY Abby interacts with TS Ben at 700 mb during one period and with an extratropical (ET) cyclone at 400 mb in a later period. Both Ben and the ET cyclone exhibited counterclockwise rotation about Abby. This case study provides some explanation of why Abby's track disagreed with the primary forecast aid models and led to greater than normal forecast errors (Chan 1986).

In Case 2, a multiple storm interaction involving TY Pat, Odessa and TS Ruby is investigated. This case includes a classic binary interaction (Fujiwhara) between Pat and Odessa about a singular point as shown in Fig. 28 (ATCR 1985).

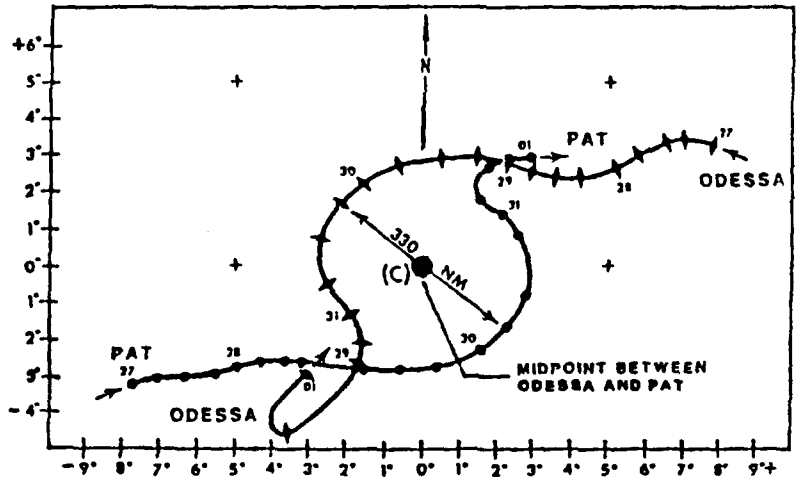

Figure 28. Binary interaction of Pat and Odessa about a singular point at (C) with inward spiral with time (ATCR 1985). Relative motion of these two typhoons is illustrated around their common midpoint.

A less dramatic binary interaction between TY Ed and TY Dinah is evaluated in Case 3. These tropical cyclones appear to bounce off each other or the ridge between them. The post-analysis (ATCR 1984) does not provide the meteorological reasoning for this event. In addition, Dinah later interacts with an anticyclone.

Case 4 is an example of how this diagnostic forecasting tool (EOF vorticity fields) evaluates weak cyclone-cyclone interactions. The topography of the Philippine Islands also contributed to this complex situation.

C. CASE 1 - SUPERTYPHOON ABBY (STAGE 1)

1. Synoptic Discussion

Chan (1986) divided the track of Abby into three segments in Fig. 29 (ATCR 1983).

(i) Between 00 UTC 5 August (denoted 0500) to 0900 when Abby rapidly intensified to maximum intensity of 75 m/s (145 kt) while moving northwestward;

(ii) Between 0906 and 1200 when Abby slowed to forward speeds of less than 2.5 m/s with an almost due north movement, and the intensity and size remained relatively constant; and

(iii) Between 1206 and 1712 when Abby steadily weakened and moved northeastward.

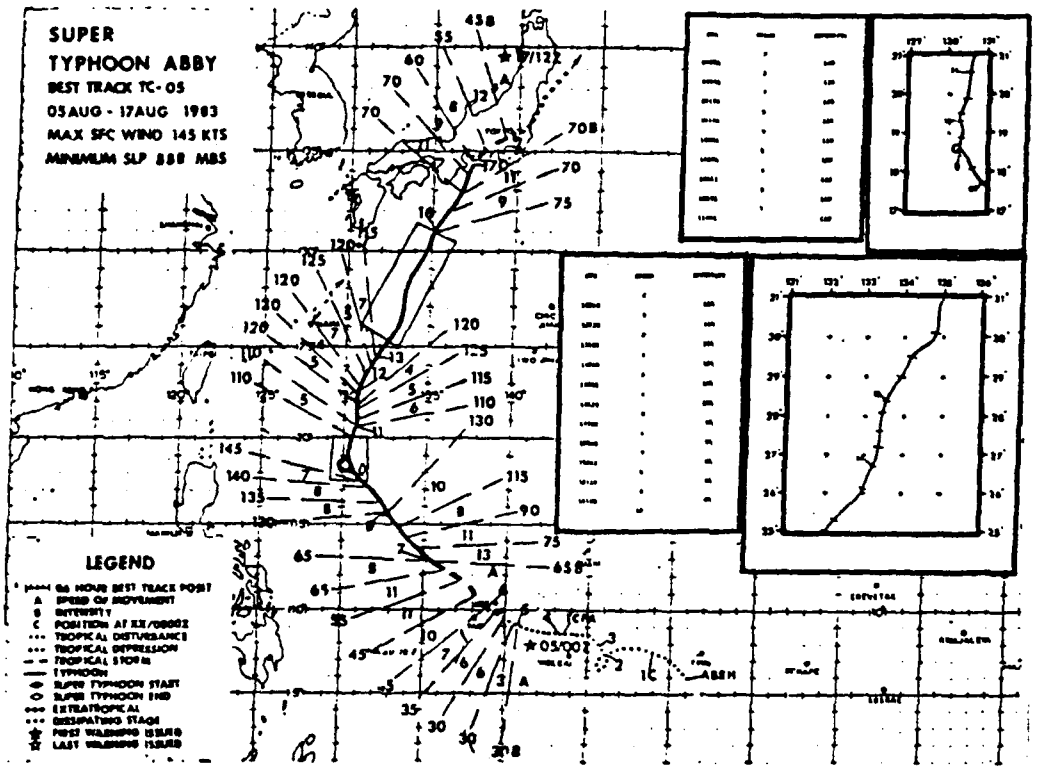

Figure 29. Best track of Supertyphoon (STY) Abby during August 1983. The intensity and movement of the storm are given in knots.

This case study focuses only on the last segment from 1200 to 1600. Chan (1986) shows the track of Abby was consistently to the right of the forecast models and the JTWC forecasts. This case is separated into two stages to illustrate interactions that Abby had with two synoptic features that may partially explain the poor performance of the forecast models. The tracks of Abby, Ben and the extratropical (ET) cyclone during stages 1 and 2 are shown in Fig. 30. Although Abby was interacting with both features between 1400 and 1500, the interaction with the ET cyclone dominated since Ben already had become absorbed in Abby's circulation.

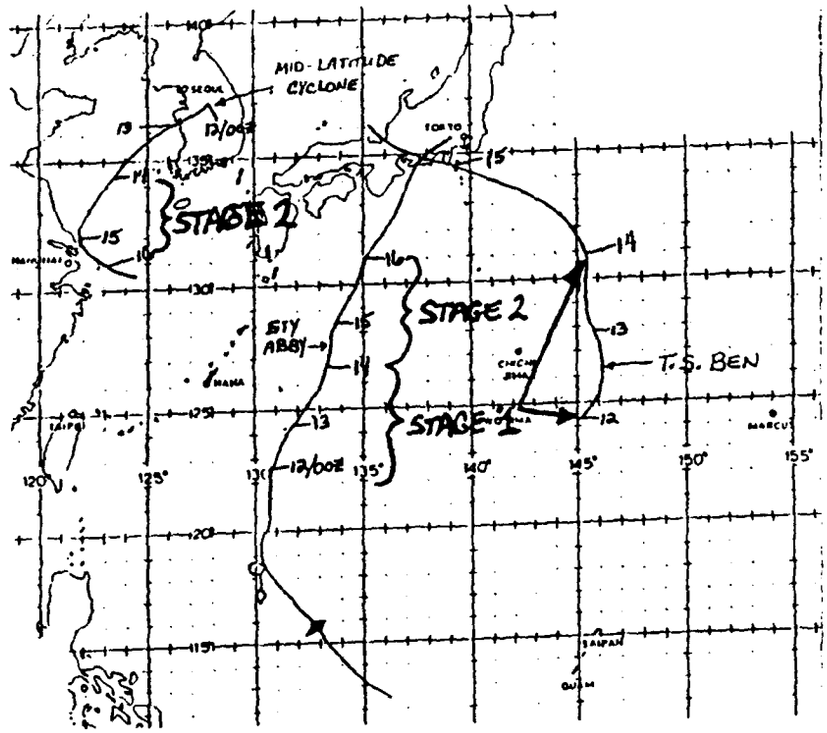

Figure 30. Tracks of Abby, TS Ben and an extratropical cyclone are illustrated with stages 1 and 2 depicting Abby's periods of significant interaction with each feature.

In stage 1, the development of TS Ben on 12 August was the result of STY Abby's upper-level outflow interacting with a Tropical Upper Tropospheric Trough (TUTT) circulation. This interaction created an area of intense upper-level divergence to the east-northeast of STY Abby beneath which TS Ben formed (Fig. 31). TS Ben moved northward along the edge of Abby's growing circulation and gradually intensified (Fig. 32 and 33). Shortly after 1400, Abby's strong upper-level outflow sheared Ben's upper-level center to the northeast. Meanwhile, Abby's deep convergent circulation appeared to absorb Ben's circulation and Ben accelerated to the northwest (Fig. 34).

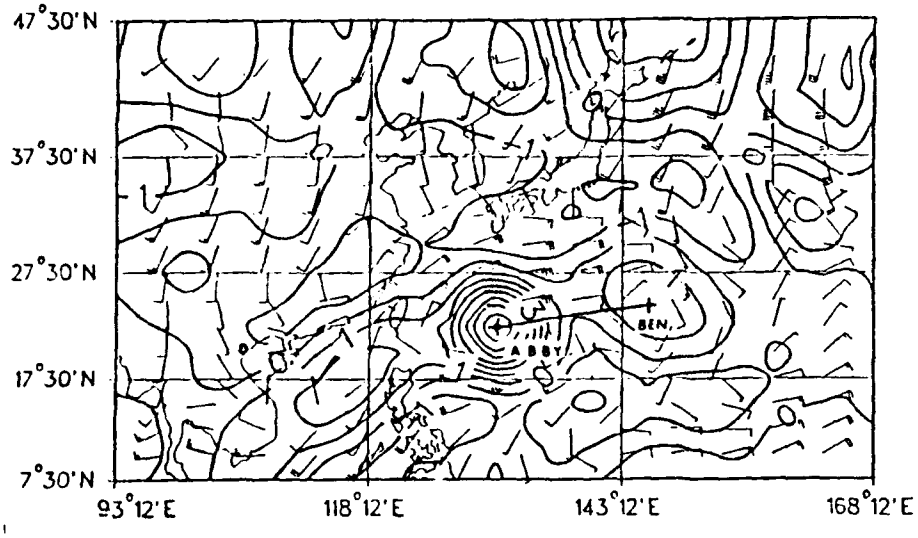

Figure 31. Vorticity and winds (kt) for 00 UTC 12 August 1983 at 700 mb showing the vorticity (contour interval 1 x 10^{-5} s^{-1}) centered on STY Abby and TS Ben just forming to the east. The solid line indicates the separation distance between the vorticity centers of Abby and Ben. The vorticity fields are reconstructed with 45 EOF's and the wind fields are reconstructed from 35 EOF's.

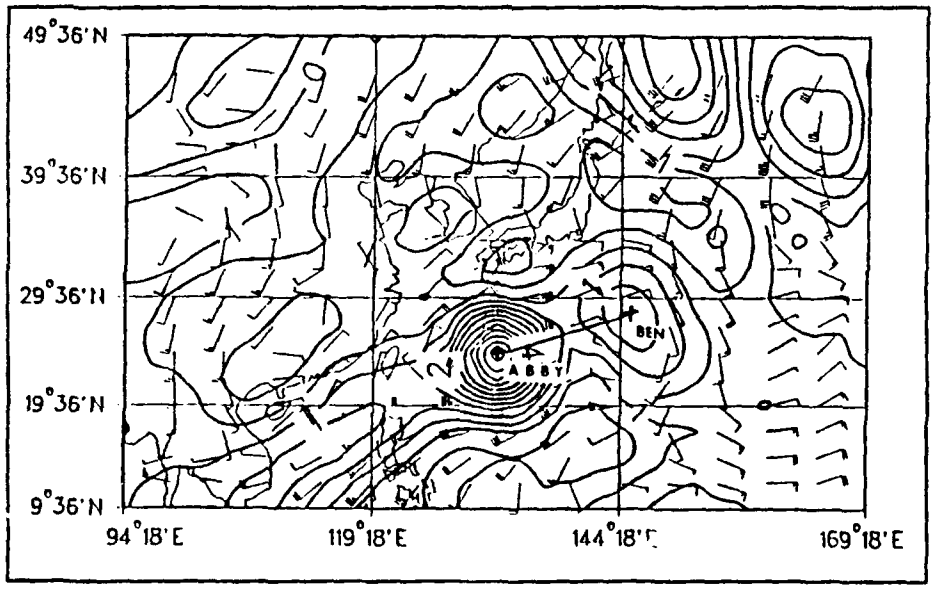

Figure 32. Vorticity and the wind field for 00 UTC 13 August 1983 at 700 mb as in Fig. 31 with TS Ben intensifying as it moves northward along the edge of STY Abby's circulation.

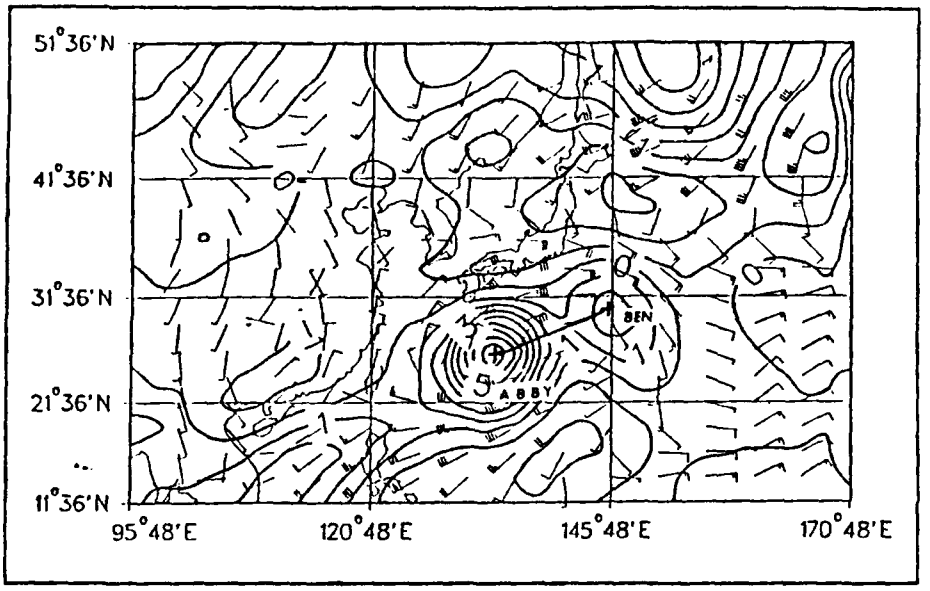

Figure 33. Vorticity and wind field for 00 UTC 14 August 1983 at 700 mb as in Fig. 31 with TS Ben intensifying as it moves northward along the edge of STY Abby's circulation.

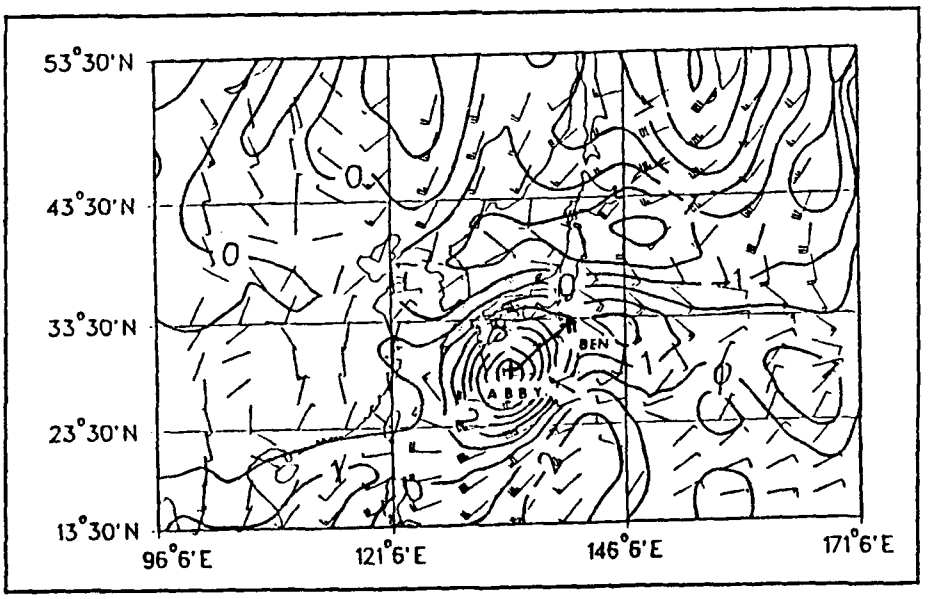

Figure 34. Vorticity and the wind field for 00 UTC 15 August 1983 at 700 mb with TS Ben accelerating to the northwest after being absorbed within STY Abby's circulation.

2. Analysis Procedures and Vortex Parameters

The separation distances between the two storm centers (cross symbols) are indicated in Figs. 31-34. Vorticity values along these lines were extracted and were fit with a fifth-order polynomial (Fig. 35). These curves permit an evaluation of each circulation's magnitude and areal extent, and indicate the separation distance changes. Vorticity values remained positive between the two systems as the separation distance decreased throughout stage 1. The magnitude and horizontal extend of Abby was steady from 1200 to 1400, but Abby seems to increase in size as it absorbed Ben into the circulation. At that time, the vorticity gradient no longer changes sign along the line between the two centers.

Estimates of vorticity magnitudes, areas extent, and their products are shown in Table 3. These semi-quantitative estimates can be used to evaluate the five secondary mechanisms. The vorticity values for 1400 (Fig. 35) are used to demonstrate how these evaluations are made. The slope of this curve changes sign at approximately 750 km from Abby's center. Therefore, Abby has a 150 km diameter circulation. Since the radius of Ben is about 400 km (from 750 to 1150 km), the diameter of Ben is about 800 km, which is about 1/2 that of Abby. Consequently, the area of Ben is about one fourth of Abby. The maximum vorticity of Abby in Fig. 35 at 1400 is about $8.5 \times 10^{-5}\ s^{-1}$, while the value for Ben is only 2.5, or approximately 1/3 that of Abby. Since the interaction effect is proportional to the product of amplitude and area, the relative effect of Ben on Abby is about 1/12 that of Abby on Ben. The strength (amplitude and area) of Abby relative to Ben is large at other time in stage 1 (Table 3). From Figs. 31-34, the separation distance decreases as the two centers rotate counterclockwise with time.

Table 3. RATIO OF THE RELATIVE VORTICITY AMPLITUDE OF TROPICAL STORM (TS) BEN COMPARED TO TYPHOON (TY) ABBY DURING STAGE ONE, showing areas of positive vorticity and the product of the two ratios. These ratios represent the relative impact of Ben on Abby during interaction at 00 UTC 12 August 1983 (1200) through 00 UTC 14 August 1983.

DATE/TIME (Z)	1200	1300	1400
AMPLITUDE	1/5	1/4	1/3
AREA $(1/r)^2$	49/64	16/81	1/4
PRODUCT	3/20	1/20	1/12

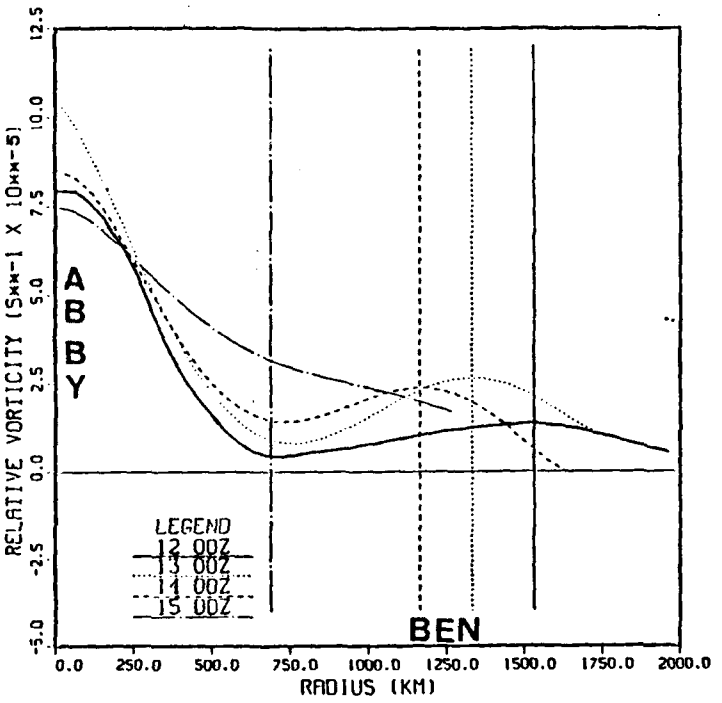

Figure 35. Vorticity along line connecting STY Abby and TS Ben. Abby is represented along the left axis (radius = 0) and the relative position of Ben is indicated by the vertical lines between 00 UTC 12 August and 00 UTC 15 August (see legend).

3. Evalutation of Secondary Effects in Stage 1

In Figs. 36-40, the effects of each mechanism are graphically illustrated to determine whether it agrees with the observed attraction or repulsion and binary rotation. Since the outer wind strength in Abby is much greater than in Ben, the Beta effect on Abby is stronger and results in a larger movement than in Ben. Because Abby is a strong vortex, the westward movement is due to the linear Beta effect dominating the nonlinear vorticity advection effect. Since Abby is expected to have a larger and more westward displacement than Ben, a repelling (increase in separation distance with time) is indicated for the Beta effect (Fig. 36). However, this conflicts with the observed attraction between Abby and Ben. Thus, the Beta effect alone can not explain Abby's north-northeast movement and the north-northwest movement of Ben.

The Fujiwhara effect (Fig. 37) supports the observed counterclockwise rotation of Ben relative to Abby. The north-northeast total movement (solid black arrow) of Abby does not agree with a predicted southeast motion (dashed arrow) due to this mechanism, probably because the weaker outer circulation of Ben had no effect on Abby's larger and much stronger circulation. However, Ben's movement may be associated with the outer circulation of Abby.

The convergent flow mechanism of Chang (1983) indicates both counter-clockwise rotation and attraction (Fig. 38), which agrees with observations. Abby's outer circulation would tend to pull Ben toward the singular point, whereas Ben's outer circulation effect on Abby probably is negligible.

The vorticity advection mechanism of DeMaria and Chang (1984) should result in Abby and Ben repelling. That is, the advection of the outer circulation of Abby on the vorticity gradient (Fig. 35) in the region of Ben should induce a secondary circulation that would have a outward component (Fig. 39). The outer circulation effect of Ben on the vorticity gradient near Abby probably is

negligible. Thus, Abby's movement to the north-northeast is approximately 90° relative to the southeast motion (towards the positive vorticity tendency) indicated by the vorticity advection effect. Although the primary vorticity advection effect associated with this mechanism is consistent with the observed counterclockwise rotation with Abby and Ben, the prediction of repelling is incorrect.

The environmental shear effect of Dong and Neumann (1986) in Fig. 40 would imply that Abby and Ben should be attracting with counterclockwise rotation. Based on Fig. 33, the monsoon westerlies south of Abby appear to be stronger than the easterly winds north of Ben. Therefore, Abby should be advected eastward faster than Ben would be westward. Because Ben is located east of the north-south axis of Abby, the storms will be advected towards one another. If Ben was located northwest of Abby with this same environmental shear, repelling would have been expected with the same counterclockwise rotation. At 1400, Ben and Abby are meridionally oriented, which produces the maximum displacement by the environmental shear. At 1200 and 1300 when Abby and Ben were located more east-west, the effects of the environmental shear were weak. The major effect during this early period is the movement of Ben northward around the eastern edge of Abby's large circulation.

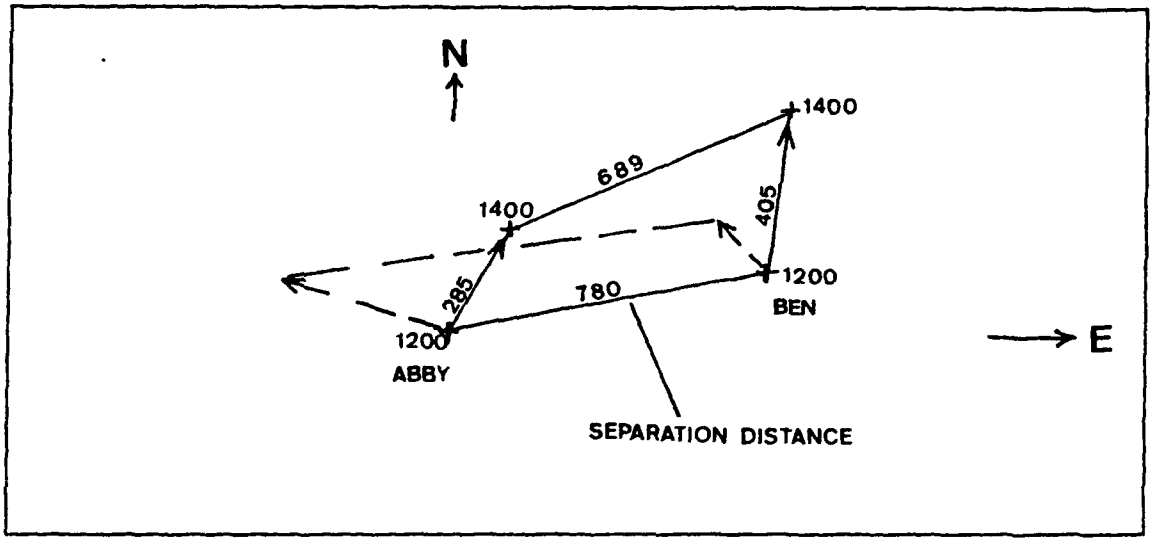

Figure 36. Beta effect in Abby-Ben case (stage 1) contributing to attraction or repulsion. Solid lines are observed movements and dashed lines are theoretical. Diagram not drawn to scale and separation distances (n mi) between the two times are estimated from Fig. 30.

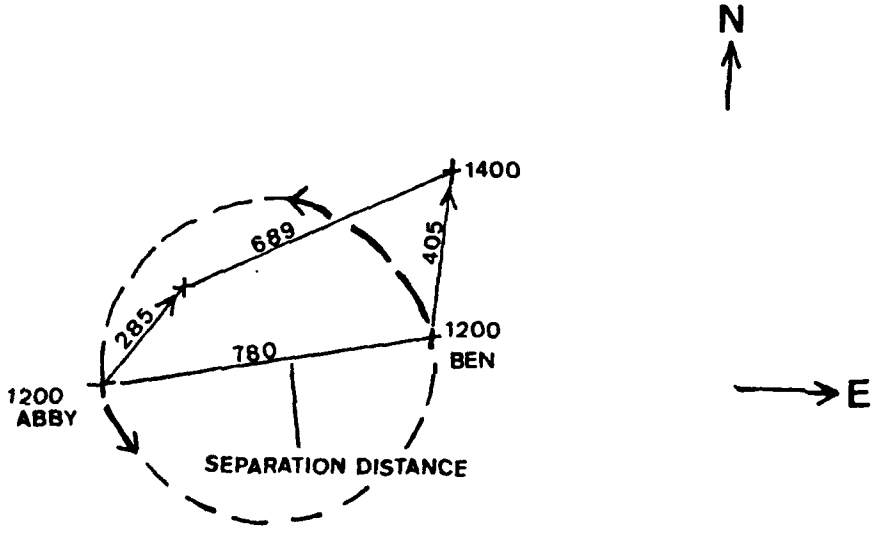

Figure 37. Fujiwhara effect applied to the Abby-Ben case (stage 1). Solid and dashed line are similar to Fig. 36. Diagrams not drawn to scale and distances estimated as in Fig. 36.

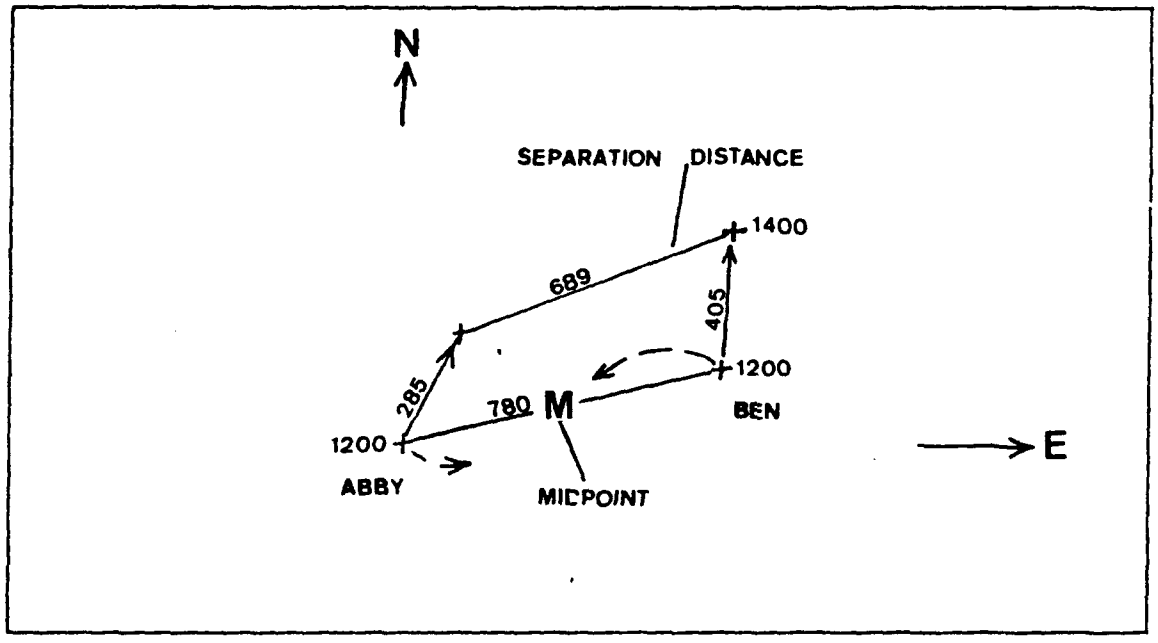

Figure 38. Convergent circulation effect of Chang (1983) for Abby-Ben case (stage 1). Labeling is the same as in Fig. 36.

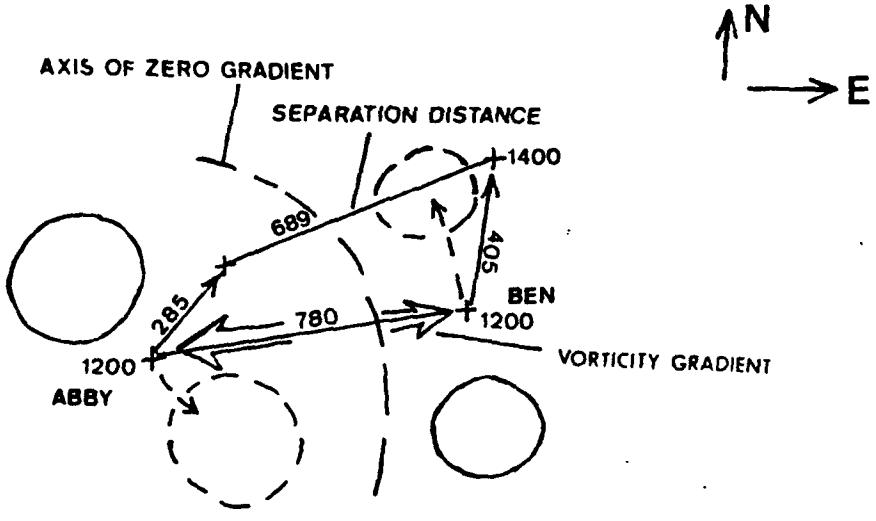

Figure 39. Vorticity advection effect of DeMaria and Chan (1984) for Abby-Ben case (stage 1). Labeling is the same as in Fig. 36. The dashed circles represent areas where relative vorticity tendency $\left(\frac{\partial \zeta}{\partial t}\right)$ changes positively with time and negatively in the solid circles. The dashed arrows point toward positive relative vorticity tendency centers.

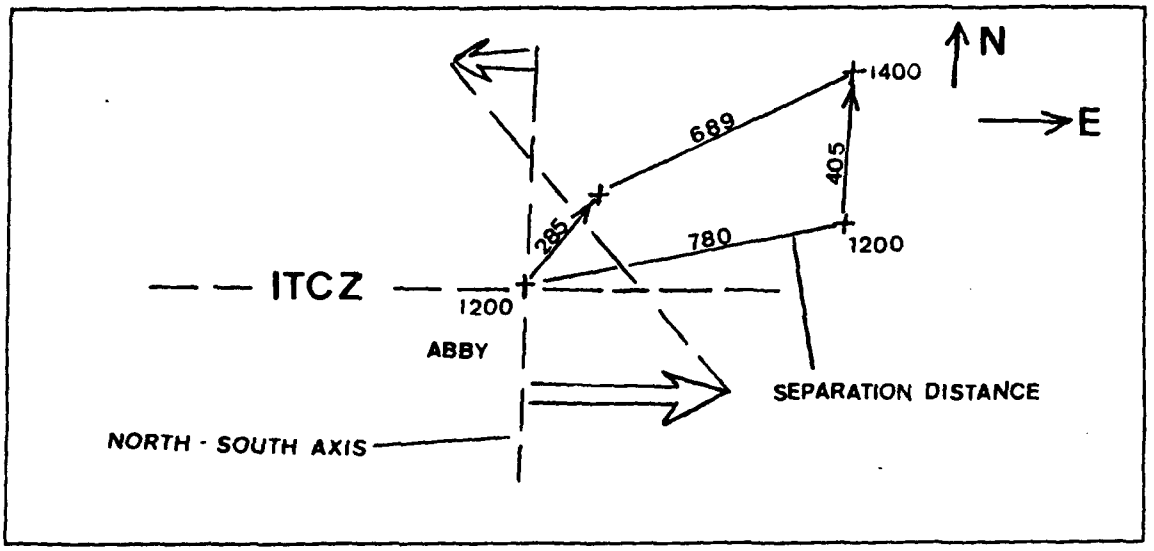

Figure 40. Environmental shear of Dong and Neumann (1986) for Abby-Ben case (stage 1). Labeling is the same as in Fig. 36. Large arrows indicate the direction of the approximate shear distribution.

Table 4 is a summary of the results for all five secondary mechanisms during stage 1. The interpretations discussed above for 1400 are similar at 1200 (00 UTC 12 August) and 1300 (00 UTC 13 August), except the environmental shear effect was weak when the two vortices were embedded in the Intertropical Convergence Zone (ITCZ).

Table 4. RELATIVE MOTION AND ROTATION OF THE TRACKS OF TY ABBY AND TS BEN DURING STAGE ONE for Five Secondary Effects between 00 UTC 12 August 1983 and 00 UTC 14 August. CCR is counterclockwise rotation and CWR is clockwise rotation.

SECONDARY EFFECTS	MOVEMENT/ROTATION		
Day/Hour (Z)	1200	1300	1400
Observed	Attract/CCR	Attract/CCR	Attract/CCR
Beta	Repel	Repel	Repel
Fujiwhara	CCR	CCR	CCR
Convergence	Attract/CCR	Attract/CCR	Attract/CCR
Advection	Repel/CCR	Repel/CCR	Repel/CCR
Shear	Weak Shear/CCR	Weak Shear/CCR	Weak Shear/CCR

D. CASE 1 - SUPERTYPHOON ABBY (STAGE 2)

1. Synoptic Discussion

On August 12, a weak cyclonic shear region at 400 mb existed over Korea between a strong midlatitude ridge and the subtropical ridge cell located north of STY Abby (Fig. 41). Abby's large circulation gradually eroded the subtropical ridge cell to the north over the next 24 h. Meanwhile, the cyclonic shear region intensified along the west coast of Korea (Fig. 42). By 1400, a clear break in the subtropical ridge (Fig. 43) allowed interaction between STY Abby and this strengthening ET cyclone to occur. Only positive vorticity values are found along the line connecting these two cyclonic centers. Comparing Fig. 43 with Fig. 33 reveals the ET cyclone feature is not distinguishable at the 700 mb level. Consequently, this circulation appeared to be restricted to the mid to upper levels. This midlatitude cyclone continued moving southwestward, and acquired many of the characteristics and dynamics of a TUTT cell. Figs. 44 and 45 illustrate the strong binary counterclockwise interaction occurring with decreased separation distances. This decrease in horizontal distance is indicated by the vertical lines in Fig. 46.

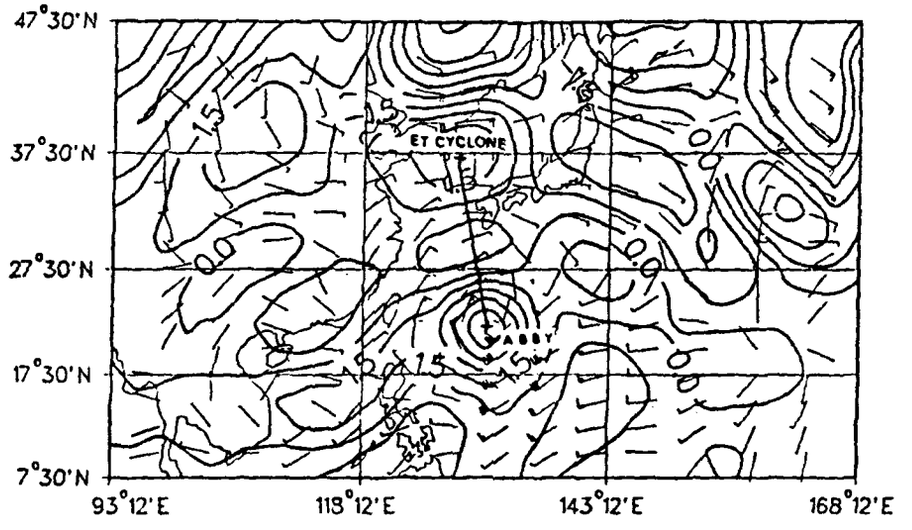

Figure 41. Relative vorticity and wind fields for 400 mb at 00 UTC 12 August. The vorticity (contour intervals 1.5 x 10-5 s^{-1}) and wind fields (kt) describe Abby and a weak cyclonic shear region over Korea. The cross symbols indicate the vorticity centers and the solid line represents the separation distances.

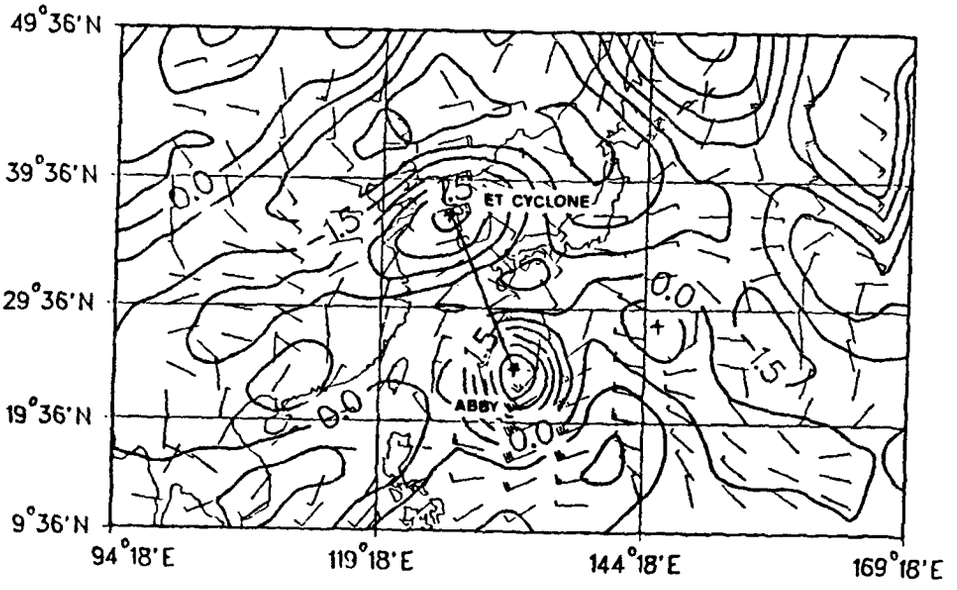

Figure 42. Relative vorticity and wind fields for 400 mb at 00 UTC 13 August similar to Fig. 41.

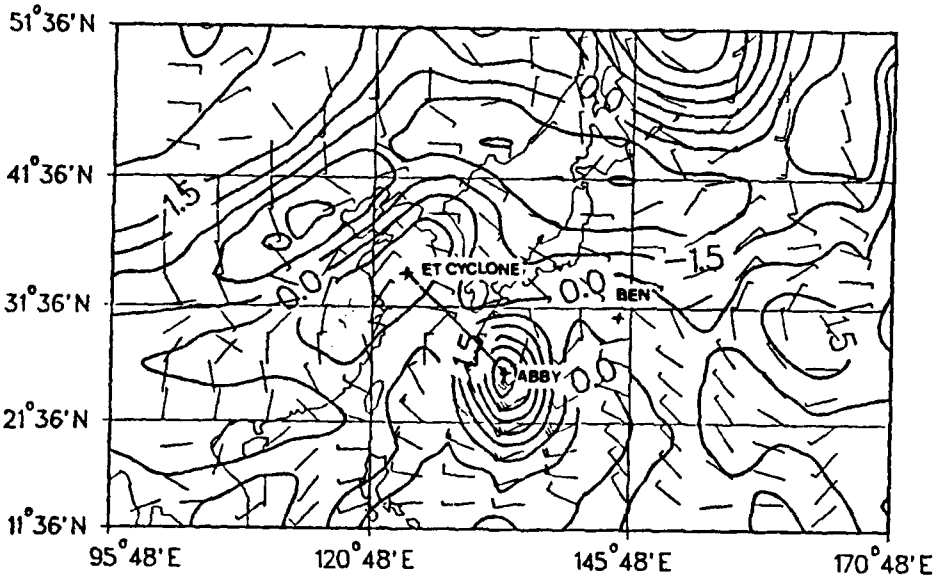

Figure 43. Relative vorticity and wind fields for 400 mb at 00 UTC 14 August similar to Fig. 41.

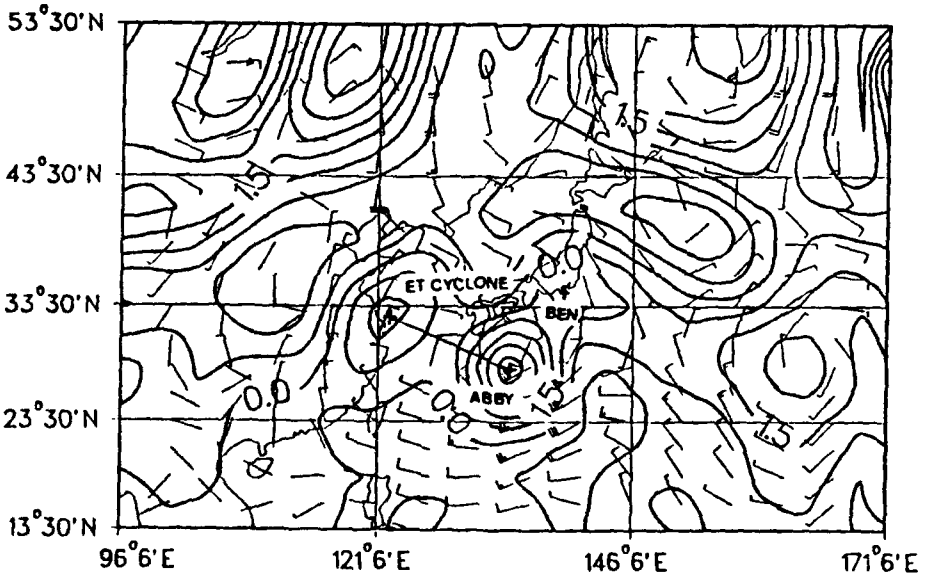

Figure 44. Relative vorticity and wind fields for 400 mb at 00 UTC 15 August similar to Fig. 41.

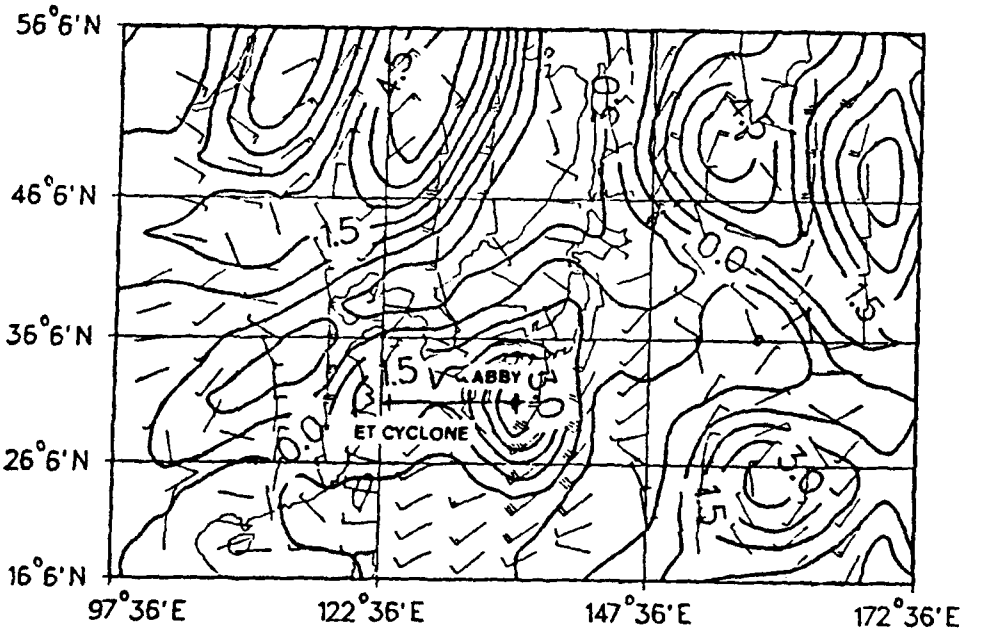

Figure 45. Relative vorticity and wind fields for 400 mb at 00 UTC 16 August similar to Fig. 41.

2. Vortex Parameters

Table 5 provides a summary of the relative amplitudes and sizes of each vortex during stage 2 of the interaction of STY Abby with and ET circulation. These estimates were obtained with similar procedures as used in stage 1. The period of strongest interaction was at 1500, when the relative vorticity gradients were greatest for each system (Fig. 46). The relative vorticity of Abby is about 8 x 10^{-5} s^{-1} ad compared to 3 x 10^{-5} s^{-1} for the ET cyclone, and the diameter of Abby is about 1300 km and 1100 km for the cyclone. Based on the product of area and magnitude, the relative effect of the ET cyclone on Abby is expected to be approximately 1/10 that of Abby on the ET cyclone.

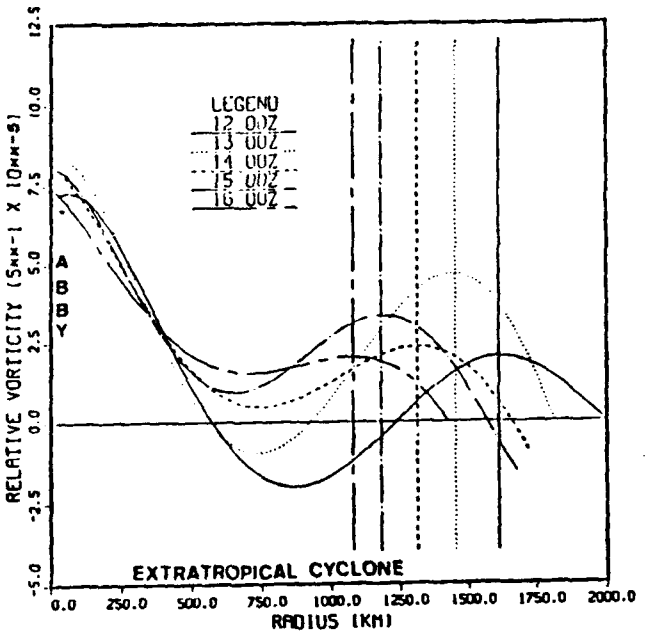

Figure 46. Vorticity of Abby and a midlatitude cyclone. STY Abby is at radius = 0.0 and an ET cyclone is represented by the vertical lines between 00 UTC 12 August and 00 UTC 16 August (see legend).

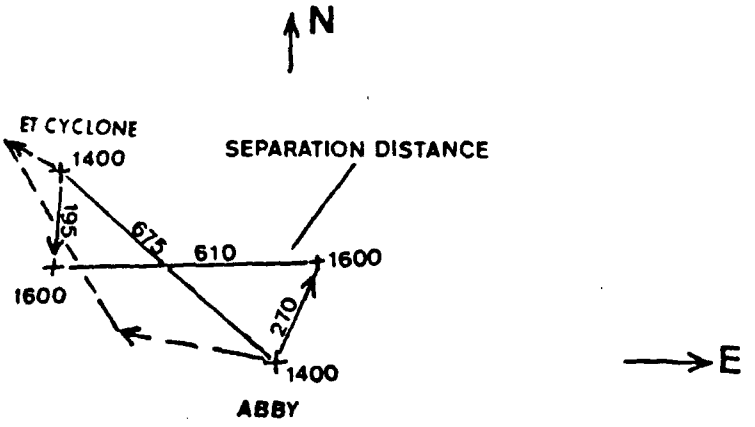

Figure 47. Beta effect during stage 2 of the interaction of STY Abby with an ET cyclone. Solid and dashed lines are similar to Fig. 36. Diagram is not drawn to scale and distances are estimated as in Fig. 36.

Table 5. RATIO OF THE RELATIVE VORTICITY AMPLITUDE OF THE EXTRATROPICAL (ET) CYCLONE CPMPARED TO TY ABBY DURING STAGE TWO, showing areas of positive vorticity and the product of the two ratios. These ratios represent the relative impact of Extratropical (ET) cyclone on Abby during interaction at 00 UTC 14 August 1983 (1200) through 00 UTC 16 August 1983.

DATE/TIME (Z)	1400	1500	1600
AMPLITUDE	1/4	3/8	1/4
AREA $(1/r)^2$	9/16	9/16	3/5
PRODUCT	1/7	1/5	1/7

3. Evaluation of Secondary Mechanisms in Stage 2

In a similar manner to stage 1, the effect of each secondary process on the binary movement of Abby and the ET cyclone at 1500 is evaluated. Each effect will be examined to determine whether it can contribute to the decreasing separation (Fig. 46) and counterclockwise rotation (Figs. 41-45).

Consider first the Beta effect with Abby and the ET cyclone. From Table 5, the magnitude of the cyclone is significantly smaller relative to Abby at 1500. Therefore, Abby should experience a greater west-northwest displacement with time that the ET cyclone, which would result in a decreasing separation distance (Fig. 47). Hence, the Beta effect is consistent with the apparent attraction between the two systems.

The Fujiwhara effect (Fig. 48) between Abby and the ET cyclone would lead to counterclockwise rotation as observed. Given the stronger outer circulation in Abby, the ET cyclone should be displaced faster, which is observed.

The convergent flow effect of Chang (1983) would suggest that the stronger outer circulation of Abby would have a large effect on the ET cyclone. Similarly, the midlevel convergence associated with the ET cyclone would tend to attract Abby. However, the ET cyclone appears to pull toward the singular point more rapidly, which suggests Abby's more extensive convergent circulation (Fig. 49) extends much deeper into the atmosphere than the typical strong typhoon. Advection by the outer wind field of each vortex would support the correct rotation.

The vorticity advection mechanism of DeMaria and Chan (1984) is shown in Fig. 50. The relative vorticity from the "col" area towards the cyclone is fairly weak compared to the gradient associated with Abby. The outer circulation effect of Abby acting on the cyclone's vorticity gradient should cause a movement towards the southwest according to the first-order advection (Fujiwhara). However, the secondary circulation effect would lead to a repelling of the ET cyclone relative to Abby. As in stage 1, this repelling motion does not agree with the observed attraction. However, this effect would account for two systems rotating counterclockwise.

It may be observed from Figs. 43-45 that the orientation of the axis between the two systems is becoming more east-west with time. When the orientation was more meridional (Fig. 49), the easterly (westerly) winds in the region of the ET cyclone (STY Abby) would tend to increase the separation distance, rather than decrease it. However, the environmental shear effect later becomes too weak to make an accurate assessment (Fig. 51).

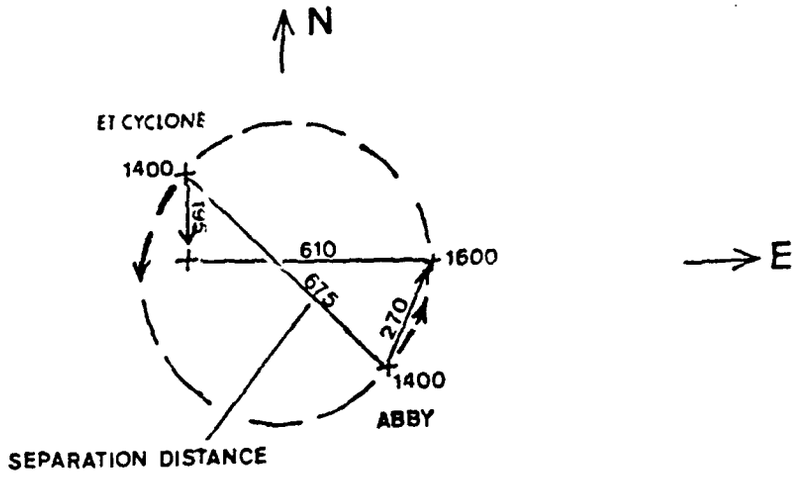

Figure 48. Fujiwhara effect during state 2 of the interaction of STY Abby with an ET cyclone. Labeling is the same as in Fig. 36.

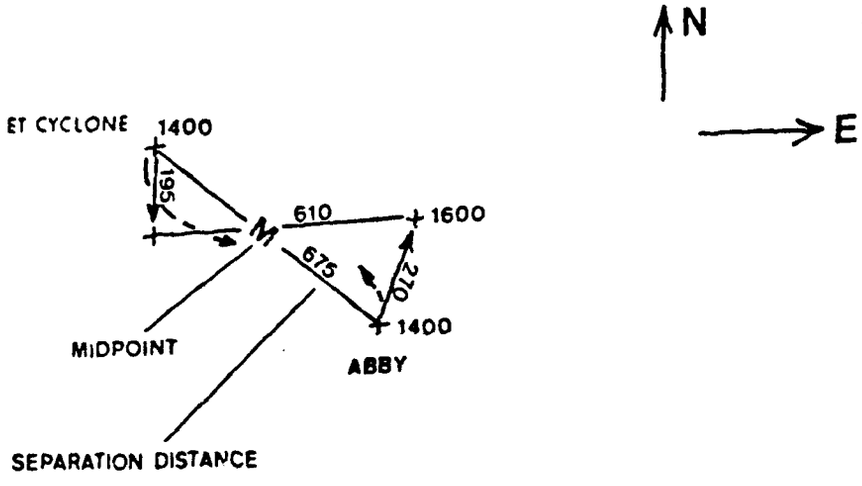

Figure 49. Convergent flow effect during stage 2 of the interaction of STY Abby with an ET cyclone. Labeling is the same as in Fig. 36.

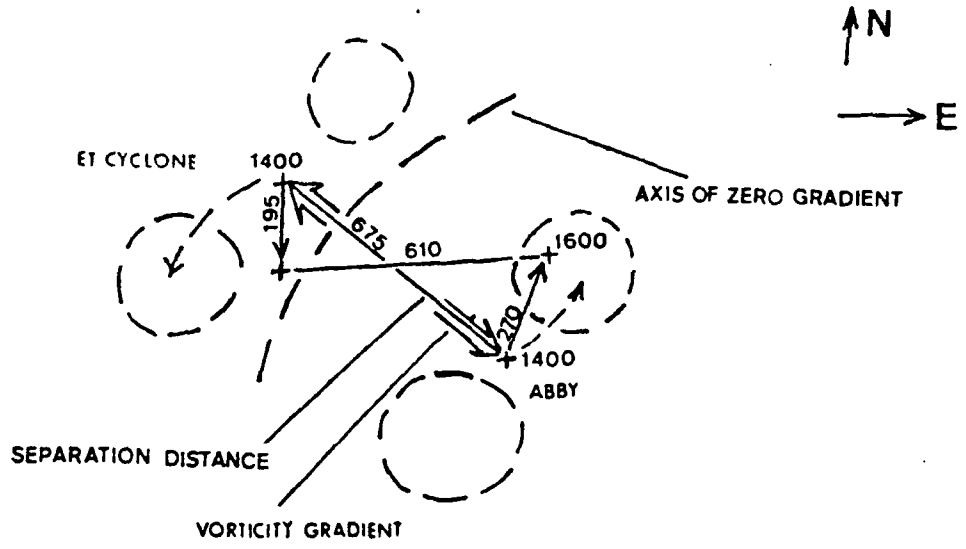

Figure 50. Vorticity advection effect during stage 2 of the interaction of STY Abby with an ET cyclone. Labeling is the same as in Fig. 36. Dashed and solid circles are represented as in Fig. 39.

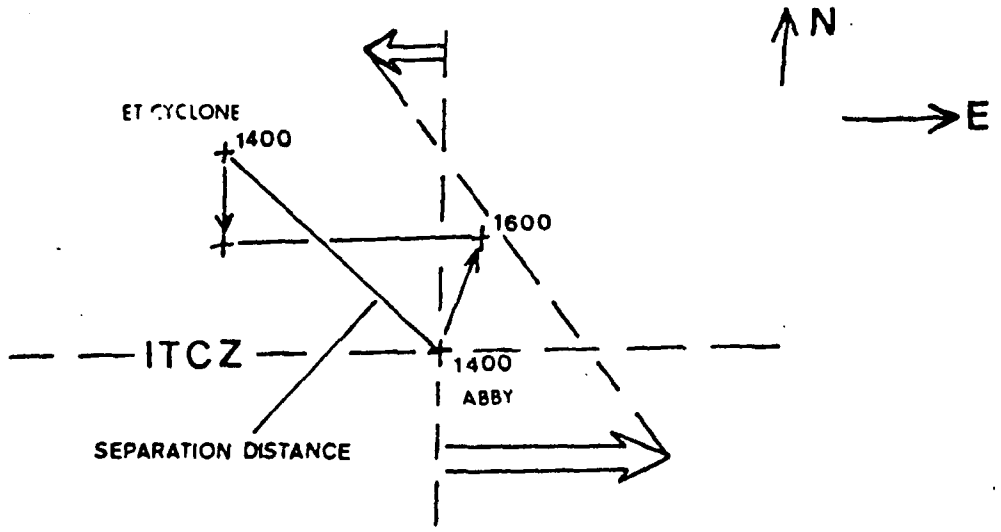

Figure 51. Environmental shear effect during stage 2 of the interaction of STY Abby with an ET cyclone. Large arrows indicate the direction of the approximate shear direction.

Table 6 is the sumary of the tendencies associated with the various effects during stage 2. The results were similar to those descirbed at 1500 except for the environmental shear effect at 1400.

Table 6. RELATIVE MOTION AND ROTATION OF THE TRACKS OF TY ABBY AND THE ET CYCLONE DURING STAGE TWO for five secondary effects between 00 UTC 14 August 1983 and 00 UTC 16 August. CCR is counterclockwise rotation and CWR is clockwise rotation.

SECONDARY EFFECTS	MOVEMENT/ROTATION		
Day/Hour (Z)	1400	1500	1600
Observed	Attract/CCR	Attract/CCR	Attract/CCR
Beta	Attract	Attract	Attract
Fujiwhara	CCR	CCR	CCR
Convergence	Attract/CCR	Attract/CCR	Attract/CCR
Advection	Repel/CCR	Repel/CCR	Repel/CCR
Shear	Repel	Weak Shear (Abby Repel)	Weak Shear (Abby Repel)

4. Summary of Mechanisms in Case 1

Supertyphoon Abby had significant interactions with two dynamic systems at different time periods and atmospheric levels. The convergent flow process was the only process to completely agree with the observed attractions in both stage 1 and 2. The Fujiwhara effect appeared to verify better in stage 2 compared to stage 1, perhaps because the relative magnitudes in stage 2 were more equal than during in stage 1. The Beta effect was complicated by multiple interactions and did not describe the observed attraction. The environmental shear process is strongly dependent on storm orientation as indicated by Dong and

Neumann (1983). That is, attraction or repulsion may be predicted for the same shear flow field if the separation axis orientation is changed by 90°. The vorticity advection effect of DeMaria and Chan (1984) could not explain the attraction observed in both stages, but did indicate the correct rotation.

E. CASE 2 - MULTIPLE STORM INTERACTION

1. Synoptic Discussion

A multiple tropical cyclone outbreak occurred in an active monsoon trough that extended west to east across the Philippine Sea between 15 and 20° N during 27-29 August 1985. Typhoon (TY) Odessa was first to develop on the eastern end of the monsoon trough, and moved northward with the trough. At the southwest end of the trough, the disturbance that eventually became TY Pat was forming. By 00 UTC 27 August 1985 (denoted 2700), the monsoon trough was oriented more northeast-to-southwest. At that time, Odessa broke out of the monsoon trough influence, as the disturbance that became tropical story (TS) Ruby began moving northeastward within the trough towards the eastern end. Within 24 h, the development of Pat and Ruby was completed, one at the southwest and the other at the northeast end of the monsoon trough. TY Odessa and TS Ruby initially decreased their separation from 2712 to 2900. Odessa turned westward on the 27th and gradually accelerated through the 28th, while Ruby broke out of the monsoon trough after 2800 and turned northwest, with a slight increase in speed. These movements paralleled the outer circulation flow of Pat's expanding wind field from 2800 to 2900. Pat and Odessa decreased their separation distance significantly throughout this period (Fig. 52). However, Pat and Ruby first increased their separation from 2700 to 2800 and then decreased from 2800 to 2900, which suggests a multiple cyclone-cyclone interaction from 2800 to 2900. The features were better defined at 700 mb compared to the 400 and 250 mb levels. Unlike Supertyphoon Abby, none of these storms had the vertically deep convective structure to have possible interactions with other comparable systems existing above 700 mb.

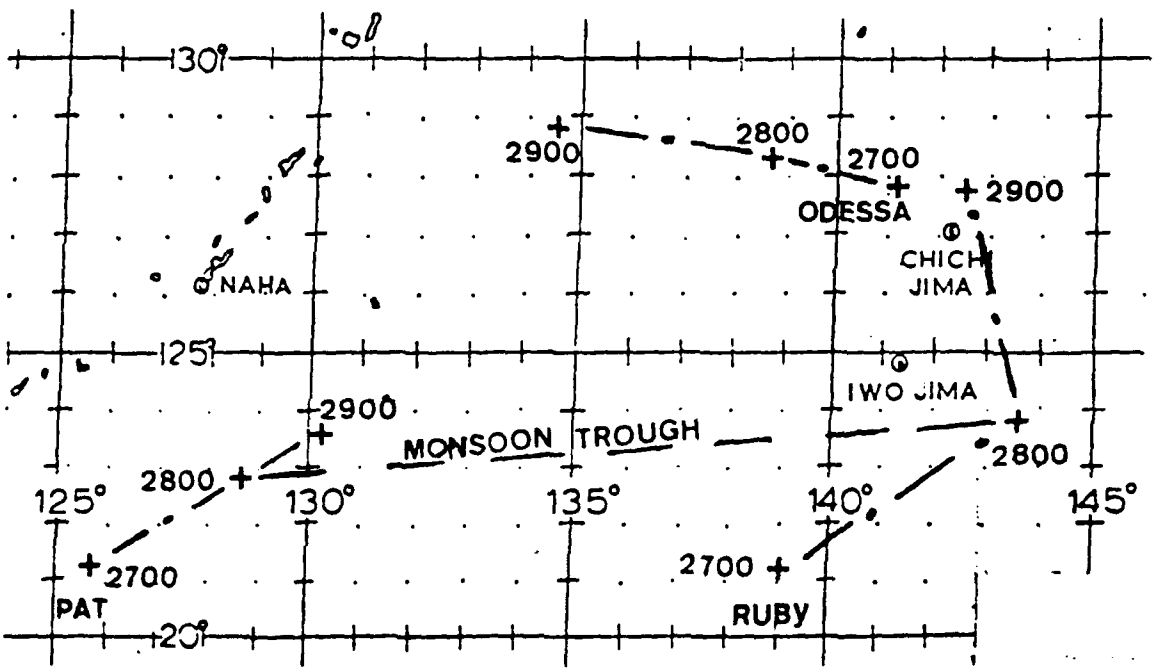

Figure 52. Separation distances (n mi) between TY Odessa and TS Ruby from 00 UTC 27 to 29 August. The cross symbols indicate the surface position.

2. Limitations Due to Grid Resolution

The limitations of the grid resolution to distinguish multiple vorticity field maxima made it more difficult to describe the interactions of Pat, Odessa and Ruby. The grid resolution of the diagnostic model is 2.5° lat. If the separation distance between two vortices is close to the grid resolution, the vorticity fields will be distorted. The interpretation of the interaction of TY Pat and Odessa was complicated by the close proximity of the maximum vorticity centers associated with Odessa and Ruby.

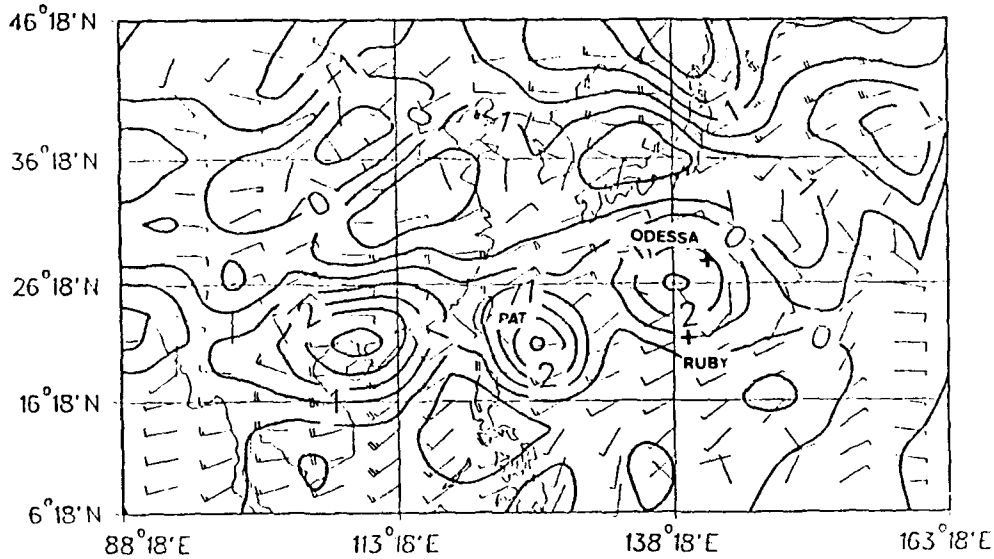

Figure 53. Relative vorticity at 700 mb for 00 UTC 27 August 1985 (contour interval 1 x 10^{-5} s^{-1}) showing TY Pat (center grid) and the interpolated maximum vorticity center located between Odessa and Ruby circulations (indicated by the cross symbol) near 26°18' N 138°18' E.

The vorticity and wind fields, which involve all three systems (Fig. 53), indicate only two maxima of vorticity instead of three. The coarse grid resolution

has caused the two vorticity centers associated with Odessa and Ruby to be represented as one maxima between the actual locations. Odessa's surface center is located approximately 400 km northeast of the maximum vorticity center (closed contour 3). There can not be that much vertical tilt between the surface and 700 mb vorticity centers in a 90 kt typhoon. In addition, the magnitude of this vorticity center is too low for a system of this intensity. Meanwhile, at that time TY Pat was only a 45 kt cyclone but was analyzed as a closed 4 contour center (Fig. 53). It appeared that the analysis of Odessa's vorticity field was degraded by the close proximity of Ruby's circulation, which was not distinguishable in Fig. 53. Since the raw vorticity field also did not display separate centers for these systems, there may not have been enough observations to define each system. The grid resolution of 278 km is inadequate to resolve two vorticity centers that were 720 km apart at 00 UTC 27 August. The vorticity fields associated with Odessa and Ruby at 2712, when the systems were separated by 650 km, is depicted along the separation axis in Fig. 54 and schematically in a larger scale representation in Fig. 55.

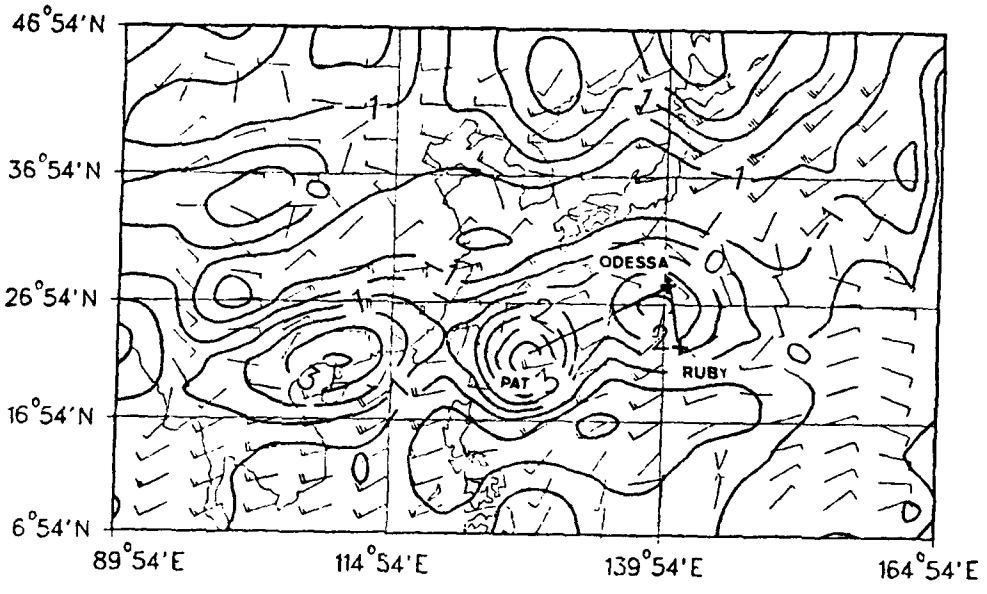

Figure 54. Relative vorticity at 700 mb for 12 UTC 27 August 1985 (contour interval 1 x 10^{-5} s^{-1}) showing TY Pat (center grid) and the interpolated center near 26°54'N 138°30'E, positioned off the axis and midpoint between Odessa and Ruby (cross symbols). Solid lines connecting storms are axes of maximum vorticities.

Odessa should be depicted as a 6 x 10^{-5} s^{-1} vorticity center in Fig. 54 compared to the 5 unit center of the weaker cyclone Pat. Ruby is only a tropical depression with a 1 or 2 unit vorticity maximum. In the schematic diagram (Fig. 55), averaging the vorticity in the top box yields about 4.5 and approximately 1.5 units in the bottom grid box. Averaging the three boxes yields a value of three. Because the circulations of Odessa and Ruby are small, these three grid boxes are interpolated to get a value of about 3 units in the corner area where two boxes share this averaged value (hatched area). Notice this closed interpolated center of three units in Fig. 55 is off-centered between Odessa and Ruby. It is biased toward the axis of the greater vorticity that exists between the two stronger storms Pat and Odessa. Ruby strengthened later into a more dominant system. This interpolated vorticity center exhibits binary motion toward the southeast and then north as Odessa and

Ruby rotate counterclockwise. Although this interpolated feature becomes more centered between these two cyclones, it becomes closer to Ruby with time (Fig. 56), perhaps because Ruby intensified and the vorticity differential between these systems was reduced. Odessa and Ruby are both near maximum intensity at 2900 (Fig. 57). If their circulation sizes are close to the grid resolution (small), they can be masked by a larger scale flow or underestimated in the relative vorticity fields. Since both their circulation sizes are smaller than the grid resolution, the EOF representation has smoothed the vorticity field within each grid box with the outer circulation field of TY Pat (largest vorticity values). Therefore, a broader 1.0 to 1.5 positive vorticity area was smoothed across both storms (Fig. 57).

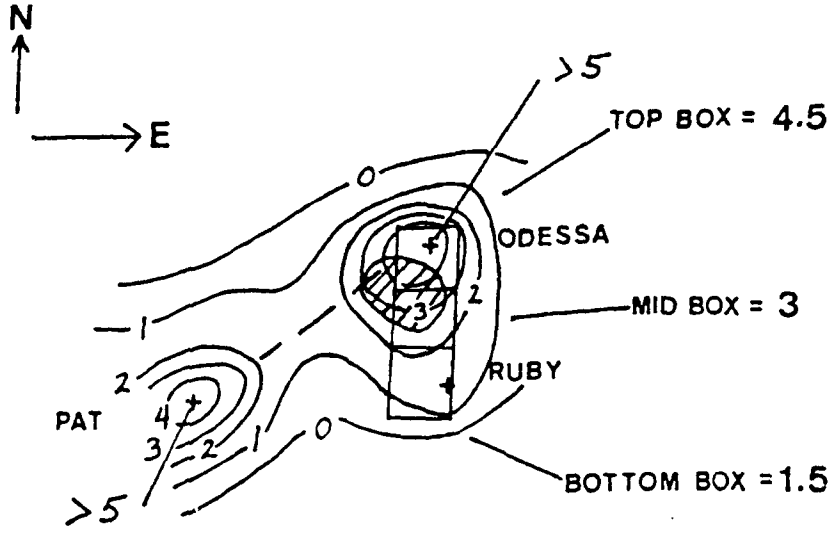

Figure 55. Schematic of the vorticity fields at 700 mb for 12 UTC 27 August 1985 associated with Odessa (top box) and Ruby (bottom). Each grid box has an area resolution of 278 km. The hatched area indicates the interpolated vorticity for both boxes.

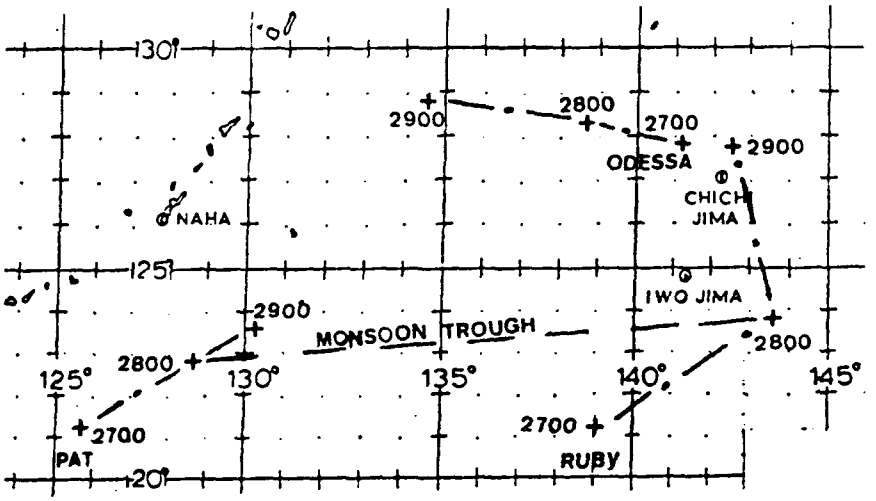

Figure 56. Binary motion of the hybrid vorticity center (HC) with respect to the binary movement of Odessa and Ruby. Notice the interpolated center moves closer to Ruby as these systems become more equal in intensity.

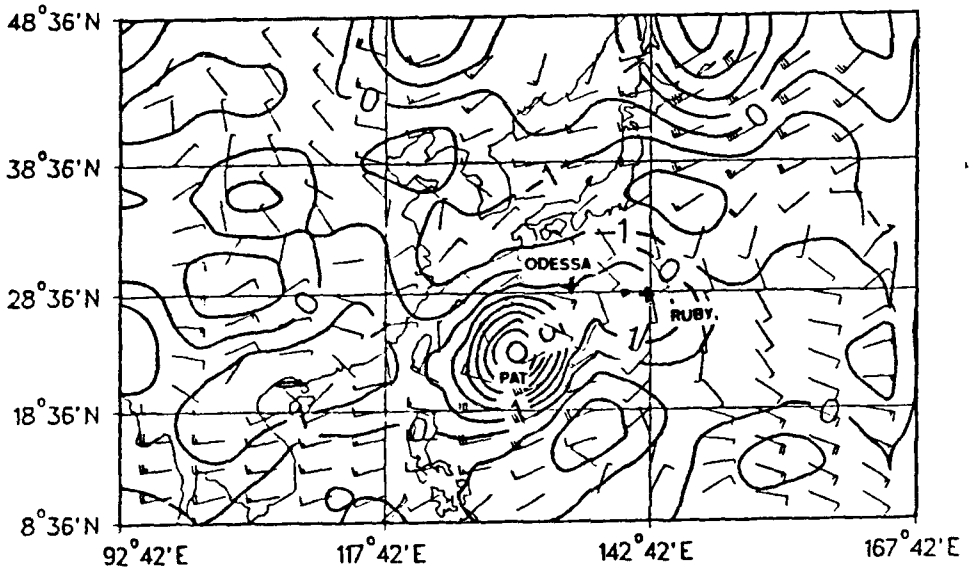

Figure 57. Positions (cross symbols) of TY Pat, Odessa and TS Ruby at 700 mb for 00 UTC 29 August. Notice the smoothing of Odessa's and Ruby's maximum vorticity centers in the outer circulation of Pat.

3. Interaction of Pat and Odessa

The grid resolution problem also affects the derived vorticity gradients (Fig. 58). The gradients along the axis connecting Pat and the interpolated vorticity feature is not representing TY Odessa's lower-level circulation. Therefore, the amplitude and areal extent of the Odessa circulation is a "hybrid" which includes Ruby's influence as well. Although the magnitudes of the secondary mechanisms between interacting cyclones would not be accurate, this distortion probably does not change the sign of the radial vorticity gradients. Therefore, the diagnostic analysis will depict the correct gradient tendencies in the qualitative description of these secondary effects.

4. Evaluation of the Secondary Mechanisms

Table 7 is a summary of the relative strengths and sizes of Pat and the interpolated vorticity center between Odessa and Ruby. As indicated from Figs. 53, 54 and 57, the separation axis is rotated counterclockwise and decreased in magnitude (attraction). After 2900, the hybrid vorticity center was absorbed into Pat's vorticity field, which eliminated the vorticity gradient toward the hybrid center.

Table 7. RATIO OF THE RELATIVE VORTICITY AMPLITUDE OF THE HYBRID CENTER (HC) COMPARED TO TY PAT with the areas of positive vorticity and the product of the two ratios. These ratios represent the relative impact of the Interpolated (Hybrid) center on Pat during interaction at 00 UTC 27 August 1983 (2700) through 00 UTC 29 August.

DATE/TIME (Z)	2700	2800	2900
AMPLITUDE	3/4	2/5	2/7
AREA $(1/r)^2$	5/4	2/5	3/10
PRODUCT	5/16	1/5	1/10<

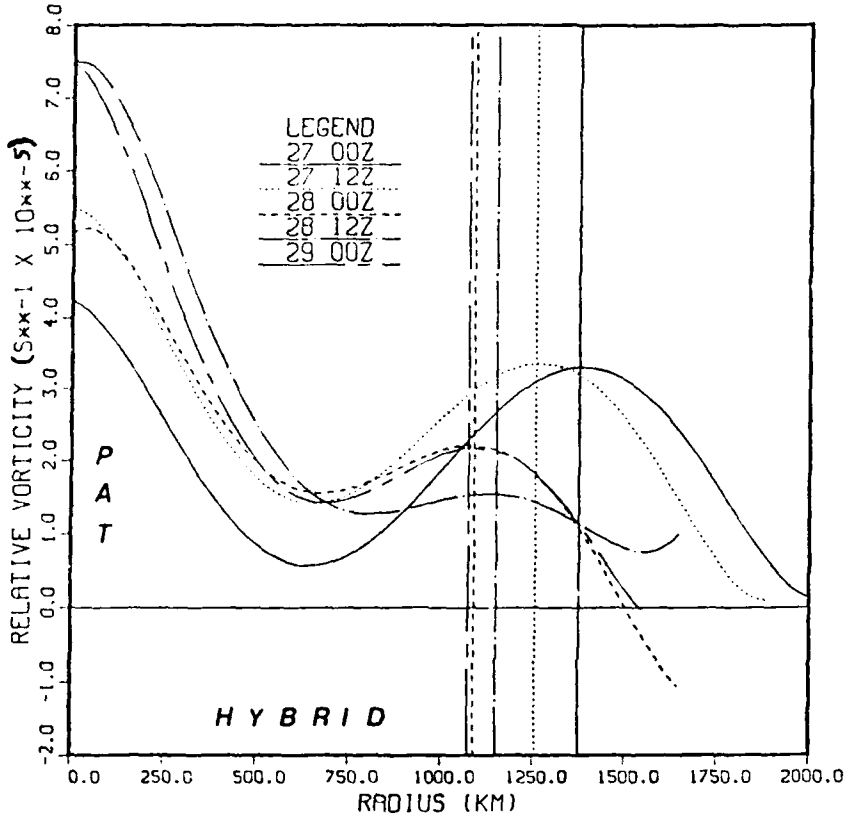

Figure 58. Vorticity along line connecting Pat and hybrid vorticity center. TY Pat is represented along the left axis (radius=0) and the relative position of the hybrid vorticity center is indicated by the vertical lines between 00 UTC 27 August and 00 UTC 29 August (see legend).

The Beta effect (similar to that shown in Fig. 36) would suggest an increasing separation in time because the greater magnitude of Pat results in a

larger northwest displacement. This relative movement would lead to a clockwise rotation. Both of these implications are not supported by the observations.

The Fujiwhara effect is clearly illustrated in Figs. 53, 54 and 57 because the separation axis rotates counterclockwise up to 2900. The binary motion as in Fig. 28 supports this rotation as well.

Both the convergent flow and the environmental shear effect supported attraction and counterclockwise rotation. The convergent flow in Pat (similar to Fig. 38) would pull the hybrid center toward the midpoint. Since the monsoon westerlies are stronger than the easterly trade wind flow (similar to Fig. 40), the orientation of these vortices in this shear field supports the observed attraction of the systems. As in Case 1, the vorticity advection effect of DeMaria and Chan would indicate a repulsion with counterclockwise rotation. Unlike Ben in Case 1, the magnitude of Odessa's vorticity field should have been stronger than Pat at the grid center. The distortions due to grid resolution again clouds the interpretation.

Table 8 is the summary of the secondary mechanisms at other time during Case 2. These results show the effects (in some unknown degree) of three cyclones interacting instead of just the cyclone-cyclone interaction of Pat and Odessa. Unfortunately, the actual effect of each mechanism is not clear because the grid resolution degrades the interpretation.

Table 8. THE RELATIVE MOTION AND ROTATION OF THE TRACKS OF TY PAT AND THE HYBRID CENTER tracks that are observed and drived for five secondary effects during stage 1 between 00 UTC 27 August and 00 UTC 29 August 1985. CCR is counterclockwise rotation and CWR is clockwise rotation.

SECONDARY EFFECTS	MOVEMENT/ROTATION		
Day/Hour (Z)	2700	2800	2900
Observed	Attract/CCR	Attract/CCR	Attract/CCR
Beta	Repel/CWR	Repel/CWR	Repel/CWR
Fujiwhara	CCR	CCR	CCR
Convergence	Attract/CCR	Attract/CCR	Attract/CCR
Advection	Repel/CCR	Repel/CCR	Repel/CCR
Shear	Attract/CCR	Attract/CCR	Attract/CCR

F. CASE 3 - INTERACTION OF TY DINAH AND TY ED

1. Synoptic Discussion

Both TY Dinah and TY Ed formed at the southern end of separate weak cold fronts that moved eastward under different midlatitude troughs. These two fronts provided the cyclonic low-level shear that enabled these disturbances to detach from the frontal zones and become isolated systems. During their first 24 h in warning status, both systems moved in atypical directions (Fig. 59) which may be attributed to the initial mid-tropospheric wind flow. As suggested by JTWC, a northeasterly flow on the south side of the narrow subtropical ridge steered Dinah southwestward during its early stages. A northerly flow west of the mid-tropospheric cyclone near 29°N and 145°E moved TY Ed initially southward and then eastward along 26°N. The ridge cell north of Dinah moved northeast under the influence of the southwest flow ahead of the cyclone east of TY Ed. A weakness in the ridge northwest of TY Dinah allowed Dinah to turn in that direction on 26 August 1984. These storms continued to move toward one another and reached their closest point of approach of 1167 km (630 n mi) at 2100 UTC 26 August (ATCR 1984). After that, the tracks of the typhoons separated significantly (Fig. 59). The turn of TY Ed toward the west-northwest appears to be due to the influence of a midlatitude short-wave trough moving east across the Sea of Japan. Meanwhile, Dinah's temporary east-northeast movement on the 27th may be attributed to the presence of Ed's upper-level anticyclonic outflow to the east-southeast (based on the JTWC post-analysis). Dinah then turned northward through the ridge break and exhibited a Fujiwhara-type binary motion with an anticyclone cell farther to the north.

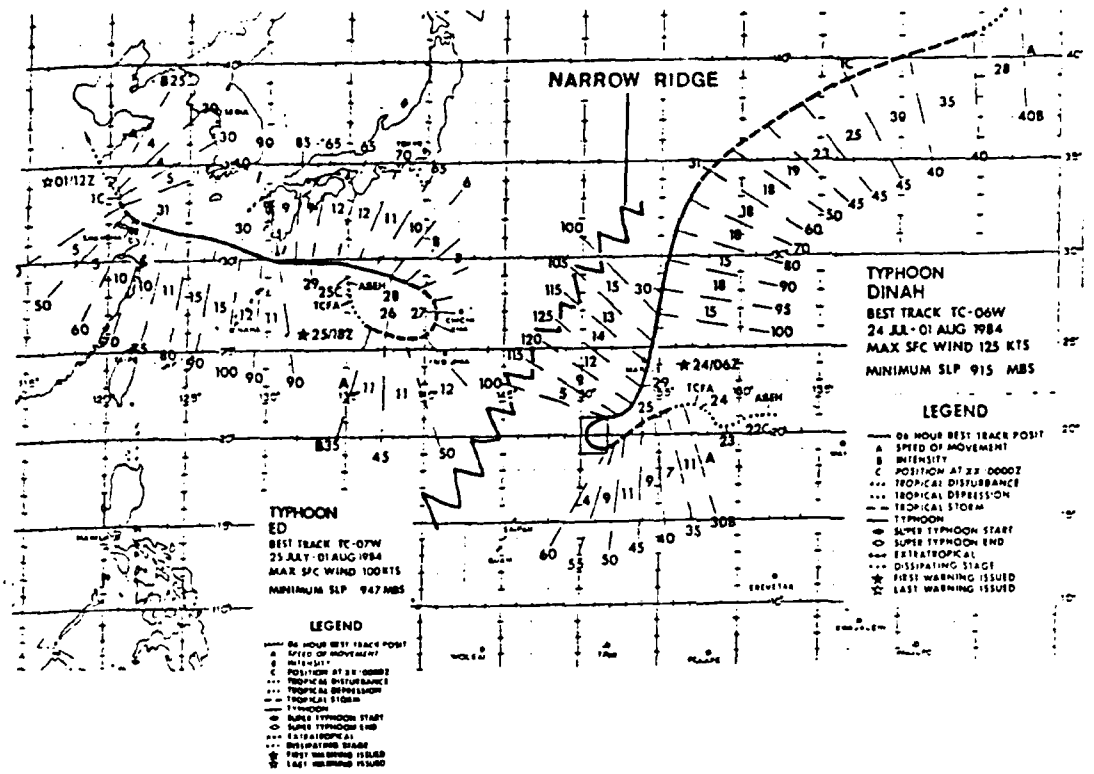

Figure 59. Tracks of TY Dinah and TY Ed during their early stage before repelling off the narrow subtropical ridge between them and resuming more climatological tracks.

Sandgathe (1987) suggested these cyclones were initially drawn toward each other as in a Fujiwhara interaction, but then were forced apart by a narrow developing ridge. However, the JTWC interpretation suggested the ridge was established between these two approaching cyclones before their repelling motion, and was not a dynamical result of the cyclones.

At 700 mb, the EOF vorticity (Fig. 60) supports the presence of the ridge through 2712, or about 15 hours after their closest point of approach (CPA). This ridge was also analyzed at 400 mb beginning at 2800. An interaction between these two systems may be indicated by the vorticity remaining positive between the

systems. This partially supports the JTWC post-analysis that attributed Dinah's east-northeast movement on the 27th to Ed's circulation. However, the vorticity magnitude of Dinah is significantly greater than Ed (Fig. 61). These vorticity maxima seem reasonable because Dinah's intensity was 20 kt greater than Ed.

During the period 2600 to 2800, the 250 mb vorticity field indicated the maximum positive vorticity associated with TY Ed was not as well defined nor stacked over the surface cyclone compared to Dinah. This is evidence of Dinah's greater organization supporting a more vertically deep positive vorticity structure.

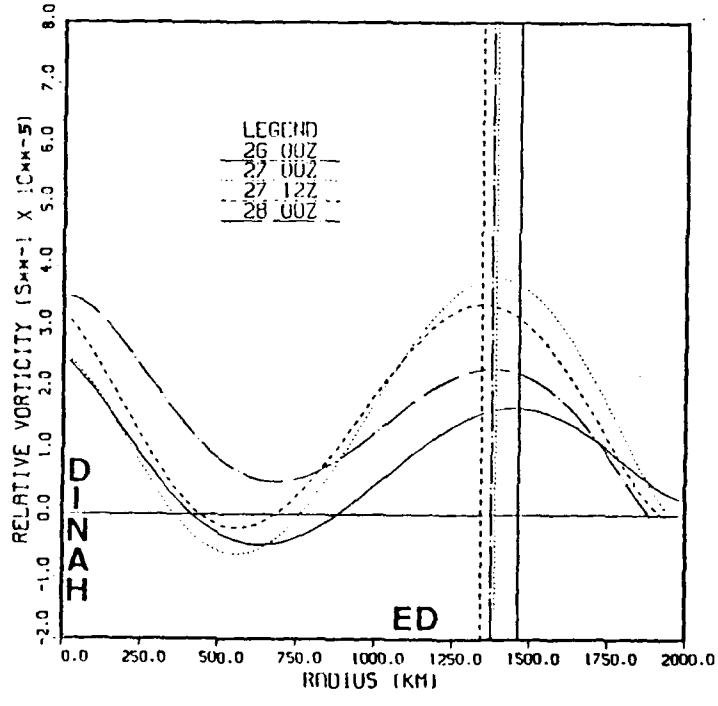

Figure 60. Vorticity at 700 mb along the axis connecting Dinah and Ed. TY Dinah is represented along the left axis (radius = 0) and Ed along the horizontal axis (vertical lines) between 00 UTC 26 July and 00 UTC 28 July 1984 (see legend).

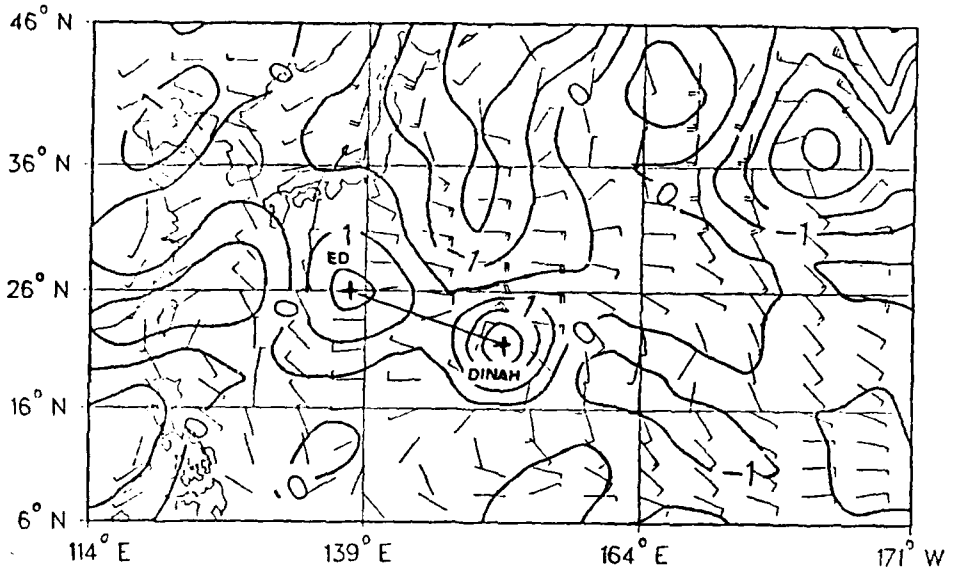

Figure 61. Vorticity at 700 mb of TY Dinah compared to TY Ed for 00 UTC 28 August 1984 shows Dinah's amplitude is larger (greater than 3 x 10^{-5} s^{-1}) vice more than 2 x 10^{-5} s^{-1} for Ed).

In summary, Dinah and Ed repelled off a ridge between then at 700 and 400 mb. An interaction only appeared possible 15 h after repelling began. At that time, an interaction did not seem to explain their respective tracks as much as other features, such as the trough over the Sea of Japan affecting Ed and the anticyclone cell in the subtropical ridge affecting Dinah.

2. TY Dinah's Interaction with an Anticyclone (AC)

TY Dinah executed a classical binary interaction with an equally strong anticyclonic circulation at 400 mb. The separation axis rotated clockwise with the vorticity centers remaining about equal distance (912 km) from 00 UTC 29 August (Fig. 63) to 00 UTC 30 August (Fig. 64), after which the separation distance decreased by about 150 km. This interaction is continued at 00 UTC 31 August

(Fig. 65). This interaction is indicated at 700 mb as well, except Dinah's vorticity is much greater (not shown). At 250 mb (not shown), the anticyclone's strength is much larger. A near equality in magnitude at 400 mb is depicted in the amplitudes of the curves in Fig. 62. The Tropical Upper-Tropospheric Trough (TUTT) located east and southeast of Dinah (Figs. 63 and 64) did not have any noticeable interaction with Dinah due to the large separation distance and weaker intensity of the TUTT.

Table 9 is a summary of the relative strengths and sizes of Dinah and the anticyclone (AC) at 400 mb. Although there was near equality in amplitudes, the areal extent more than offset the ratio in favor of the AC. The size of the mass circulation of a vortex appears to contribute as much as amplitude in determining the total relative strength. This observation is supported by comparing Table 7 (Case 2) with Table 9 (Case 3). In Case 2, TY Pat's mass circulation was much larger than the hybrid vorticity center, which consisted of two much smaller vortices. This is especially evident at 00 UTC 28 August 1985 in case two. Pat's intensity is only slightly greater than Ruby's but significantly less than TY Odessa's. Yet, Pat's relative strength is much greater, due at least in part to the significant areal size differences between Pat's large circulation and the other two much smaller size wind fields.

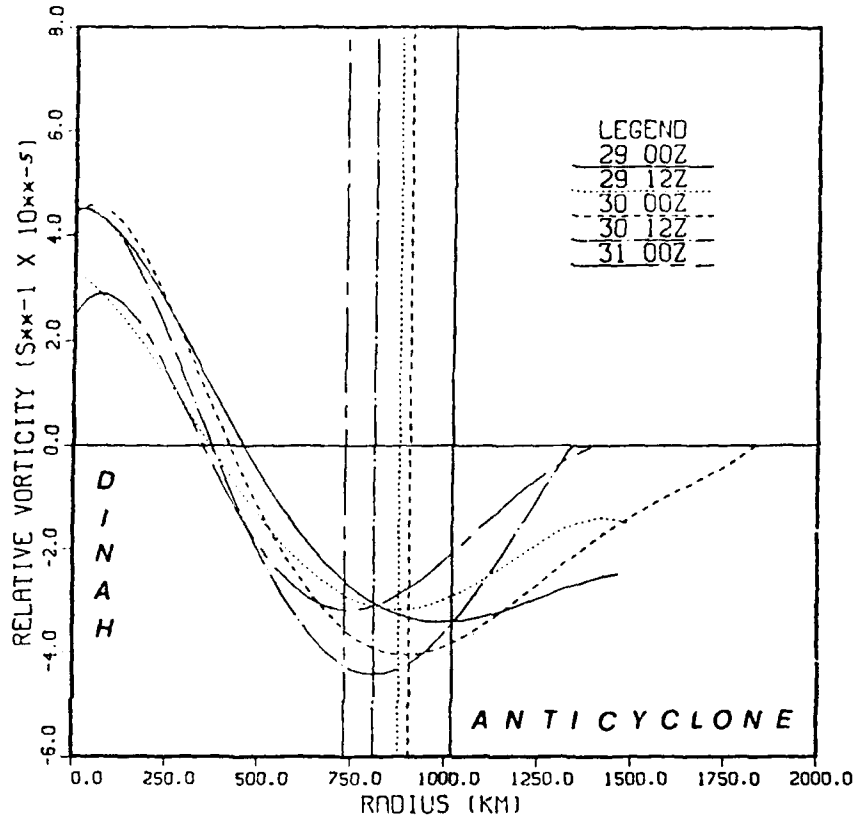

Figure 62. Vorticity at 400 mb along the a connecting Dinah and the AC. Dinah is represented along the left axis (radius=0) and the positions of the AC are indicated by the vertical lines between 00 UTC 29 and 00 UTC 30 August (see legend).

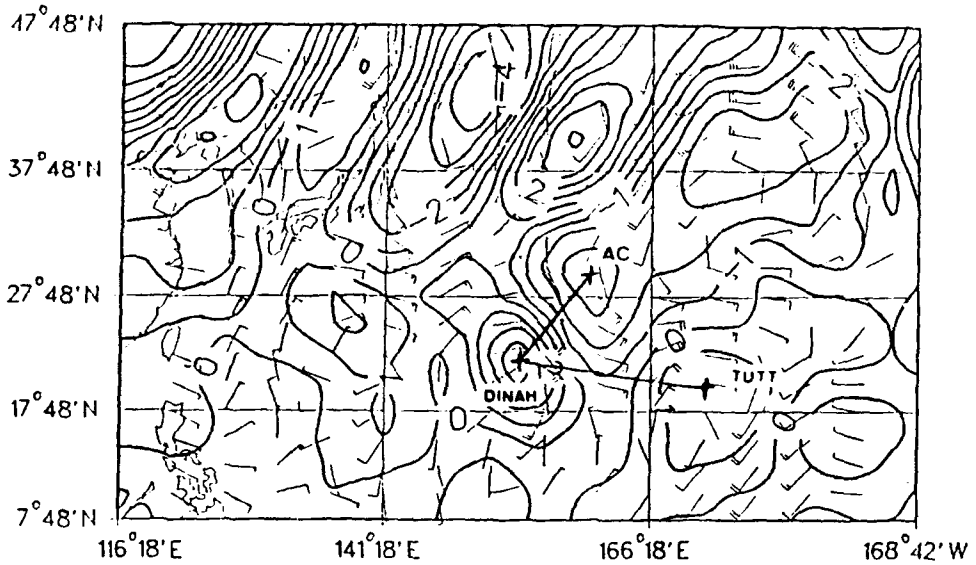

Figure 63. Relative vorticity and wind fields for 400 mb at 00 UTC 29 August. The vorticity (contour intervals 1.5 x 10^{-5} s^{-1}) and wind fields describe the interaction between Dinah (center of grid) and the anticyclone. The cross symbols indicate the vorticity centers with the solid line representing the separation distance.

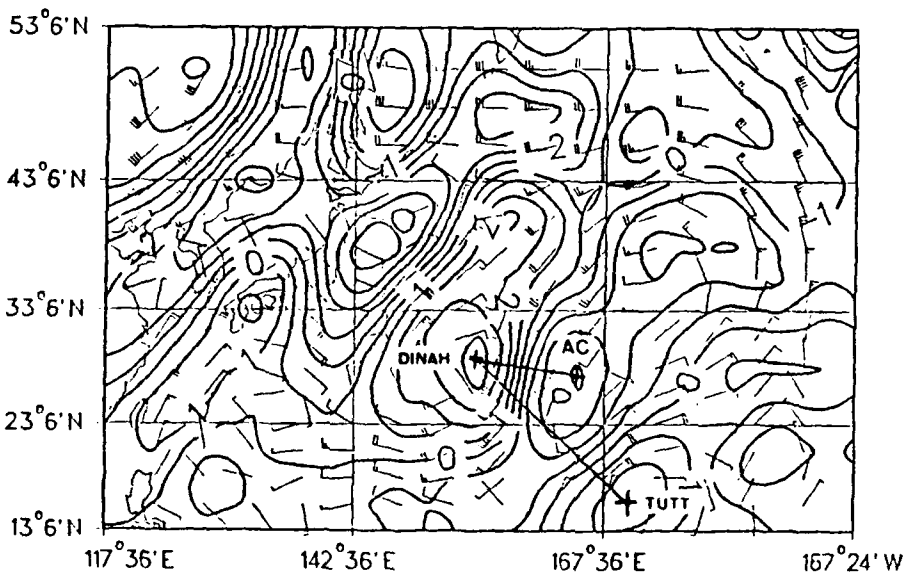

Figure 64. Relative vorticity and wind fields for 400 mb at 00 UTC 30 August similar to Fig. 63.

Table 9. RATIO OF THE RELATIVE VORTICITY AMPLITUDE OF THE ANTICYCLONE (AC) COMPARED TO TY DINAH showing the areas of positive vorticity and the product of the two ratios which represents the relative impact of the Anticyclone on Dinah during interaction at 00 UTC 29 July 1984 (2900) through 00 UTC 31 July.

DATE/TIME (Z)	2900	3000	3100
AMPLITUDE	3/4	4/5	1
AREA $(1/r)^2$	49/16	25/16	4
PRODUCT	3	5/4	4

3. Evaluation of Secondary Effects Between TY Dinah and an Anticyclone

The secondary effect interpretations of an anticyclonic circulation can be applied similarly as discussed earlier with a cyclone. The opposing interacting wind fields of Dinah and the anticyclone (AC) do not significantly complicate the interpretation of these effects. Figure 66 shows that isolating the linear Beta part of the theory on each circulation would depict a westward movement for both Dinah and the anticyclone and north (south) motion for the nonlinear vorticity advection effect for the cyclone (anticyclone), respectively. Neither attraction nor repulsion was indicated from the Beta effect from 2900 to 3000 as these two circulations rotated counterclockwise around each other at an equal distance (Figs. 63 and 64). By isolating the Beta effect it appeared both the linear and nonlinear part processes had and equivalent effect on each circulation, which is supported in part by the constant separation distance maintained during this period. In addition, the vorticity fields in Figures 63 and 64 suggest each system had equal and opposite vorticity magnitudes of 3 and 4 units, respectively. It appears that this equal and

opposite equality nullified the Beta effect and allowed other secondary processes to me more dominate in determining the type of motion (clockwise rotation) of these system shown in figures 63-65. When the anticyclone's negative vorticity magnitude became greater than Dinah's positive value by 3100 (Figure 67), a decrease in the separation distance occurred, which perhaps indicates a greater westward displacement by the AC due to a larger Beta effect at that time.

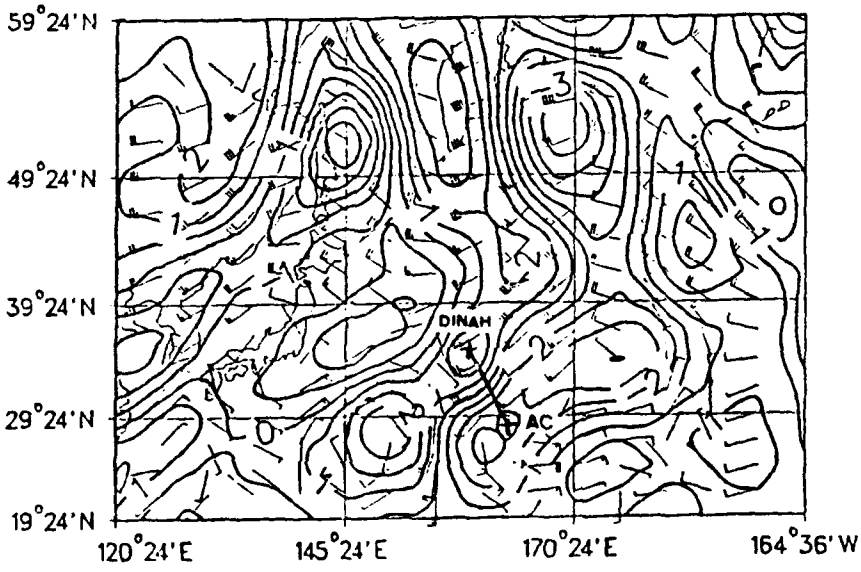

Figure 65. Relative vorticity and wind fields for 400 mb at 00 UTC 31 August similar to Fig. 63.

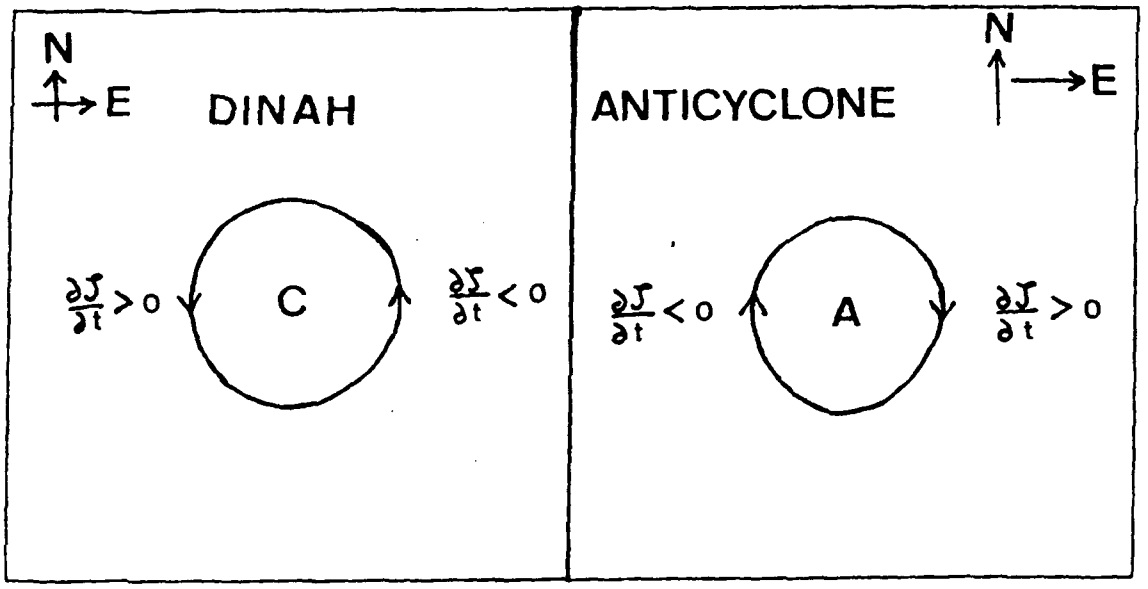

Figure 66. Linear Beta effect for Dinah and the anticyclone (AC). The letter C indicates cyclonic circulation and the letter A indicates anticyclonic circulation.

The Fujiwhara effect does not lead to a binary type of rotation with these circulations of nearly equal and opposing flow from 2900 to 3012. Rather, this cyclone-anticyclone couplet oriented north-south would tend to propagate westward during this period. When the anticyclone's circulation became larger at 3100 (Fig. 65), Dinah experience more advection from the AC's outer circulation, which resulted in a clockwise rotation, in agreement with the observations (cross symbols of each system in Fig. 68).

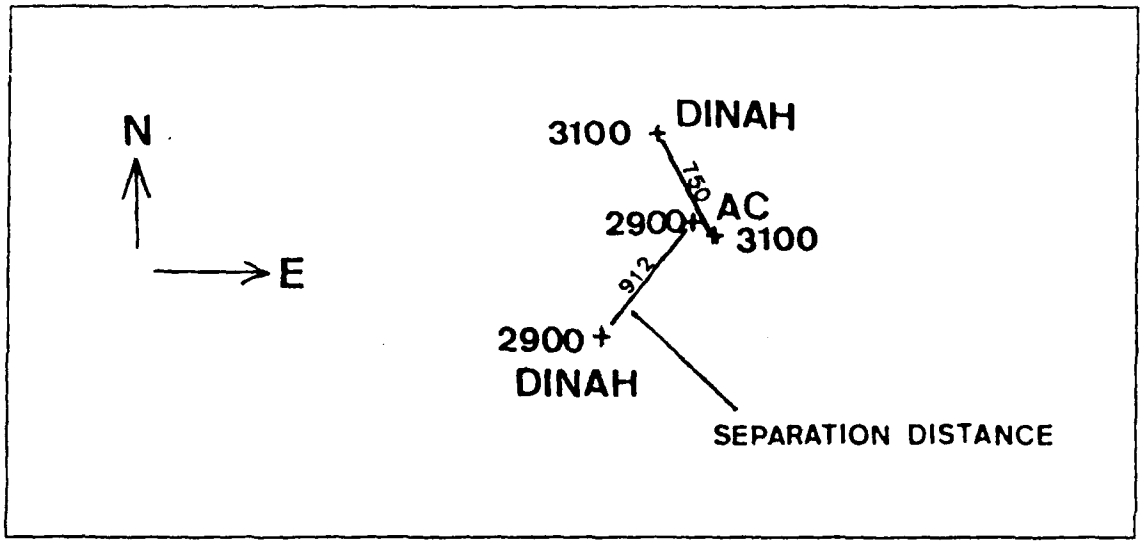

Figure 67. Separation distances and relative positions of Dinah and the AC (anticyclone). Solid lines are separation distances at those time periods. Diagram is not drawn to scale and distances are estimated from Figs. 63 and 65.

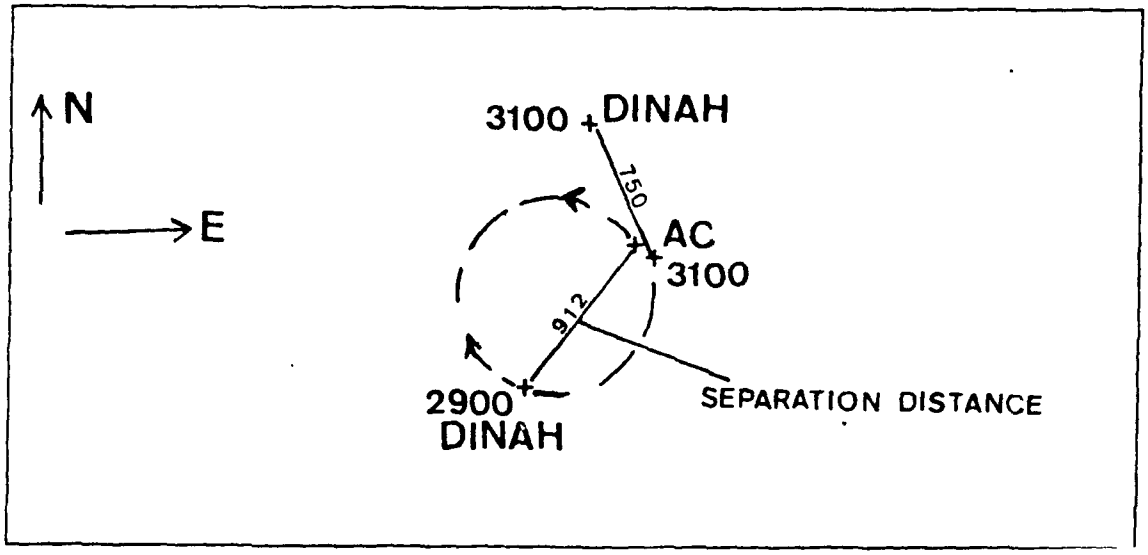

Figure 68. Fujiwhara effect between Dinah and the AC at 400 mb. Solid lines are similar to Fig. 67. Dashed lines depict the theoretical movement associated with

the Fujiwhara theory. Diagram is not drawn to scale and distances are estimated as in Fig. 67.

The convergent flow mechanism of Chang applied to a cyclone-anticyclone pair would support constant separation distance for equal strength systems through 3000, and then repelling at 3100 when the anticyclone's outer circulation effect on Dinah becomes greater (Fig. 69). For 2900 and 3000, there was not any defined rotation because the magnitudes were about equal. As indicated above, the anticyclone becomes dominant at 3100 and results in a clockwise rotation.

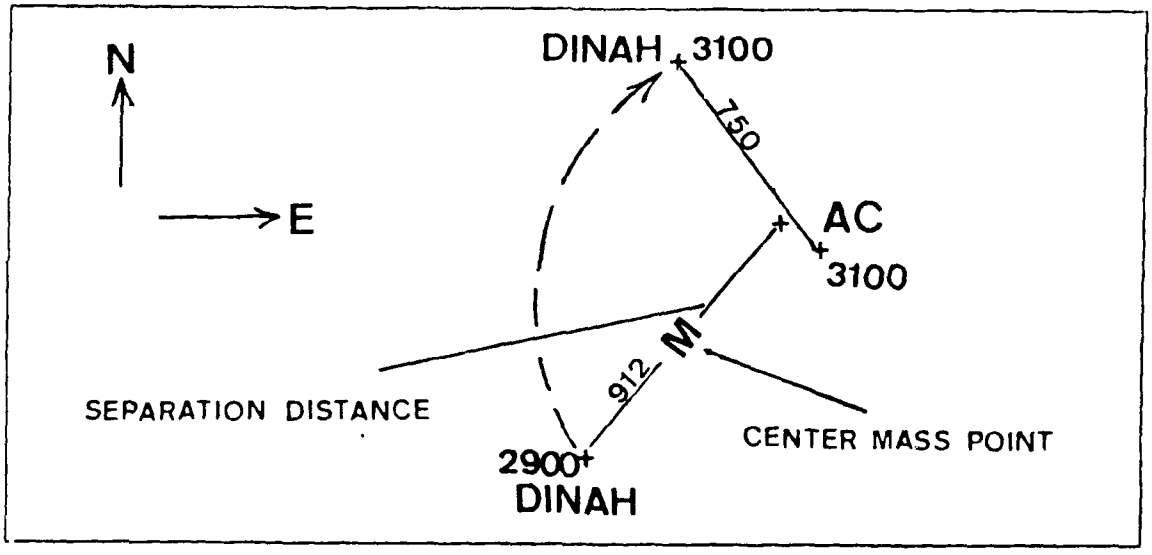

Figure 69. Convergent flow effect between Dinah and the AC at 400 mb for 00 UTC 31 August. Solid lines are similar to Fig. 67. Dashed lines show the direction of each system as they rotated about each other. The dotted lines depict the theoretical movement in accordance with the convergent flow theory. Diagram and distances are not drawn to scale.

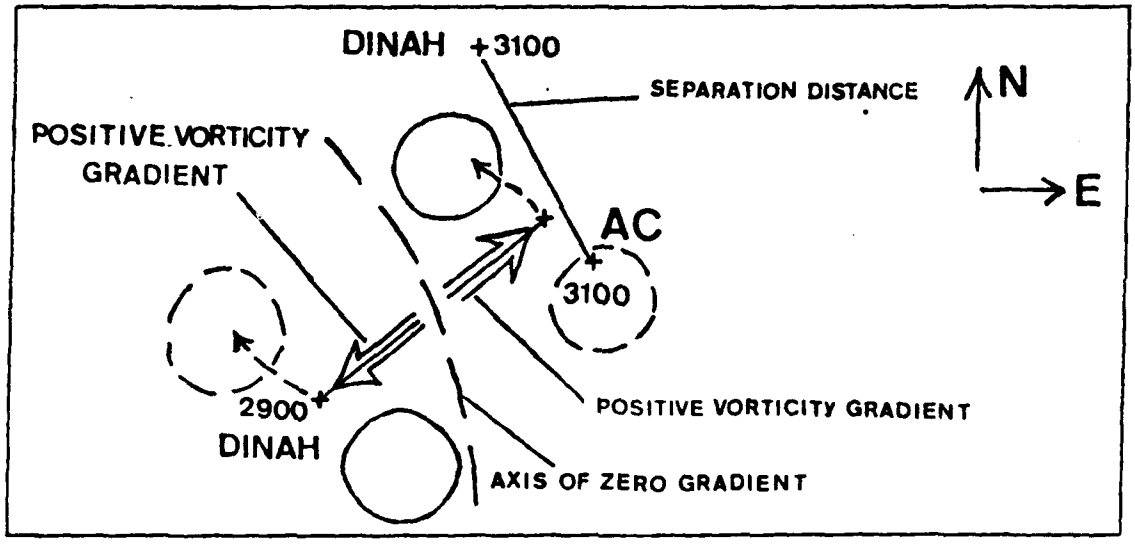

Figure 70. Vorticity advection effect between Dinah and the AC at 400 mb. Labeling is the same as in Fig. 36. The dashed circles represent areas where relative vorticity tendencies ($\partial\zeta/\partial t$) change positively with time and negatively in the solid circles. The dashed arrows point toward positive tendencies for the cyclone and negative tendencies for the anticyclone.

The environmental shear effect of Dong and Neumann would indicate a repelling motion at 2900 (Fig. 71) since the westerly midlatitude flow in Fig. 63 is stronger to the north of the AC than the weak and variable flow south of Dinah. At 3000, the shear flow is not effective (Fig. 64) because of the east-west orientation of the two systems. At 3100 (Fig. 65), the shear flow indicates an attraction because the stronger midlatitude westerlies would advect Dinah eastward, while the weaker subtropical easterlies south of Dinah would advect the AC westward. This

advection would create a clockwise rotation of the separation axis, in agreement with observations.

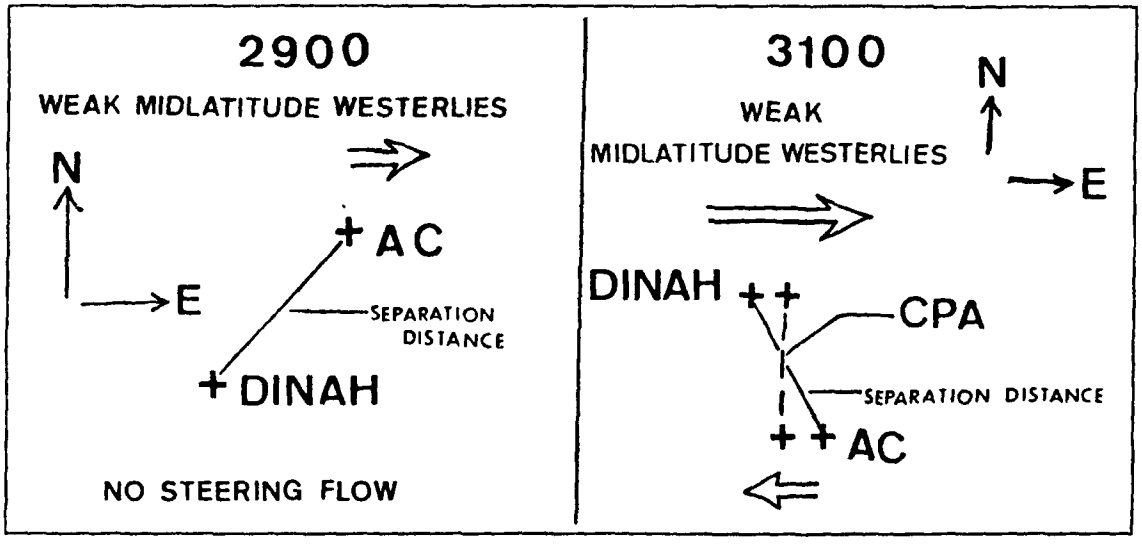

Figure 71. Environmental shear effect for Dinah and the AC at 400 mb.

Table 10 is a summary of the secondary effects for Case 3. A combination of the relative magnitudes and the orientation of the Dinah-AC pair complicated and masked the proper interpretation in terms of the secondary proceses to explain the ultimate movement and roataion of such features. The convergent effect would suggest a repelling motion whereas attraction is observed (Fig. 69). From the environmental shear, a repelling motion is evident at 2900 (Fig. 71), with only weak midlatitude westerlies advecting the AC a small distance eastward while negligible flow south of Dinah (Fig. 63) results in little movement in any direction. Then at 3100 (Fig. 65), attraction is evident after the oreintation of these two features has shifted 90° due to their rotation (Fig. 71) while the shear field remained unchanged.

Table 10. RELATIVE MOTION AND ROTATION OF THE TRACKS OF TY DINAH AND THE ANTICYCLONE during stage 1 for five secondary effects between 00 UTC 29 July 1984 and 00 UTC 31 July. CCR is counterclockwise rotation and CWR is clockwise rotation.

SECONDARY EFFECTS	MOVEMENT/ROTATION		
Day/Hour (Z)	2900	3000	3100
Observed	Attract/CWR	Attract/CWR	Attract/CWR
Beta	Neither/CWR	Neither/CWR	Neither/CWR
Fujiwhara	Undefined	Undefined	Undefined
Convergence	Repel/CWR	Repel/CWR	Repel/CWR
Advection	Attract/None	Attract/None	Repel/CWR
Shear	Repel/CWR	Repel/CWR	Attract/CWR

G. CASE 4 - INTERACTION OF TY MAC AND TS NANCY

1. Synoptic Discussion

This interaction involved two weak circulations in the South China Sea. TY Mac formed in the Philippine Sea and weakened significantly while moving westward across the central Philippine Islands. TY Mac never regained typhoon intensity after crossing the islands. Meanwhile, TS Nancy was developing in the monsoon trough just east of Hainan Island. Mac turned to the northwest in the South China Sea in response to Nancy's presence (Fig. 72). After TS Nancy turned to the southwest due to an apparent interaction with TY Mac (Fig. 72), Nancy eventually crossed the southern end of Hainan Island and tracked into Vietnam. The magnitudes of the 700 mb vorticity maxima were indicative of relatively weak systems embedded in the monsoon trough. Despite satellite cloud signatures that

indicated stronger upper-level vortices for both systems, only weak vorticity maxima at 400 and 250 mb were analyzed.

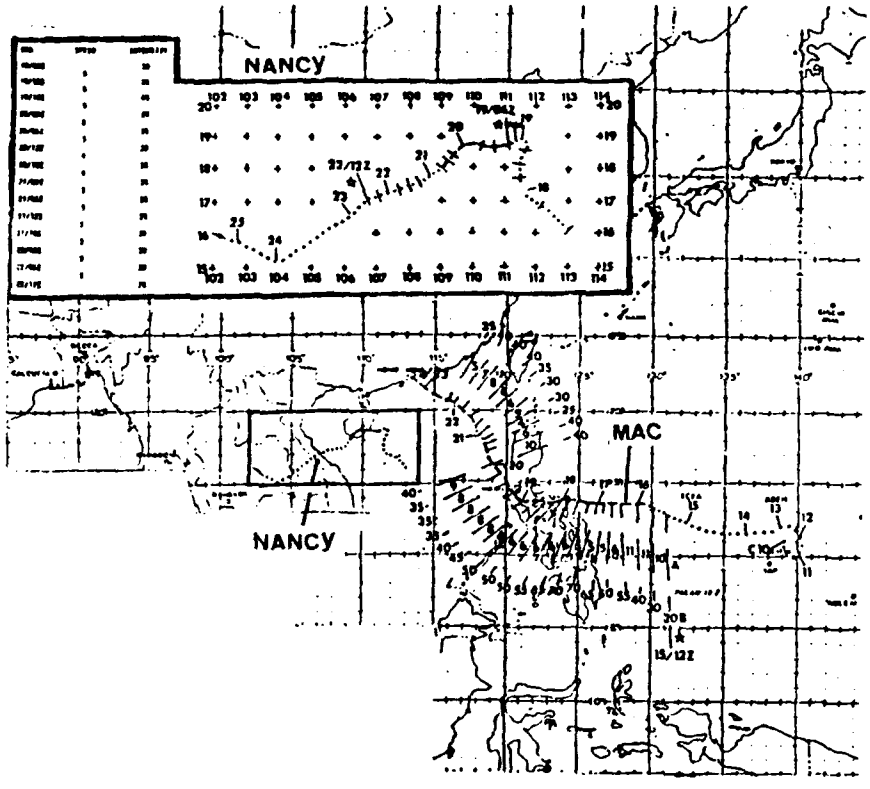

Figure 72. Tracks of weakened TY Mac and TS Nancy in the South China Sea (September 1979) suggests a cyclonic binary movement.

After Mac crossed the Philippines on 19 August, many of the Philippine rawinsonde observations were not available for the next 12 to 24 h. The Philippines is the primary source of rawinsonde data in an otherwise very sparse and vast western North Pacific region. Without the Philippine information, this region is nearly void of data. Consequently, the wind and the resultant vorticity fields across the Philippines could be strongly influenced by extrapolated data from the

midlatitudes. Interaction with the rugged topography of the Philippines may also have affected TY Mac's vorticity structure.

In summary, the vorticity field in Fig. 73 appeared to be smoothed due to paucity of data. This lack of data means the analysis was completed using observations from farther away, which likely resulted in a degraded analysis. The lack of an analyzed positive center for Mac in the eastern South China Sea, where a negative vorticity field is depicted, supports this interpretation. A better description of the fields is found at 2100 and at later times.

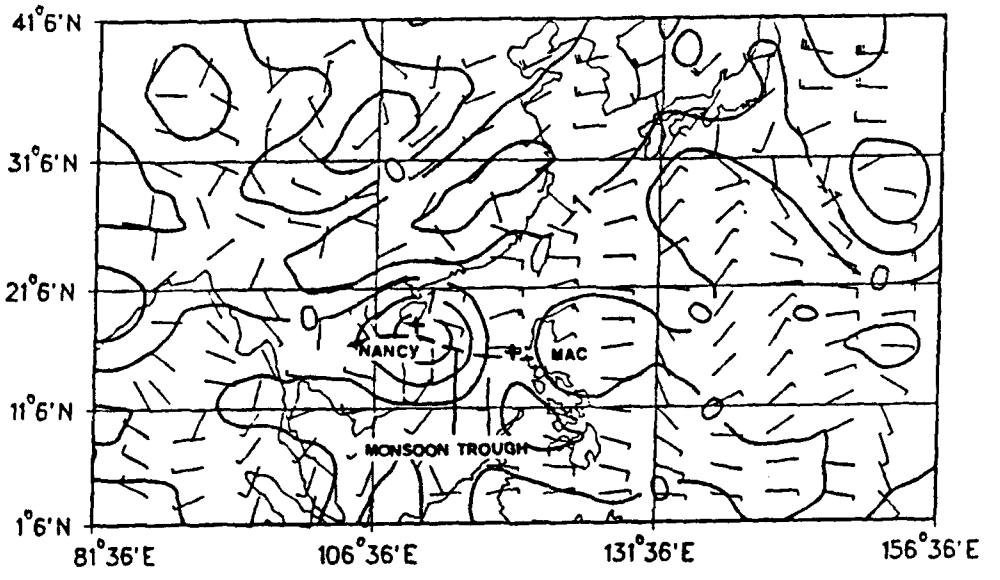

Figure 73. Vorticity field at 700 mb for TY Mac on 00 UTC 20 September 1983 which is distorted due to paucity of upper-air soundings over the Philippines after Mac's transit across that area on the 19th.

2. Evaluation of Secondary Effects on the Interaction of Weak Cyclones

The vorticity gradients in Fig. 74 indicate interaction only after 2012, because negative vorticity values (ridging) existed between the two storms at 1912 through 2012. The vorticity analysis in Fig. 73 has negative vorticities in the location of a significantly weakened TY Mac, which results in a positive vorticity gradient toward TS Nancy at 2112. This single gradient in Fig. 74 is depicted by the dashed curve without any slope change. Only the curves at 2212 and 2312 support binary interaction due to distinct vorticity gradients associated with each cyclone. This binary interaction occurred only after these two storms had passed their CPA at 2112, as indicated by the vertical lines in Fig. 74, and showed repelling (vertical lines moving to the right with time) along with the counterclockwise rotation (Fig. 75). Table 11 indicates Nancy had the greater relative magnitude up to 2212 with only a single vorticity gradient present up to 2100. Thereafter, the relative strength of Mac became larger than Nancy beyond 2212 and a vorticity gradient existed for each system.

Table 11. RATIO OF THE RELATIVE VORTICITY AMPLITUDE OF TS NANCY COMPARED TO TY MAC showing the relative imapct of TS Nancy on Mac during the interaction period at 12 UTC 22 September 1979 through 12 UTC 23 September.

DATE/TIME (Z)	2212	2312
AMPLITUDE	4/3	3/4
AREA $(1/r)^2$	9/4	4/9
PRODUCT	3	1/3

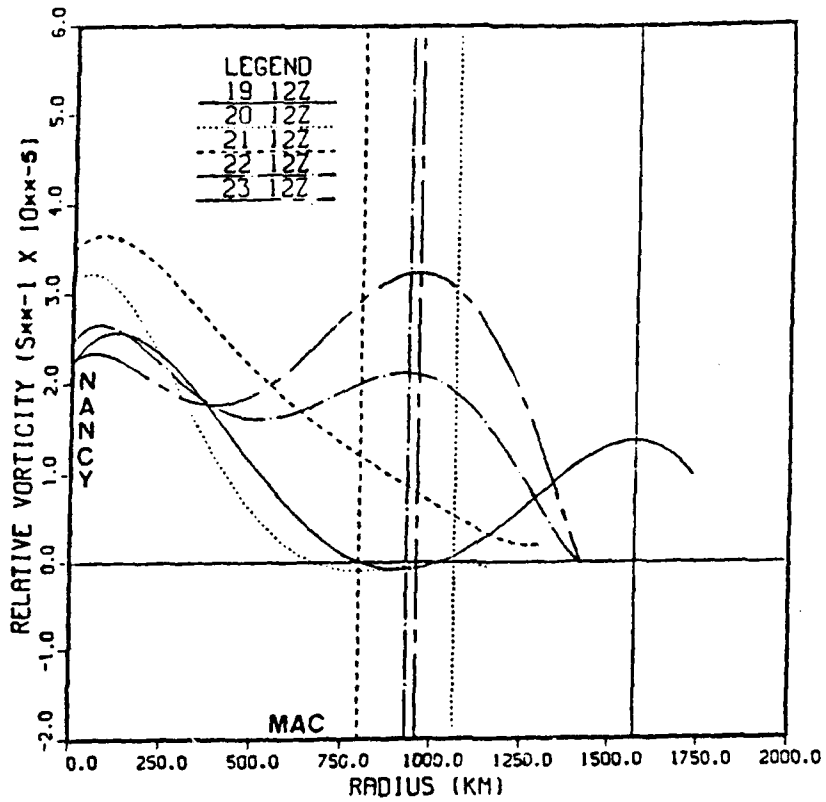

Figure 74. Vorticity along the axis connecting Mac and Nancy at 700 mb from 12 UTC 19 September to 12 UTC 23 September 1979. TS Nancy is represented along the left axis (radius=0) and the relative positions of TY Mac are indicated by the vertical lines during this period. TS Nancy and TY Mac indicate mutual attraction at 12 UTC on 22 and 23 September, after their closest point of approach (CPA) on the 21st.

These results are somewhat suspect because of the analysis ambiguities indicated above and the uncertainties in the vorticity gradients in Fig. 74. No interaction was probable at 1912 and 2012 because of the small negative vorticity values between Mac and Nancy. Nevertheless, an attraction was occurring.

The Beta effect (Fig. 75) would indicate weak repulsion through 2112, and then weak attraction by 2312 when Mac was larger than Nancy and was located to the northeast. However, this is in disagreement with the observations.

Although the Fujiwhara effect depicts the correct rotation (similar to Fig. 48), the magnitudes would be difficult to estimate because the outer wind profile on each system is uncertain due to the paucity of data. Because they were weak features in a smoothed analysis, the low-level environmental flow associated with the monsoon trough (depicted in Fig. 72) may be a better indication of the actual effect.

The convergent flow effect indicates attraction (similar to Fig. 38) with counterclockwise rotation. This supports the observed attraction until 2112, but not the repulsion at 2212 and 2312.

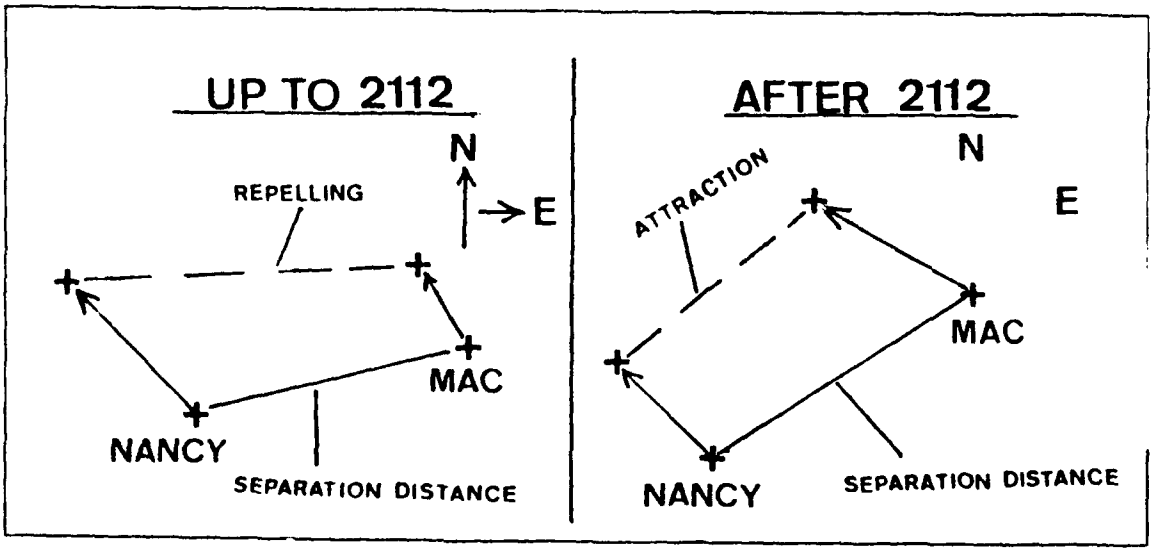

Figure 75. Beta effect between TY Mac and TS Nancy at 700 mb from 12 UTC 19 September and 12 UTC 23 September. Solid lines are the initial separation distances. Arrows indicate actual movement. Dashed lines are the resultant distance axes.

Similar to Fig. 50, the vorticity advection secondary effect would indicate weak repulsion with disagrees with the observed attraction at 1912 and 2012. Unlike the other cases, a single vorticity gradient exists between Mac to Nancy at these times. After 2100, vorticity gradients for each system become reestablished and support this secondary mechanism's repulsion effect at 2212 and 2312.

The environmental shear effect is negligible until 2212 due to the east-west orientation of the storms. After 2212, this effect remained negligible even though the storms became more north-south oriented. This type of movement would support the counterclockwise rotation that was observed. In this case, the easterly flow south of the subtropical ridge steered Mac westward as did Nancy because of its location north of the subtropical ridge, which caused the separation distance to decrease. Both systems continued moving westward with the apparent attraction due to Mac's faster westward movement under the influence of the subtropical ridge low-level easterlies that were stronger away from the monsoon trough axis. Therefore, the shear effects did not contribute throughout this cyclone interaction period.

In summary, the secondary effects evaluation is degraded without reliable wind and vorticity field analysis due to the sparsity of data. The weak interaction event involved attraction during the first half of the time period and repulsion in the last half. Counterclockwise rotation was evident throughout the period. Table 12 is a summary of the secondary effects for Case 4 during the two time periods. The only secondary effect that correctly evaluated the observed events throughout the entire period (1912-2312) was the Fujiwhara effect. However, the outer wind field of each storm seemed too weak to influence the movement of the other in the latter period (2200-2312) compared to the vorticity advection effect. Overall, this

interaction case seemed to be too weak and was influenced too much by the monsoon trough that dominated the environmental wind field in which these storms were embedded. This appears to have hindered a proper evaluation of the shear effect on cyclone-cyclone movement.

Table 12. RELATIVE MOTION AND ROTATION OF THE TRACKS OF TS NANCY AND TY MAC for five secondary effects between 12 UTC 19 September 1979 and 12 UTC 23 September. CCR is counterclockwise rotation and CWR is clockwise rotation.

SECONDARY EFFECTS	MOVEMENT/ROTATION	
Day/Hour (Z)	1912 TO 2112	2200 TO 2312
Observed	Attract/CCR	Repel/CCR
Beta	Repel/CCR	Attract/CCR
Fujiwhara	CCR	CCR
Convergence	Attract/CCR	Attract/CCR
Advection	Repel/CCR	Repel/CCR
Shear	Negligible (weak shear)	Negligible (weak shear)

VI. CONCLUSIONS AND RECOMMENDATIONS

The study suggests that Empirical Orthogonal Functions (EOF's) are an effective tool to represent the relative vorticity fields, and these fields may be used to improve the forecaster's understanding of tropical cyclone interactions with adjacent synoptic features. Four cases with various types of interaction illustrate different scenarios from which to evaluate the secondary mechanisms. Each of the secondary effects was treated independently. These scenarios involved:

(1) interaction of two tropical cyclones (strong and weak intensities);

(2) interaction of multiple tropical cyclones;

(3) interaction of a tropical cyclone and a midlatitude cyclone; and

(4) interaction of a tropical cyclone and an anticyclone.

The EOF representation of vorticity features is less noisy than the original fields of Sherman (1988). More cases are needed to verify that the EOF vorticity representation of the axis of maximum relative vorticity describes the movement of the tropical storm as well as in case of STY Marge in Fig. 27 (Sherman, 1988). If so, 12-h operationally-analyzed wind fields could be used in a prognostic model to construct vorticity patterns to predict short-term tropical cyclone tracks. These EOF vorticity fields should be made available to the Typhoon Duty Officer at JTWC as an additional forecast aid or as a check against other prognostic models. Interpretations in terms of vorticity dynamics could be used as a guidance tool to evaluate if and when the objective track forecast aids are performing satisfactorily (Case 1-STY Abby).

The vorticity values along the separation axis are used to represent the amplitudes and areal extents of the interacting synoptic features. In general, the accuracy of the EOF vorticity field representation depends on how well the wind

field is depicted from available data (rawinsondes and pilot reports). Although these data are very sparse in the western North Pacific under the best of circumstances, the more intense systems with larger areas extents (tropical or extratropical) are better analyzed. Such case studies involving STY Abby and the ET cyclone in stage 2 of Case 1, TY Pat in Case 2, and TY Dinah and the Anticyclone in Case 3 appear to support such analyses. Even the TUTT in Case 3, though too distantly separated to interact with Dinah, appeared to be analyzed accurately throughout the case study period.

In Case 2, which involved an intense but small areal extent circulation (TY Odessa), the magnitude of the relative vorticity fields were under-represented due to smoothing from a coarse grid resolution of 2.5° lat. Another major problem with Case 2 was the difficulty of interpreting interacting features in close proximity (less than 3 gridpoints). A grid interval of 278 km requires too much interpretation and causes too much smoothing of the vorticity field, which significantly degrades the evaluation of the secondary mechanisms. In Case 4, relatively weak and shallow cyclones and paucity of data acounted for the suspect analysis, especially prior to 1200 UTC 20 September 1979.

The EOF-derived fields clearly illustrated that tropical cyclones may interact at different levels with a variety of tropical and midlatitude features. In Case 1, Supertyphoon Abby interacted with another cyclone (Tropical Storm Ben) at 700 mb during stage 1. The relative vorticity fields showed no significant circulation features associated with Ben above 700 mb which was dominated by the outer cyclonic circulation of Abby at 400 mb and an anticyclonic outflow at the 250 mb level. Ben's shallow vertical structure was consistent with its relatively weak intensity. During stage 2, STY Abby interacted with a midlatitude cyclone at 400

mb. Although Abby was well developed through all levels of the atmosphere, the upper-level cyclone was evident only from 250 down through 700 mb, and had the largest relative vorticity magnitudes at 400 mb.

In Case 2, two nearly equal intensity cyclones were interacting with well defined circulations from the surface through 250 mb. In a normal situation, it would be reasonable to consider that these two cyclones would interact with the most intensity at the 400 mb level. However, TY Pat had a rather large areal extent of vorticity, while Odessa's was too small to be properly resolved. Therefore, the analysis did not show a separate wind field and vorticity gradient associated with Odessa. Rather, a displaced false (hybrid) center was defined at 700 mb. Perhaps the close proximity of another relatively weak intensity system (TS Ruby) also influenced the level and placement of this hybrid center. Eventually, both Odessa and Ruby became completely absorbed in Pat's outer circulation. It appeared from this case study that the intensity, areal extent and close proximity equally influenced this end result of a poor representation of the interaction.

Case 3 was similar to Case 1 in that Dinah interacted with Ed in stage 1, and then with the anticyclone during stage 2. It appeared that a Dinah-Ed interaction was prohibited by a blocking narrow ridge that was evident from the surface through 400 mb. If any interaction occurred, it was restricted to the 250 mb level on 27 August as suggested from the JTWC post-analysis. In stage 2, the interaction scenario mirrored that of Case 1.

In Case 4, two weak intensity cyclones with relatively shallow vertical structures revealed only a mild interaction. It seemed these cyclones were more influenced by the well-developed monsoon trough. Only the 700 mb analysis suggested any interaction. Even at this level, the weak intensity, the separation

distance and the absence of any vorticity gradient with Mac earlier in the case study period made the analysis of cyclone-cyclone interaction difficult to interpret.

These case studies revealed the strongest interactions between two systems occurred where the vorticity magnitudes and gradients were large. Thus, two intense interacting features may extend to 400 or 250 mb, whereas weaker circulation features are restricted to lower atmospheric levels (700 mb).

The convergent flow effect of Chang (1983) depicted the observed attraction or repulsion and rotation for most situations. The only scenario in which this mechanism did not agree with the observations was during the interaction periods involving the weak cyclones (Case 4) and in Case 3 with opposing circulations (TY Dinah and the anticyclone).

Application of the Beta effect was complicated during the multiple cyclone interactions (Case 2), because the environmental vorticity gradient is not due only to the earth vorticity gradient. Both the Beta and the environmental shear effect (Dong and Neumann) were very dependent on the relative storm orientations. Many times the western North Pacific monsoon trough is not aligned in a zonal direction to contribute to interacting cyclone movements due to these secondary effects.

The Fujiwhara effect verified better with scenarios involving stronger and nearly equal circulations. In Case 3 with opposing circulations (Dinah and the anticyclone), this effect did not explain the observed clockwise rotation even when the two systems were equal in magnitude (prior to 3100). The vorticity advection effect of DeMaria and Chan (1984) did not explain the attraction or repelling motion in any of the cyclone-cyclone scenarios, but did apply in situations involving

opposing circulations (Case 3). However, this effect supported the correct rotation in the four cases.

More case studies are needed to test the applicability of these five secondary effects. Given the wind data in the western North Pacific region are sparse, the derivatives for the vorticity field computations are inherently noisy. This may explain why the mechanisms that do not involve higher order derivatives, such as the Fujiwhara effect and the convergent flow effect of Chang (1983), seem to be more reliable. The goal of the additional case studies should be to develop a set of "Thumb Rules" for forecasting, which also might be employed in an artificial intelligence scheme in the JTWC computer network. Such an artificial intelligence approach could assist the forecaster by suggesting which of the mechanisms best depict the ambient environment and possible cyclone track.

Finally, a method should be developed to separate the environmental vorticity from the tropical cyclone vorticity. This separation would isolate the cyclone circulation from the ambient environment and allow a clearer depiction of the steering flow. The availability of these EOF-derived relative vorticity fields should provide the forecaster with many displays to improve understanding of cyclone interactions. Hopefully, a better understanding of the cyclone-cyclone and cyclone-environmental interactions will lead to improved forecasts in the future.

LIST OF REFERENCES

ATCR, 1979: Annual Tropical Cyclone Report. NAVOCENCOMCEN/JTWC, COMNAVMARIANAS BOX 17, FPO San Francisco, CA, 191 pp.

ATCR, 1983: Annual Tropical Cyclone Report. NAVOCENCOMCEN/JTWC, COMNAVMARIANAS BOX 17, FPO San Francisco, CA, 196 pp.

ATCR, 1984: Annual Tropical Cyclone Report. NAVOCENCOMCEN/JTWC, COMNAVMARIANAS BOX 17, FPO San Francisco, CA, 219 pp.

ATCR, 1985: Annual Tropical Cyclone Report. NAVOCENCOMCEN/JTWC, COMNAVMARIANAS BOX 17, FPO San Francisco, CA, 274 pp.

Chan, J. C.-L., 1986: Supertyphoon Abby - An example of present track forecast inadequacies. *Weather and Forecasting*, **1**, 113-126.

DeMaria, M., 1985: Tropical cyclone motion in a nondivergent barotropic model. *Mon. Wea. Rev.*, **113**, 1199-1210.

DeMaria, M., and J. C.-L. Chan, 1984: Comments on "A numerical study of the interactions between two tropical cyclones." *Mon. Wea. Rev.*, **112**, 1643-1645

Dong, K., and C. J. Neumann, 1986: The relationship between tropical cyclone motion and the environmental geostrophic flows. *Mon. Wea. Rev.*, **114**, 115-122.

Elsberry, R. L., 1986: Some issues related to the theory of tropical cyclone motion. Tech. Rep. NPS-63-86-005, Naval Postgraduate School, Monterey, CA, 25 pp.

Halsey, W. F., and J. Bryan III, 1947: *Admiral Halsey's story.* McGraw-Hill Company, Inc., 310 pp.

Kutzbach, J. E., 1967: Empirical eigenvectors of sea-level pressure, surface temperature and precipitation complexes over North America. *J. Appl. Meteor.*, **6**, 791-802.

Lorenz, E. N., 1956: Empirical orthogonal functions and statistical weather prediction. Department of Meteorology, Massachusetts Institute of Technology, Cambridge, MA. Scientific Report 1, Statistical Forecasting Project, 48 pp.

Meanor, D. H., 1987: Vertical wind shear as a predictor of tropical cyclone motion. M.S. thesis, Naval Postgraduate School, Monterey, CA, 74 pp.

Neumann, C. J., 1982: Trends in forecasting the tracks of Atlantic tropical cyclones. *Bull. Amer. Meteor. Soc.*, **62**, 1473-1485.

Peak, J. E., W. E. Wilson, R. L. Elsberry and J. C.-L. Chan, 1986: Forecasting tropical cyclone motion using empirical orthogonal function representation of the environmental wind fields. *Mon. Wea. Rev.*, **114**, 2466-2477.

Preisendorfer, R. W., and T. P. Barnett, 1977: Significance tests for empirical orthogonal functions. *Proc. 5th Conf. on Probability and Statistics in Meteorology and Atmospheric Sciences,* Amer. Meteor. Soc., Boston, MA, 169-172.

Sandgathe, S. A., 1987: Opportunities for tropical motion research in the Northwest Pacific region. Tech. Rep. NPS-63-87-006, Naval Postgraduate School, Monterey, CA, 36 pp.

Schott, T. B., 1985: Applications of wind empirical functions in tropical cyclone motion studies. M.S. thesis, Naval Postgraduate School, Monterey, CA, 99 pp.

Shaffer, A. R., 1982: Typhoon motion forecasting using empirical orthogonal function analysis of the synoptic forcing. M.S. thesis, Naval Postgraduate School, Monterey, CA, 150 pp.

-----, and R. L. Elsberry, 1982: A statistical-climatological tropical cyclone track prediction technique using an EOF representation of the synoptic forcing. *Mon. Wea. Rev.*, **110**, 1945-1954.

Sherman, B. T., 1988: Synoptic patterns related to tropical cyclone recurvature. M.S. thesis, Naval Postgraduate School, Monterey, CA, 131 pp.

U.S. Naval Weather Service, 1975: *Numerical Environmental Products Manual.* NAVAIR 50-1G-522, 155 pp.

Wilson, W. E., 1984: Forecasting of tropical cyclone motion using an EOF representation of wind forcing. M.S. thesis, Naval Postgraduate School, Monterey, CA, 87 pp.

INITIAL DISTRIBUTION LIST

		No. Copies
1.	Defense Technical Information Center Cameron Station Alexandria, VA 22304-6145	2
2.	Library, Code 52 Naval Postgraduate School Monterey, CA 93943-5002	2
3.	Chief of Naval Research 800 N. Quincy Street Arlington, VA 22217	1
4.	Oceanographer of the Navy Naval Observatory 34th and Massachusetts Avenue, NW Washington, DC 20390-5000	1
5.	Commanding Officer Naval Oceanographic Command NSTL, MS 39522-5000	1
6.	Commanding Officer Fleet Numerical Oceanography Center Monterey, CA 93943-5005	1
7.	Chairman (Code MR/Hy) Department of Meteorology Naval Postgraduate School Monterey, CA 93943-5000	1
8.	Chairman (Code OC/Co) Department of Oceanography Naval Postgraduate School Monterey, CA 93943-5000	1
9.	Professor Russell L. Elsberry (Code MR/Es) Department of Meteorology Naval Postgraduate School Monterey, CA 93943-5000	1
10.	Dr. G. J. Holland BMRC, P. O. Box 1289K Melbourne, Victoria 3001 Australia	1

11. LT Mark J. Gunzelman, USN — 1
DMA-H/TC
6500 Brookes Lane
Washington, DC 20315

12. Mr. Paul Dobos (Code MR/Db) — 1
Department of Meteorology
Naval Postgraduate School
Monterey, CA 93943-5000

13. Commanding Officer — 1
Naval Oceanographic and Atmospheric
Research Laboratory (NOARL)
Monterey, CA 93943-5006

14. Mr. Ron Miller — 1
Naval Oceanographic and Atmospheric
Research Laboratory (NOARL)
Monterey, CA 93943-5006

15. Chairman, Department of Meteorology — 1
Florida State University
Tallahassee, FL 32306

16. Director, — 1
Joint Typhoon Warning Center
COMNAVMARIANAS Box 17
FPO San Francisco, CA 96630

17. Library Acquisitions — 1
National Center for Atmospheric Research
P. O. Box 3000
Boulder, CO 80307-5000